



**UNIVERSITY OF LEEDS**

This is a repository copy of *Liquid crystal displays*.

White Rose Research Online URL for this paper:  
<https://eprints.whiterose.ac.uk/120360/>

Version: Accepted Version

---

**Book Section:**

Jones, JC [orcid.org/0000-0002-2310-0800](https://orcid.org/0000-0002-2310-0800) (2018) Liquid crystal displays. In: Dakin, JP and Brown, RGW, (eds.) Handbook of Optoelectronics: Enabling Technologies. Series in Optics and Optoelectronics, 2 . CRC Press , Boca Raton, FL, USA , pp. 137-224. ISBN 9781482241808

---

© 2018 by Taylor & Francis Group, LLC. This is an Accepted Manuscript of a book chapter published by CRC Press in Handbook of Optoelectronics: Enabling Technologies on 06 Oct 2017, available online: <https://www.crcpress.com/9781138102262>. Uploaded in accordance with the publisher's self-archiving policy.

**Reuse**

Items deposited in White Rose Research Online are protected by copyright, with all rights reserved unless indicated otherwise. They may be downloaded and/or printed for private study, or other acts as permitted by national copyright laws. The publisher or other rights holders may allow further reproduction and re-use of the full text version. This is indicated by the licence information on the White Rose Research Online record for the item.

**Takedown**

If you consider content in White Rose Research Online to be in breach of UK law, please notify us by emailing [eprints@whiterose.ac.uk](mailto:eprints@whiterose.ac.uk) including the URL of the record and the reason for the withdrawal request.



[eprints@whiterose.ac.uk](mailto:eprints@whiterose.ac.uk)  
<https://eprints.whiterose.ac.uk/>

# Liquid Crystal Displays

J. Cliff Jones

*Soft Matter Physics, School of Physics and Astronomy, University of Leeds, Leeds, UK*

IN J.P. Dakin and R.G.W. Brown, (2017) Handbook of Optoelectronics, CRC Press.

Objective	2	4.5 <i>Ferroelectric Liquid Crystal Displays</i>	59
1. Introduction	2	4.5 <i>In-Plane Switching LCDs</i>	63
2. Liquid Crystals and their display relevant physical properties	3	4.5.1 <i>Introduction</i>	63
2.1 <i>Orientalional Order</i>	3	4.5.2 <i>Basics of IPS Operation</i>	64
2.2 <i>General Anisotropic Physical Properties</i>	6	4.5.3 <i>Fringe Field Switching Mode</i>	67
2.3 <i>Formulating Liquid Crystal Mixtures</i>	10	4.6 <i>Vertically Aligned Nematic Modes</i>	67
2.4 <i>Functional Liquid Crystal Compounds</i>	12	5. LCDs for non-mainstream and Niche Markets	70
3. Basics of Liquid Crystal Devices	15	5.1 <i>Introduction</i>	70
3.1 <i>Basics of Display Construction</i>	15	5.2 <i>Cholesteric LCDs</i>	70
3.2 <i>LCD Polarisation Optics</i>	21	5.2.1 <i>Temperature, Strain and Gas Sensors</i>	70
3.3 <i>Basic Operation: Electrically Controlled Birefringence Mode</i>	22	5.2.2 <i>Bistable Cholesterics</i>	70
3.4 <i>Passive Matrix Addressing and the Multiplexing Limit</i>	28	5.3 <i>Bistable Nematic LCDs and ZBD</i>	71
3.5 <i>Thin Film Transistors and Active Matrix Addressing</i>	32	5.4 <i>Polymer Dispersed Liquid Crystals</i>	75
4. Standard LCD Modes	38	5.5 <i>Liquid Crystal on Silicon (LCoS)</i>	79
4.1 <i>Overview</i>	39	6. LCD Modes for potential future applications	80
4.2 <i>Dynamic Scattering Mode</i>	43	6.1 <i>Introduction</i>	80
4.3 <i>Twisted Nematic Mode</i>	44	6.2 <i>Pi-Cell</i>	82
4.3.1 <i>Introduction</i>	44	6.3 <i>Analogue Ferroelectric Liquid Crystal Modes</i>	82
4.3.2 <i>The OFF State and TN Design</i>	44	6.4 <i>N*-SmC*</i>	82
4.3.3 <i>The ON State and Optical Compensation</i>	49	6.5 <i>Anti-ferroelectric liquid crystals</i>	83
4.3.4 <i>Single Polariser Reflective Mode TN</i>	51	6.6 <i>Deformed helix mode ferroelectric liquid crystal.</i>	83
4.4 <i>Supertwist Nematic LCDs</i>	54	6.7 <i>The Electroclinic Effect</i>	83
		6.8 <i>Blue Phase TFT Displays</i>	83
		6.9 <i>Cholesteric Flexoelectricity and</i>	86

<i>the Uniform Helix Mode</i>	
6.10 <i>Liquid Crystal Lasers</i>	86
7. Conclusions	89
Acknowledgements	89

References	89
Suggested Further Reading	98

## Objective

Over the past half-century, Liquid Crystal Displays have grown to be one of the most successful optoelectronic technologies, becoming an integral part of communication devices and often an enabling technology. This success has required many adaptations to meet the requirements of ever-increasing complexity and performance. Indeed, it is the adaptability of liquid crystal devices that grounds their success. After outlining the basic physics of liquid crystals and device construction, the various modes used in commercial displays will be reviewed, both for mainstream and niche markets, together with a summary of the important complimentary technologies. Finally, liquid crystal devices that have promise for future applications in optoelectronics will be discussed.

## 1 Introduction

On May 28<sup>th</sup> 1968, the cinema audience at the Loews Capitol Movie Theatre on Broadway, New York, USA would have been astounded by the vision of the future presented to them in Stanley Kubrick's masterpiece *2001: A Space Odyssey* [1]. Amongst the technological advances envisaged, from an International Space Station, video telephony to the omnipresence of computers, the viewers will have been no less captivated by the tablet computers that astronauts Dave Bowman (Keir Dullea) and Frank Poole (Gary Lockwood) apprise themselves with from the BBC12 podcast, after being awoken from hibernation. Those devices had flat panel displays able to present full colour, video information, something that would be as unfamiliar to the audience in 1968, as it is familiar to us now. Just one block away, at the Headquarters of *RCA* in the Rockefeller Plaza on 6<sup>th</sup> Avenue, George Heilmeyer was at a press conference [2] to announce his recently published patent of the

technology that would eventually lead to Kubrick's vision becoming reality: the first practical liquid crystal display, or LCD [3, 4].

Although the first device utilising liquid crystal electro-optical effects dates back to 1934 [5], the era of LCD research had begun in earnest with the ground breaking inventions at *RCA* in the mid 1960s [2, 6, 7]. This work was driven by *RCA* CEO David Sarnoff's dream for "hang on the wall" television displays [6] and inspired by the work of George Gray [8] of Hull University in the UK, Glenn Brown at Kent State University in the US [9] and Richard Williams [10, 11] at *RCA*'s Sarnoff Laboratories in Princeton. LCDs offered both reflective mode and backlit transmissive modes, in displays with a simple construction, light weight and flat form factor. Display power consumption and operating voltages were attractively low and suited for being driven by CMOS circuitry.

Soon after Heilmeyer's invention of the Dynamic Scattering Mode liquid crystal display [3, 4], *RCA* terminated their LCD investment, but the seed had been sown. Research groups from around the world, notably from Europe [12] and Japan [7, 13], entered the field, stimulated by the *RCA* Press announcement. Having teamed up with Martin Schadt at Hoffman La Roche in Switzerland, ex-*RCA* researcher Wolfgang Helfrich invented the twisted nematic LCD in 1970 [14], a device with a more attractive optical appearance than its Dynamic Scattering Mode predecessor, and a design that was to become the mainstay of flat panel displays for the following three decades. In the UK, Gray's group had formulated the first stable room temperature liquid crystal compounds [15] allowing mixtures with operating temperatures below zero degrees centigrade [16] to be formulated by Peter Raynes at the Royal Signal and Radar Establishment in Malvern, UK. In Japan, Tomio Wada at *Sharp* led a joint collaboration with Dainippon Ink and Chemicals that launched the

world's first commercial LCD, incorporated in *Sharp's* electronic calculator EL-805 in early 1973.

The promise of flat-screen, low power, high information content displays that met Sarnoff's goal for television displays seemed imminent [17]. Developments in the fabrication of LCD devices [7, 12, 13] led to early success in applications such as wristwatches and pocket calculators. However, it would take a further three decades of investment, invention and development before the LCDs replaced the dominant cathode ray tube displays used in televisions. Today's state-of-the-art ultra-high resolution LCDs for UHDTV combines technologies such as thin-film transistors behind each colour sub-pixel, optical compensation layers to give the widest angle of view, new alignment modes and addressing methods to achieve 120Hz frame rates, liquid crystal mixtures that can operate from -20°C to +80°C to produce displays from several mm to over 100" diagonal, at a price affordable for mass market adoption. Although it took this period to achieve Sarnoff's goal, the roadmap includes many consumer products that have been enabled by the emerging LCD: flat screen desktop monitors, laptop computers, mobile phones and tablets. LCDs are the purveyors of the Internet age.

There is a plethora of different liquid crystal display types, each with properties that have been optimized for different markets. After reviewing some basics of liquid crystal science and display construction, a selection of typical LCD modes is described in this chapter, together with some of the more esoteric devices that meet the needs of niche markets or are yet to achieve commercial success.

## 2 Liquid Crystals and their display relevant physical properties

### 2.1 Orientational Order

Although discovered by Friedrich Reiner in 1888 [18], the true nature of liquid crystals, and the oxymoronic term *liquid crystal* itself, was described a year later by Otto Lehmann [19, 20]. The type of liquid crystal used in all devices to date is formed from rigid rod-like (calamitic) organic compounds, such as

those shown in figure 1. There are a variety of liquid crystal phases that may appear between the isotropic liquid and solid crystal of certain organic compounds. Another, less common expression for liquid crystals is the term mesogenic, with molecules capable of forming liquid crystals being called mesogens, and the various phases termed mesophases. The simplest of the liquid crystal phase is the nematic (denoted N for shorthand), figure 1a), which has no positional order, as with a conventional isotropic liquid, but the liquid crystal phase has long-range orientational order of the long molecular axes. The molecular axes tend to orientate in a common direction called the director, represented by the unit vector  $\mathbf{n}$ . This orientational order leads to crystal-like anisotropy of physical properties such as the refractive indices, dielectric constants and conductivities. However, the lack of positional order means that the nematic is fluid, and can flow when perturbed. The statistical distribution of the molecular axes is quantified by order parameters. For a cylindrically symmetric phase, such as the nematic, which is composed of cylindrical molecules, the degree of order is defined using the S order parameter:

$$S = \frac{1}{2} \langle 3 \cos^2 \xi - 1 \rangle \quad , \quad (1)$$

where the brackets  $\langle \rangle$  represent the statistical average over the coherence volume of the material, and the deviation from the director of an individual long molecular axis is  $\xi$ . The anisotropic physical properties of the liquid crystal are related to S, which varies with temperature with the approximate form [21]:

$$S = \left( 1 - \frac{T}{T_{NI}} \right)^{\nu} \quad , \quad (2)$$

where  $\nu$  is a material constant, typically  $0.15 \leq \nu \leq 0.2$ , and  $T_{NI}$  is the nematic to isotropic transition temperature and T is the temperature below  $T_{NI}$ . Above  $T_{NI}$ ,  $S = 0$  by definition. This expression neglects the weakly first order nature of the nematic to isotropic phase transition, which jumps immediately

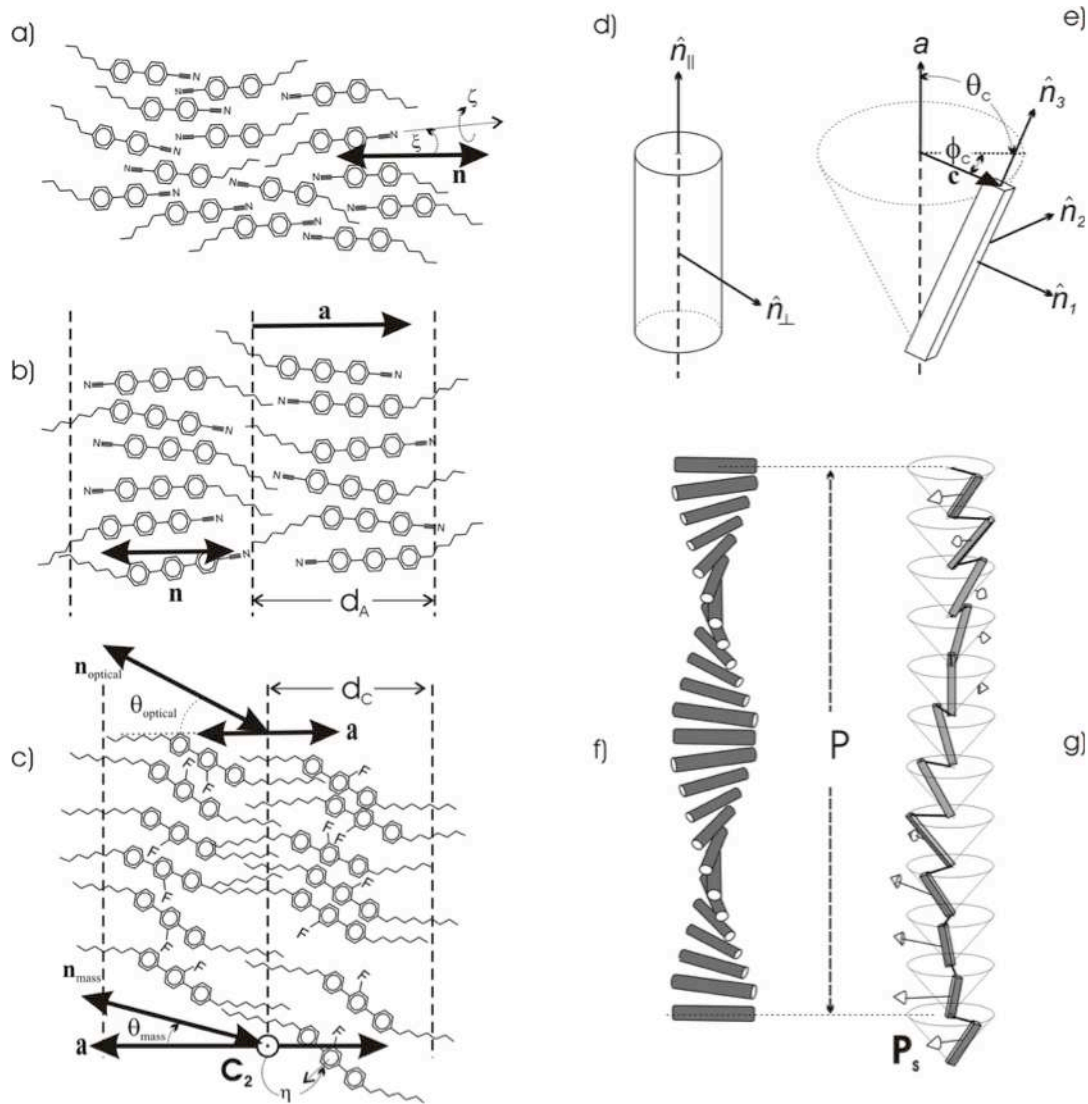


Figure 1. Some liquid crystals basics: a) Schematic representation of: a) the nematic phase and the  $\mathbf{n}$  director; b) the smectic A phase; and, c) the smectic C phase. The principal axes for; d) the cylindrical nematic and smectic A phases, and e) the monoclinic smectic C. The spontaneous twist of the chiral nematic or cholesteric and definition of the helical pitch length  $P$  are shown in f), and the spontaneous twist / bend of the chiral smectic C and ferroelectric spontaneous polarisation  $P_s$  are shown in g).

from 0 to about  $S = 0.43$  at  $T_{NI}$  in actuality. However, equation (2) is satisfactory a couple of  $^{\circ}\text{C}$  below  $T_{NI}$ , predicting typical nematic materials to have  $S \approx 0.60$  to  $0.80$  for typical nematic material at ambient temperatures.

A phial containing a nematic liquid crystal is milky in appearance. Unlike the common colloidal fluids with this type of behaviour (such as milk itself), this appearance occurs for a pure, single compound. It arises because, although the liquid crystal molecules tend to point in the same direction locally, this

direction changes over micron length scales due to thermal fluctuations, causing strong Tyndall scattering of the light. When heated to the isotropic liquid, the scattering disappears suddenly and the liquid is clear; for this reason, the temperature of the liquid crystal to isotropic transition (for example,  $T_{NI}$ ) is often termed the *clearing point*.

Almost all LCDs sold are based on the simple nematic type of liquid crystal, because it is the easiest to handle and most well understood. However, there are many other phases that can form that are intermediate between the liquid and crystal states, from those with higher degrees of order (layered smectics, helical cholesterics, and columnar phases), those using different shaped molecules (discs, banana-shaped, bowl-shaped, main-chain and side-chain polymeric) to those systems where the liquid crystal nature is due to changes in concentration, rather than, or in addition to, temperature, (lyotropic and chromonic phases). The interested reader is referred to reference [22] for a comprehensive review on all aspects of liquid crystal science. For the present chapter, only the smectic and cholesteric phases are considered because of their (limited) application to displays. Smectic liquid crystal phases have some degree of positional order in addition to orientational order. The simplest smectics are termed smectic A and C (for which the shorthand SmA and SmC is used, respectively) and they exhibit one-dimensional positional order, to form layers of nematic-like material. The layers of such phases are described by the unit vector  $\mathbf{a}$ . Smectic A have  $\mathbf{n}$  parallel to  $\mathbf{a}$ , figure 1b), whereas the director  $\mathbf{n}$  is at an angle  $\theta_C$  to  $\mathbf{a}$  in the smectic C phase, figure 1c). Both the nematic and smectic A (SmA) phases have cylindrical symmetry about  $\mathbf{n}$ , figure 1d), whereas the SmC has monoclinic symmetry. Nematics comprised, at least in part, of chiral molecules undergo a spontaneous twist of the director, to form a helical structure figure 1f). Chiral nematics, represented by  $N^*$ , are often called cholesterics after the first liquid crystal behaviour was observed for this phase in a compound derived from cholesteryl benzoate [18]. A full  $2\pi$  rotation of the  $\mathbf{n}$  director is defined as the pitch length,  $P$ , which may vary from sub-micron in some pure compounds, to

several hundreds of microns in a nematic material doped with a small concentration of a cholesteric dopant. In the chiral smectic C phase (SmC\*), figure 1g), the loss of mirror symmetry induced through the addition of chirality has two notable effects. Firstly, the  $\mathbf{n}$  director undergoes a spontaneous twist and bend deformation (so that the  $\mathbf{c}$  director forms a twist in a similar way to the cholesteric), again with pitch  $P$ . Secondly, the combination of the loss of the mirror-plane with the monoclinic symmetry of the smectic C leads to a spontaneous ferroelectric polarisation  $\mathbf{P}_s$  in the plane of the layers and normal to the tilt plane [23]. As the  $\mathbf{c}$ -director precesses about the layer normal in a helical fashion, so the net ferroelectric polarisation cancels out throughout the bulk of the phase.

Liquid crystal phases are formed for molecules that comprise both a rigid core structure and pendant flexible hydrocarbon chains. The occurrence, temperatures and phase sequences of liquid crystals depend on the relative proportion of the flexible chains and rigid core: the flexible groups are needed to space the cores sufficiently to prevent crystallisation but sufficiently small to allow orientational ordering of the cores. Predicting the temperature range over which liquid crystal phases form is a complex subject, requiring skill and experience for the synthetic chemist. For the simple rod-shaped calamitic molecules used in commercial displays, the transition from isotropic to liquid crystal phase is related to the length of the molecule. However, viscosity is also dependent on molecular size, and so most practical liquid crystal compounds are formed from two or three ring structures to keep viscosity low and switching speeds high. The ring structures in the core may be benzene, cyclohexane, pyrimidine, thiophene, etc., joined together with para- substitution (e.g. 1,4 benzene) or with near-linear linking groups (such as esters, ethyl groups), and terminated on one or both sides with alkyl chains. In each case, the molecular core retains its near-cylindrical symmetry with each of any low energy conformers allowed by the core, such as rotations about the ester or ethyl linkages. Table 1 lists a range of different compounds that are typical for nematic liquid crystal mixtures, together with some of

the key physical parameters [24] related to typical device behaviour.

## 2.2 General Anisotropic Physical Properties

All liquid crystal displays operate because of the combination of the anisotropic physical properties combined with fluidity exhibited by liquid crystals. Tensorial anisotropic physical properties such as the refractive indices and electric permittivities can be diagonalised to give principal values parallel ( $\hat{\mathbf{n}}_{||}$ ) and perpendicular ( $\hat{\mathbf{n}}_{\perp}$ ) to the director, [25]. Most commercially available devices use reorientation of the director induced by an applied electric field  $\mathbf{E}$  coupling to the dielectric tensor  $\boldsymbol{\varepsilon}$ , to reduce the electro-static free energy  $G_E$ , given by:

$$G_E = -\frac{1}{2}\mathbf{D}\cdot\mathbf{E} = -\frac{1}{2}\varepsilon_0(\mathbf{E}\cdot\boldsymbol{\varepsilon}\cdot\mathbf{E}) = -\frac{1}{2}\varepsilon_0\Delta\varepsilon(\mathbf{n}\cdot\mathbf{E})^2 \quad (3)$$

where the dielectric anisotropy  $\Delta\varepsilon$  is the difference of the principal components  $\varepsilon_{||} - \varepsilon_{\perp}$ . Equation (3) predicts that the director tends to reorient parallel to the applied field if the material has a positive  $\Delta\varepsilon$ , and perpendicular to the field if  $\Delta\varepsilon$  is negative. Similarly, many devices rely on changes of optical retardation from the material birefringence  $\Delta n$  ( $= n_{||} - n_{\perp} = n_e - n_o$ ), where  $e$  and  $o$  refer to the extra-ordinary and ordinary rays respectively) to give the perceived optical modulation. For example, if viewed between crossed polarisers, a device will appear isotropic, and therefore black, when viewed along the optic axis (parallel to  $n_e$ ) and will exhibit some white light transmission when viewed in a direction at an angle to the optic axis due to the effect of the optical retardation.

The physical parameters depend on both chemical structure and temperature. Anisotropic properties, such as  $\Delta n$  and  $\Delta\varepsilon$  are also related to the order parameter  $S$ , whereas the fluid properties, such as density, bulk viscosity and the mean refractive indices and permittivities, are primarily related to absolute temperature. The uniaxial refractive indices are given by [25]:

$$n_o^2 = 1 + \frac{\rho N_A h F}{M \cdot \varepsilon_0} \left\{ \bar{\alpha} - \frac{1}{3} \Delta\alpha S \right\} \quad (4)$$

$$n_e^2 = 1 + \frac{\rho N_A h F}{M \cdot \varepsilon_0} \left\{ \bar{\alpha} + \frac{2}{3} \Delta\alpha S \right\}$$

where  $\rho$  is the density,  $N_A$  Avogadro number,  $M$  the molecular weight,  $\bar{\alpha}$  is the mean molecular polarisability, and  $\Delta\alpha$  is the difference between the molecular polarisability parallel to the long  $\alpha_l$  and short  $\alpha_t$  axes. The cavity field factor  $h$ , and the Onsager reaction field  $F$  relate to the internal field experienced by an average molecule, approximated for a spherical cavity by:

$$h = \frac{3\bar{\varepsilon}}{2\bar{\varepsilon}+1} \approx 1 \quad ; \quad F = \left\{ \frac{1}{1 - \frac{2\rho N_A \bar{\alpha} (\bar{\varepsilon}-1)}{3 M \cdot \varepsilon_0 (2\bar{\varepsilon}+1)}} \right\} \approx 1 \quad (5)$$

where mean anisotropic properties are expressed using a bar above the symbol, such as for the mean polarisability on the molecular scale:

$$\bar{\alpha} = \frac{1}{3}(2\alpha_t + \alpha_l) \quad , \quad (6)$$

and permittivity and refractive index on the macroscopic scale:

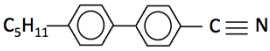
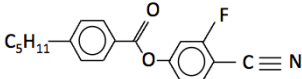
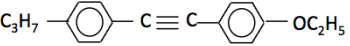
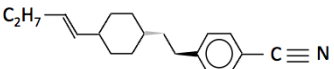
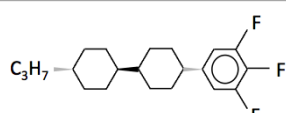
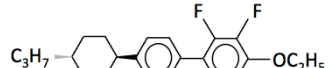
$$\bar{\varepsilon} = \frac{1}{3}(2\varepsilon_{\perp} + \varepsilon_{||}) \quad ; \quad \bar{n} = \frac{1}{3}(2n_o + n_e) \quad (7)$$

The birefringence is given by:

$$\Delta n = \frac{\rho N_A h F}{M \cdot \varepsilon_0} \left\{ \frac{\Delta\alpha}{3\bar{n} - n_o} \right\} S \quad , \quad (8)$$

and is largely dictated by the polarisability anisotropy  $\Delta\alpha$  of the constituent molecules. The density  $\rho$  is usually close to that of water at 20°C, with a selection of nematic compounds  $\rho = 990 \pm 50 \text{ kgm}^{-3}$  [26], and with a near linear temperature dependence through the

Table 1: Typical Nematic Liquid Crystal Compounds and their physical properties.

#	Compound structure	use	$T_{NI}$ ; mpt / °C	$\Delta n$	$\Delta \epsilon$	$K_{11}$ ; $K_{22}$ ; $K_{33}$ /pN	$\gamma_1$ / Pa.s
1		TN	35 23	0.237	+21.6	7.4 4.3 10.4	0.112
2		TN	(24) 70	0.182	+50.2	$k_{33} / k_{11}$ = 1.78	0.270
3		STN	95 88	0.300	+2.3	$k_{33} / k_{11}$ = 1.38	0.054
4		STN	74 68	0.17	+22.5	11.2 6.6 24.3	0.170
5		TFT	94 65	0.073	+8.3	9 7 17	0.025
6		VA	145 67	0.156	-5.9		0.217

LC phases that is typically  $-1\text{kgm}^{-3}\text{K}^{-1}$ . Thus, the temperature dependence of the birefringence is dominated by the order parameter  $S$ . A calamitic liquid crystal has a positive birefringence because  $\Delta\alpha$  is positive for the cylindrical molecular core structures. If the rigid core is short and comprises weakly polarisable saturated moieties such as cyclohexanes, the birefringence will be low. It will be higher for longer, unsaturated groups such as phenyls and ethynes, reaching  $\Delta n \approx 0.4$ , but more typically being maximum at  $\Delta n \approx 0.26$  for light stable compounds.

Similarly, the uniaxial electric permittivities are given by [25]:

$$\epsilon_{\perp} = n_o^2 + \frac{\rho N_A h F^2}{3M \cdot \epsilon_0 k T} \mu^2 \left\{ 1 + \frac{1}{2} (1 - 3 \cos^2 \beta) S \right\} \quad (9)$$

$$\epsilon_{\parallel} = n_e^2 + \frac{\rho N_A h F^2}{3M \cdot \epsilon_0 k T} \mu^2 \{ 1 - (1 - 3 \cos^2 \beta) S \}$$

where  $\beta$  is the angle between the molecular dipole  $\mu$  and the long molecular axis. The dielectric anisotropy is:

$$\Delta \epsilon = n_e^2 - n_o^2 - \frac{\rho N_A h F^2}{6M \cdot \epsilon_0 k T} (1 - 3 \cos^2 \beta) \mu^2 S \quad (10)$$

and

$$\bar{\epsilon} = 1 + \frac{\rho N_A h F}{M \epsilon_0} \left( \bar{\alpha} + \frac{\mu^2}{3kT} \right) \quad (11)$$

There is more freedom for controlling the dielectric anisotropy than for birefringence by placement of strong dipole moments onto the core structure. Strongly positive materials result from polar moieties such as cyano- terminal groups, or 3,4,5 substitution of fluoro- groups onto a terminal phenyl group. Such placement ensures that  $\beta$  is kept low, with  $\Delta\epsilon \approx +50$  being readily achievable. It is harder to make strongly negative materials for a number of reasons. Firstly, the  $n_e^2 - n_o^2$  term of equation (10) is always positive and leads to  $\Delta\epsilon \approx +2$  even if there is a negligible dipole moment. Equation (10) predicts that transverse dipoles, where  $\beta \approx 90^\circ$ , are only half as efficient at contributing to a negative  $\Delta\epsilon$ , due to the cylindrical symmetry. Moreover, bulky polar side groups detract from the rod-like shape of the molecule that leads to liquid crystallinity. Nevertheless, mixtures with  $\Delta\epsilon \approx -6$  have been achieved for modern LCD TV applications. Note, equation (10) also predicts that a dipole moment at  $\beta = 48.2^\circ$  contributes equally to  $\epsilon_{\parallel}$  and  $\epsilon_{\perp}$ ; even a large dipole moment oriented at  $\beta \approx 52^\circ$  gives  $\Delta\epsilon \approx 0$ .

Implicit in the definition of liquid crystal behaviour is the concept of orientational elasticity and the energetic cost associated with deforming the director field. Whereas, a crystal solid has elasticity associated with the positional translation of the constituent molecules, the liquid crystal has elasticity associated with changing director orientation. The curvature strain tensors of phases with cylindrical symmetry contain terms in splay, twist and bend deformations, [27] as shown in figure 2a). The elasticity of the chiral nematic is equivalent to that of the achiral nematic, but includes  $2\pi/P$  subtracted from the twist term to represent the spontaneous twist of director. The elastic bulk free-energy density for nematics and cholesterics  $G_K$  is given by:

$$G_K = \frac{1}{2} \iiint \left[ k_{11} (\nabla \cdot \mathbf{n})^2 + k_{22} \left( \mathbf{n} \cdot \nabla \times \mathbf{n} - \frac{2\pi}{P} \right)^2 + k_{33} (\mathbf{n} \times \nabla \times \mathbf{n})^2 \right], \quad (12)$$

where  $P = \infty$  for the usual achiral nematic case, and  $k_{ii}$  ( $i = 1, 2, 3$ ) are the splay, twist and bend elastic constants, respectively.

The elastic constants are important to the display engineer because they dictate the amount of deformation induced by the applied electric field. Both splay and bend elastic constants contribute to distortions in the plane of the director and deforming torque, whereas twist occurs where the distortion is perpendicular to the director and torque. There have been extensive studies of the relationship between molecular structure and the elastic constants, because of this important role they play in the operation of liquid crystal displays. To a first approximation, the temperature dependence of the elastic constants follows  $S^2$ , a relationship that holds well for  $k_{11}$  and  $k_{22}$ , where the ratio  $k_{22}/k_{11}$  is relatively insensitive to temperature and chemical structure with  $0.5 \leq k_{22}/k_{11} \leq 0.8$ , and usually  $k_{22}/k_{11} \approx 0.5$ . The behaviour of the bend elastic constant  $k_{33}$  is more complex [28], with  $k_{33}/k_{11}$  being both temperature dependent and showing a strong dependence on structure, with values ranging from:  $1.0 \leq k_{33}/k_{11} \leq 2.2$ . Approximating the constituent molecules of the liquid crystal to rigid, hard rods of length  $L$  and diameter  $W$  leads to the approximate relationship:

$$k_{33}/k_{11} \sim L^2 / W^2 \quad (13)$$

which provides a useful rule of thumb for the LC mixture designer. However, there is a strong influence on this elastic ratio from short-range local ordering in the nematic phase, due to intermolecular dipole correlations or local smectic ordering. For example, smectic local ordering of positive  $\Delta\epsilon$  materials leads to a higher  $k_{33}/k_{11}$ .

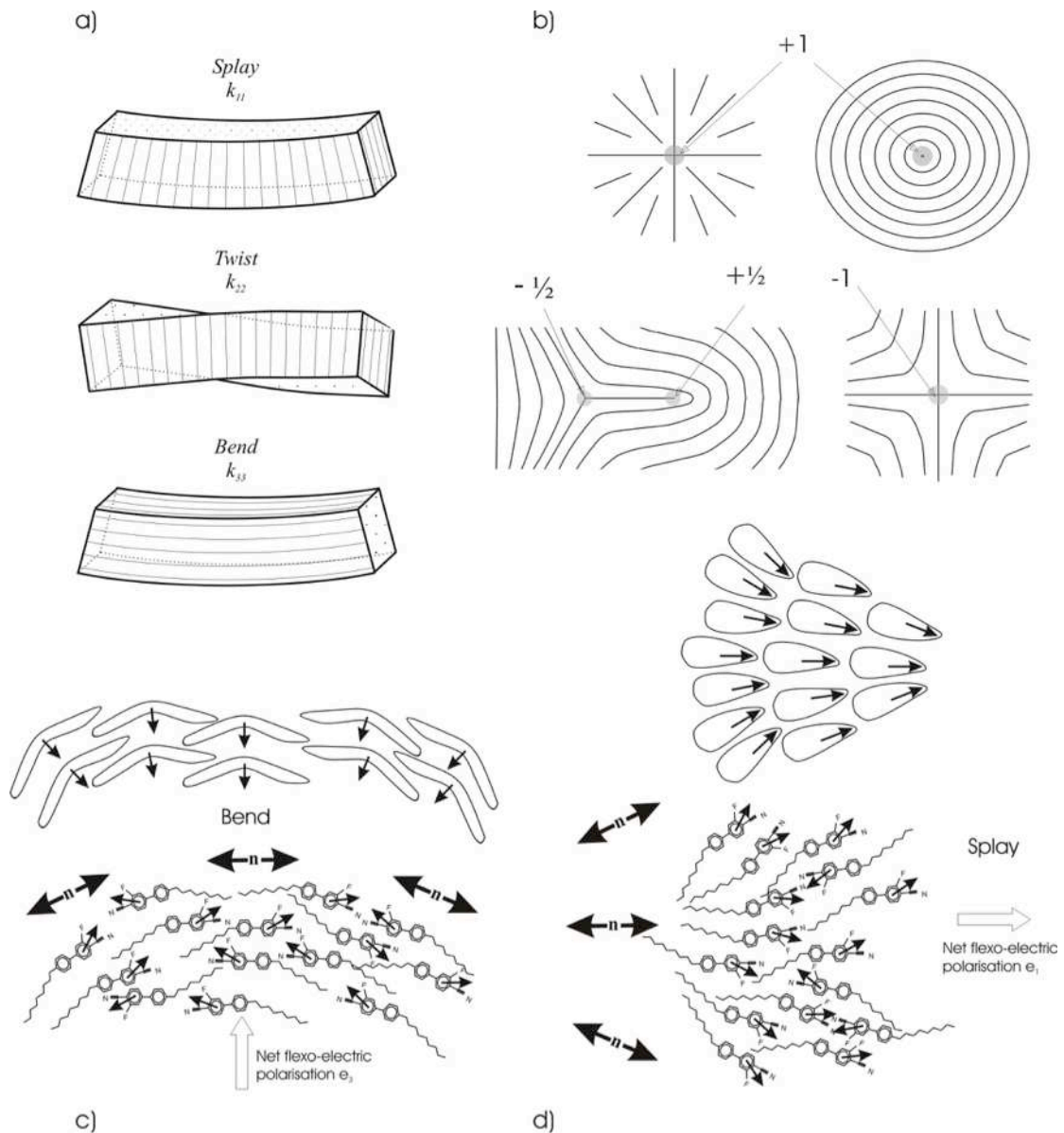


Figure 2. Nematic elasticity and disclinations: a) Splay, Twist and Bend deformations; b) Line disclinations of strength  $+1$ ,  $+1/2$ ,  $-1/2$  and  $-1$ . In each case the disclination continues normal to the page, and the director remains invariant in this direction (cylindrical symmetry). The defect core is indicated in grey; c) flexoelectric behaviour from banana-like molecules in a bend deformation; and, d) flexoelectric behaviour from wedge-like molecules in a splay deformation.

Liquid-like fluidity of a liquid crystal is dictated by the viscosity, which determines the switching speed of LCDs. How quickly the director reorients with respect to a deforming torque is determined by the ratio of the viscosity and the elastic constants. However, even for the simplest nematic

case, there are five viscosity coefficients [29], describing flow of the director in directions parallel and perpendicular to the director and shear force directions. The effect of fluid flow can play an important part in device behaviour, such as the optical bounce that occurs in twisted-nematic displays due to

backflow [30]. Full understanding of these effects requires numerical modelling [31]. For simplicity, back-flow is often ignored, and the time dependence of director reorientation without coupling to mass flow is represented by the single twist viscosity  $\gamma_1$ . Viscosity has a strong temperature dependence related to the change in order as well as the Arrhenius dependence common to liquids [32]:

$$\gamma_1 = (a_1 S + a_2 S^2) e^{\frac{U}{kT}} \quad (14)$$

with  $a_1$  and  $a_2$  are material dependent constants,  $U$  is the activation energy for molecular movement,  $k$  is the Boltzmann constant and  $T$  is the absolute temperature. Most commercial liquid crystal mixtures are based on aromatic systems, where  $a_1 \gg a_2$  for compounds with low birefringence,  $a_2 \gg a_1$  for highly birefringent compounds, and  $a_1 \approx a_2 \approx 10^{-14} \text{ s.m}^{-2}$  and  $U \approx 0.3 \text{ eV}$  for  $\Delta n \approx 0.18$ . At low temperatures, the viscosity often deviates from this Arrhenius type of behaviour as it diverges towards a low temperature glass transition. The standard Vogel-Fulcher-Tammann equation has been applied successfully to a range of nematic compounds [26]:

$$\log \gamma_1 = A + \frac{B}{T - T_0} \quad (15)$$

where  $A$  and  $B$  are material dependent constants, and  $T_0$  is a temperature that is typically about  $20^\circ\text{C}$  below the liquid crystal glass transition.

Continuum descriptions of the director field are not always satisfactory, since the director field often also includes topological discontinuities, called defects or disclinations [27]. Indeed, it was the thread-like appearance of nematic samples containing such defects that originally led to the naming of the phase, from the Greek for thread (*nematos*). Both point defects and line defects are common; examples of nematic line disclinations with different strengths are shown in figure 2b). At each discontinuity in the director field, there is local melting of the phase and the liquid crystal order is zero at the disclination core,

which is typically of the order of 10nm in diameter. For the nematic phase, disclinations of strengths  $+1$ ,  $-1$ ,  $+\frac{1}{2}$  and  $-\frac{1}{2}$  are common, with  $+\frac{1}{2}$  and  $-\frac{1}{2}$  appearing as pairs and usually form defect loops, or may terminate at interfaces such as the containing substrates of a device. Avoiding defects is a key part of the design of most liquid crystal displays, although recently there has been an resurgence of interest in the potential applications for liquid crystal devices with controllable formation of topological defects, such as the zenithal bistable display described in section 5.3.

The constituent molecules for the liquid crystal do not exhibit perfect cylindrical symmetry but have more complex shapes. For example, they may not have a two-fold rotational symmetry about either their short or long axes, leading to “wedged” or “banana” molecular shapes, respectively. Normally, the nematic includes all possible orientations of the molecules that maintain the symmetry of the phase. However, with bend and splay deformations, the distribution of asymmetric molecules is shifted slightly as the molecules pack. For example, banana-like molecules will tend to orient so that molecular curvature follows that of the director field, figure 2c). Similarly, the apex of wedge-like molecules points into the splay, figure 2d). In either case, any molecular dipole will then contribute to a macroscopic polarisation [33] and flexo-electric terms are required in the free energy. The degree of polarisation for splay and bend deformations is represented by the flexoelectric coefficients  $e_1$  and  $e_3$  respectively, which are dependent on the material shape, dipole moments and density.

### 2.3 Formulating Liquid Crystal Mixtures

Table 1 includes some of the important display-related physical properties for a number of common nematic compounds, including temperatures for the nematic to isotropic transition  $T_{NI}$ , as well as the room temperature values for the optical, electrical, elastic and viscous properties. Each of these compounds is stable at operating temperatures and when exposed to light, allowing device lifetimes of scores of years to be achieved. As shall be shown

through the following sections, the properties of each of the compounds might be suited to different display technologies. For example, devices using optical scattering effects require a high birefringence to become strongly scattering whereas polarised light displays using the retardation effect of the liquid crystal, often require a lower birefringence to enable higher device spacing (and hence higher yields). Modes such as the supertwist nematic require  $k_{33}/k_{11}$  to be high, whereas the simpler twisted nematic display requires  $k_{33}/k_{11}$  to be kept low. Such requirements are rarely isolated, being combined with a range of target physical properties, such as appropriate temperature range of the required liquid crystal phase, low viscosity, to more complex needs, such as low temperature dependence of elastic constant ratios, etc. This necessitates mixtures to be used, frequently involving scores of components.

Properties such as the birefringence  $\Delta n$ , the isotropic to nematic transition temperature  $T_{NI}$ , and splay elastic constant  $k_{11}$  depend roughly linearly with concentration. The dielectric anisotropy  $\Delta\epsilon$ , and twist and bend elastic constants  $k_{33}$  and  $k_{22}$  are slightly more complex, because of the effects of dipole correlations and smectic ordering. For example, the epoch-making compound pentyl-cyano-biphenyl (5CB, compound 1 in Table 1) has a measured  $\Delta\epsilon$  of about 15 close to room temperature can be treated as  $\Delta\epsilon$  of about 24 when adding into mixtures. This is because the anti-parallel dipole correlations of the pure compound that effectively reduce the parallel dipole moment are disrupted in a multi-component mixture. Care still has to be taken when formulating mixtures, since the breaking of the dipole correlations can lead to the unmasking of smectic behavior: it is quite common for a mixture of polar and apolar nematic compounds to exhibit an unwanted smectic phase despite neither component having smectic behaviour. Such a phase is called an “injected” smectic and arises because the dipole correlations of the polar compound were preventing the formation of the smectic layers.

Ignoring the order parameter related terms in equation (14) and considering the viscosity to follow

the Arrhenius behaviour of conventional liquids then the viscosity of an  $n$  component mixture is given by:

$$\log(\gamma_1) = \sum_i^n C_i \cdot \log(\gamma_1)_i \quad (16)$$

where  $i = 1, 2, 3, \dots, n$ , and  $C_i$  is the concentration of component  $i$  such that  $\sum_i^n C_i = 1$ . This logarithmic concentration dependence means that highly viscous additives can be used at low concentration without increasing the mixture viscosity significantly. For example, it is common practice to increase the clearing point through the addition of three or four ringed compound where the linear increase in  $T_{NI}$  is accompanied with a disproportionately small viscosity increase.

None of the compounds in Table 1 show a room temperature liquid crystal phase, rather freezing to a crystal form. The liquid crystal phases usually supercool below the melting point, because of the strong first order nature of crystallisation; this is particularly true in a thin container such as an LCD, where crystallisation is suppressed by the surfaces. However, LCDs require operation typically between  $-20^\circ\text{C}$  to  $+70^\circ\text{C}$ , and to be stored for months down to  $-40^\circ\text{C}$ . Such temperature ranges require the formation of eutectic mixtures to suppress melting, at concentrations approximated by the Schroeder-Van Laar equation:

$$\ln(C_i) = -\frac{\Delta H_i}{R} \left( \frac{1}{T} - \frac{1}{T_i} \right) \quad (17)$$

where  $R$  is the Rydberg constant,  $C_i$ ,  $\Delta H_i$  and  $T_i$  are the molar concentration, enthalpy of freezing and melting point of the  $i$ th component, respectively. This provides a guide for the material scientist to calculate the eutectic composition, given that, at the eutectic temperature, the concentrations sum to 100%. In practice, more thorough empirical methods [34] are required to formulate commercial mixtures. Table 2 includes the composition of three typical positive  $\Delta\epsilon$  eutectic mixtures, E7, ZLI2293 and ZLI 4792 together with their important physical properties.

Table 2 Physical properties of selected nematic LCD mixtures. Data collected from references [35 - 37].

Mixture	E7	ZLI 1132	ZLI - 4792
Typical Use	Passive Matrix TN		Active Matrix TN
Composition			
Nematic Temperature range (°C)	S < -30 N 58 I	S < -6 N 71 I	S < -40 N 92 I
$\Delta n$ ; $n_o$ (589nm, 20°C)	0.2253 ; 1.5211	0.1396 ; 1.4830	0.0969 ; 1.4794
$\Delta\epsilon$ ; $\epsilon_1$ (1kHz, 20°C)	13.8 ; 5.2	13.1 ; 4.6	5.2 ; 3.1
$k_{11}$ ; $k_{22}$ ; $k_{33}$ (pN, 20°C)	11.7 ; 8.8 ; 19.5	1.95	13.2 ; 6.5 ; 18.3
Dynamic bulk viscosity $\eta$ (cP, 20°C)	465	200	150
Twist viscosity $\gamma_1$ (mPa.s, 20°C)	180	250	109
Flexo-electric coefficients $e_1 + e_3$ ; $e_1 - e_3$ (pCcm <sup>-2</sup> , 20°C)	+15 ; 12.2		10  ; -15

## 2.4 Functional Liquid Crystal compounds

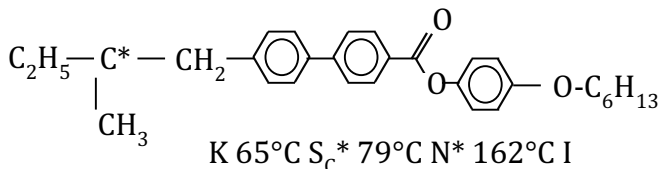
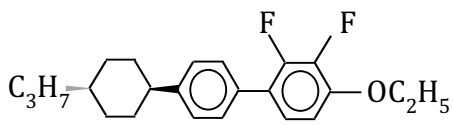
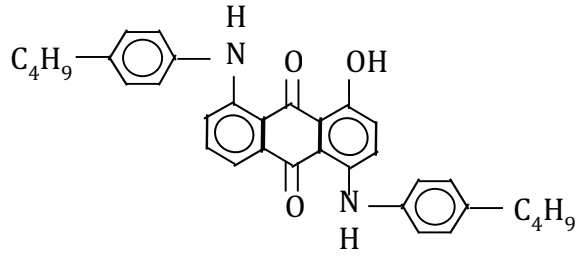
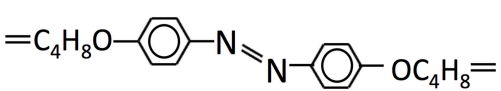
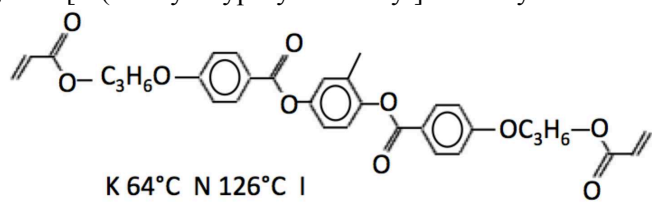
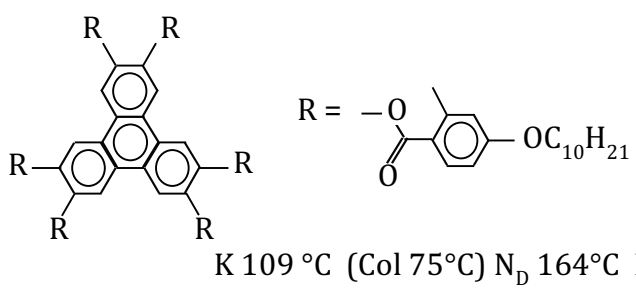
As shall be shown, it is not just the nematic phase that is used for LCDs. A variety of mesogenic compounds have been used to impart some new functionality to the system. Table 3 lists examples of mesogenic

compounds, which are used for important display-related purposes, as summarised below.

1. The inclusion of one or more chiral centres (denoted \*) in the flexible end chain of a mesogen imparts a tendency for spontaneous twist of the director. The material may exhibit inherent cholesteric (N\*) or chiral SmC\*

- phases (such as CE3 in Table 3) or may induce chirality through doping into a nematic or SmC host material. The important characteristic of the chiral compound as a dopant is its helical twisting power and handedness. These are related to molecular structure through various empirical rules, such as those of reference [38].
2. Smectic phases occur with longer terminal chain groups on the mesogenic core. The formation of tilted phases, such as the SmC occurs with suitable placement of transverse dipole moments, though precise control of phase transition temperatures and sequences remains somewhat an art for the chemist [e.g., reference 39].
  3. Pleochroic and fluorescent dyes can be added to liquid crystals to give appropriate optical functionality. Pleochroic dyes such as the anthraquinone shown in table 3 have reasonably good miscibility in the cyano-biphenyls, leading to anisotropic absorption that is much greater parallel to the director, than perpendicular to it [40]. This is used in Guest-Host displays, where the polariser is replaced by the constituent dye mixed into the liquid crystal, allowing switching of the appropriate wave bands between absorbing and transmitting states. Performance is dictated by the combined order parameter of the system and the direction of the dye transition moment with respect to the liquid crystal director.
  4. Including a central azo- moiety into the core of a mesogen allows photo-induced realignment of the director due to anisotropic absorption of the dye. Irradiating the molecule with polarised light causes reorientation of the dye molecule to the direction normal to the polarisation, usually via transition between the trans- and- cis isomers. This may be used to effect photo-reorientation of the nematic director, either reversibly [41], or irreversibly by combining the azo-mesogen into polymerisable groups [42].
  5. Reactive mesogens have become a major tool for the displays field [43]. These compounds exhibit conventional liquid crystal behaviour, either individually or when used in mixtures. The inclusion of a photo-reactive group in one or both of the terminal end-chains allows the material to be polymerised by exposure to UV light. Hence, the reactive mesogen may be aligned appropriately (through interaction with the surface, electric fields or polarised light) and that liquid crystal structure stabilised by polymerising the reactive mesogen. The solubility of the reactive mesogens is high and so a variety of systems are possible, from linear elastomers, to polymer stabilised networks and gels, and liquid crystal polymers. The photo-reactive groups are often acrylates, and so may also be used in conjunction with standard acrylate cross-linkers and photo-initiators. Reactive mesogens have been used widely, from creating patterned optical retarders, functional alignment layers, to creating templates for extending the temperature range of narrow liquid crystal phases.
  6. Discotic liquid crystals have a symmetry axis that is parallel to the short molecular axis [44]. This leads to distinctive physical properties, such as negative birefringence, one-dimensional conductivity and semiconductivity, and the formation of columnar rather than smectic phases. Many of the other anisotropic physical properties, such as the order parameter, permittivities and elastic constants are similar to those of their calamitic (i.e. rod -like) counterparts. A particularly important application for LCDs is the use of polymerisable discotic liquid crystals to form optical compensation plates.

Table 3 Examples of Functional Mesogenic Compounds

#	Compound	Use	Key properties
1	(+)-4-n-Hexyloxyphenyl- 4-(2-methylbutyl)biphenyl-4'-carboxylate (CE3)  $K\ 65^{\circ}C\ S_C^* 79^{\circ}C\ N^* 162^{\circ}C\ I$	N* ; Chiral Dopant; Ferroelectric compound	Helical twisting power; Induced Ferroelectric polarisation.
2	2,3-difluoro-1-ethoxy-4-[ <i>trans</i> -4-propyl cyclohexyl] biphenyl 	VAN S <sub>C</sub> ; FLC Host	Low $\gamma_1$ High $\partial\epsilon$ N phase; Wide S <sub>C</sub>
3	Example Anthraquinone dye 	Pleochroic Dye	High Order Parameter; High dichroism; High miscibility
4	1,2-Bis(4-hex-5-enyloxyphenyl)diazene 	Optically induced reorientation	Solubility; S; Absorption efficiency
5	RM257: 1,4-Bis[4-(3-acryloxypropyl benzoxy)]-2-methylbenzene.  $K\ 64^{\circ}C\ N\ 126^{\circ}C\ I$	Bifunctional Reactive Mesogen	Solubility; Photo-reactivity
6	DB126: triphenylene hexa-(2-methyl-4-n-decyloxy)benzoate  $R = -O-C6H4-CH3-CO-$ $K\ 109^{\circ}C\ (Col\ 75^{\circ}C)\ N_D\ 164^{\circ}C\ I$	Discotic Nematic. Acrylate version used for optical compensator films	Negative $\Delta n$

### 3 Basics of Liquid Crystal Devices

#### 3.1 Basic Display Construction

Much of the basic scientific understanding of liquid crystals was available in the first half of the twentieth century. Mauguin [45] had found that, contrary to the optical rotation caused by a quarter-wave plate, polarised white light could be guided by a liquid crystal with a twisted structure, allowing light to be transmitted between crossed polarisers by samples with a twist of  $90^\circ$ . Fréedericksz had shown field induced switching and the existence of a critical threshold for magnetic [46] and electric [47] fields applied to a uniform sample. Châtelain [48] achieved uniform alignment of the liquid crystal director using thinly spaced samples and rubbing to define the orientation. Such scientific advances prompted the first liquid crystal device to be patented by the Marconi Wireless Company in the UK in 1936 [49]. However, the first LCD commercialisation had to wait until the early 1970s, and the availability of various other components, many of which were invented and developed independently for other applications. These associated technologies include:

- **Glass.** Typically 0.7mm thick, polished glass is remarkably optically uniform ( $n = 1.520 \pm 0.005$ ), transparent (91% transmission from 320nm to 700nm) and flat ( $\pm 0.1 \mu\text{m}$ ). Together with its excellent mechanical, thermal and economic properties it is hard to imagine a better substrate material. Today's 40" TV displays are made on \$2B production lines that handle Generation 10 glass (2850mm x 3050mm), though most small displays are still made using Generation 4 production lines (550mm x 650mm). Two types are common: soda-lime glass for low cost displays and boro-silicate glass for high-end TFT (thin-film-transistor) displays. The latter has a low alkali ion content and so adds far fewer ionic impurities to the contacting LC that would otherwise prevent the TFT maintaining its charge across the pixel. Recently, ion-implanted reinforced glass and

ultra-thin ( $<100\mu\text{m}$ ) glass have been used for high-end displays, particularly for use in portable display applications and curved screen HDTV.

- **Indium Tin Oxide.** Following the initial work done in the mid 1960s at Philips [50, 51], and in the Far East at the Japanese Government Research Institute [52], ITO has become the dominant transparent conductor for the display industry, as well as for many other applications. The layer is sputtered onto the glass surface at between 50nm to 200nm, depending on the display requirements. The thin layer causes loss of light through interference and reflection, but these thicknesses usually lead to about 88% and 85% transmissivity of the glass overall, and correspond to sheet resistances of  $80 \Omega/\square$  and  $15 \Omega/\square$  respectively. It is important to understand how sheet resistance works: a square of ITO gives a resistance of  $15 \Omega$  regardless of its area. Calculation of the resistance of any electrode requires the number of squares to be multiplied by the sheet resistance. So, for example, the resistance of a display electrode that is 10cm long and  $200 \mu\text{m}$  wide is typically about  $15 \Omega/\square \times L/W = 7.5 \text{k}\Omega$ .
- **CMOS circuitry.** Complimentary Metal-Oxide-Semiconductor integrated circuits were invented by Wanlass at Fairchild in 1963 [53], whereby p-type and n-type transistors are used in parallel to provide low power logic circuitry (and hence suitable for use with battery operated equipment) and logic output voltages of between 3.5 and 5V, which could be used directly to address the liquid crystal. The first LCD product was launched by *Sharp* in April 1973: the EL-805 electronic calculator. The CMOS provided both the logic for the calculator operation and the driving circuitry for the dynamic scattering mode LCD. This was followed in October 1973 by the 06LC

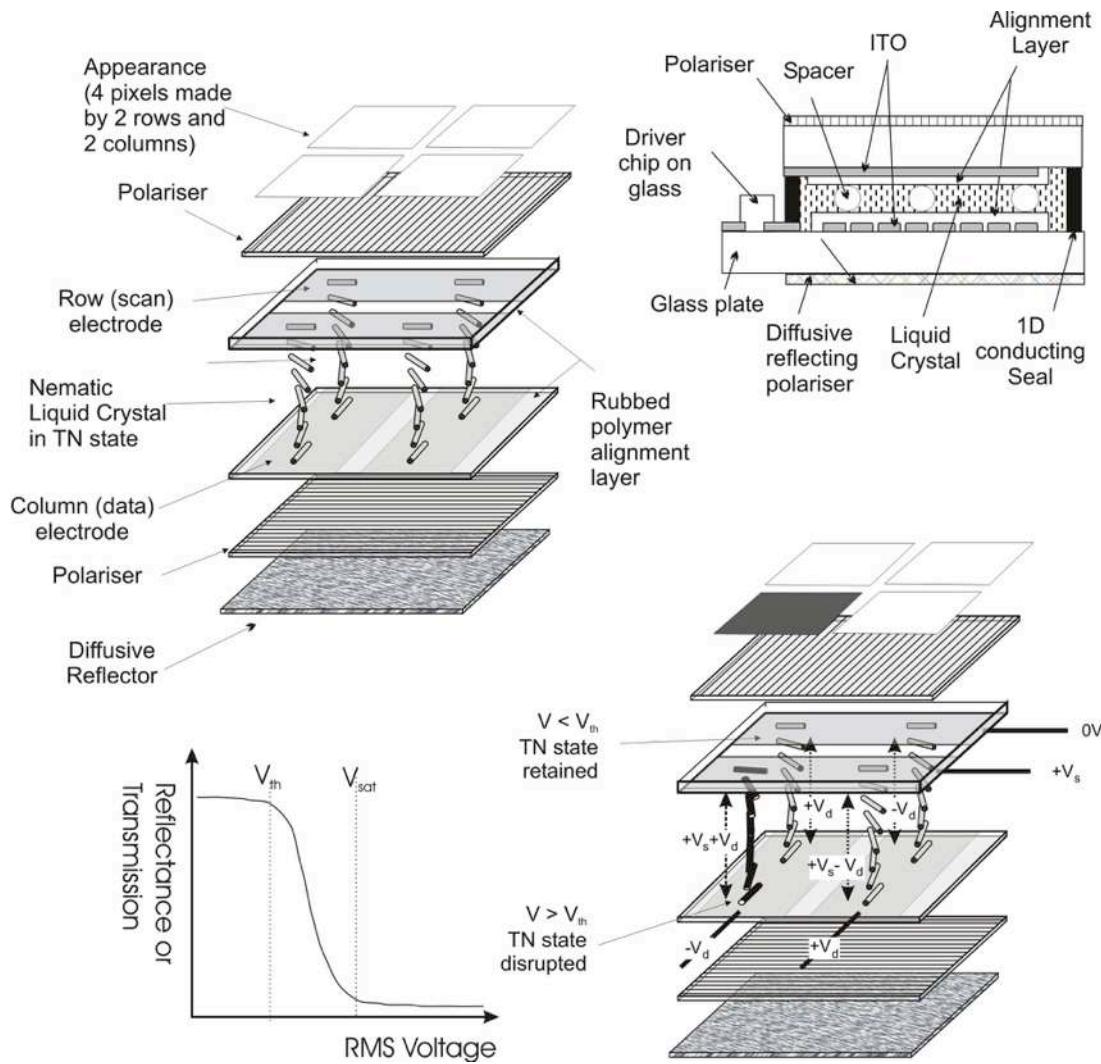


Figure 3. Construction and operation of a twisted nematic LCD: a) Schematic diagram of a 4 pixel TN in the off-state; b) cross section of a modern chip-on glass LCD; c) Typical electro-optic response for a monostable LCD, such as the TN; d) Schematic diagram of the 4 pixel TN with voltage  $V_s$  applied to one row, and data  $\pm V_d$  applied to the columns, such that one pixel (bottom left) is switched dark.

digital watch from Seiko, which used a twisted nematic LCD.

- **Polarising film.** Although prism and wire-grid polarisers were established technologies, Land's invention of iodine doped stretched polymer film polarisers in 1929 [54] and the subsequent use of polymerised dichroic nematics by Dreyer in 1946 [55] enabled low cost flat-panel displays to operate by

controlling the polarisation state. Today's polarisers use aligned silver nano-particles, and comprise protective films, adhesives, release liners and other filters required for different display purposes [56].

- **The thin-film transistor** [57] was invented at RCA by Paul Weimar in the early 1960s. The original demonstration used Tellurium as the semiconductor but other materials researched

at that time included Silicon, Germanium, Cadmium Selenide and Cadmium Sulphide. Most displays today use either amorphous or poly-crystalline silicon.

There are various different types of liquid crystal display but many of the design principles and modes of operation are common throughout. Consider the common twisted nematic LCD [14] shown in figure 3. The display is formed from two containing plates, the front one at least being transparent, and coated with transparent conducting electrodes, such as indium tin oxide (ITO). The plates are spaced a few microns apart by glass beads, adhered together and the laminate filled with the liquid crystal material and sealed. The most common substrates in use are 0.5mm or 0.7mm glass, though optically isotropic plastic substrates may also be used for low weight and flexibility. Reflecting metal foil layer has been used as the rear-substrate where flexibility and high temperature thermal processes are required for a reflective display. The ITO is etched to form the appropriate electrode pattern. This is often a series of rows and column electrodes on the opposing internal faces of the device. In such an arrangement, the electrodes form a parallel plate capacitor, wherein the individual pixels are formed in the regions of overlap of the rows and columns. Of course, other designs are possible, such as polar co-ordinates (formed from axial and radial electrodes), alphanumeric characters and icons, or inter-digitated electrodes on one of the substrates to provide an in-plane electric field. The most sophisticated displays, used from mobile phones to HDTV use a thin-film transistor (TFT) on one of the plates, addressed using copper bus lines to provide the signals to a pixel electrode. In these instances, the opposite plate is a single electrode, held at earth.

Creating an electro-optic effect requires some optical property, such as the reflectance or transmittance for a backlit display, to be changed with an applied field. Today's commercial LCDs almost exclusively use re-orientation of the director from some initial pre-aligned state, dictated by alignment layers on the inner surfaces of the display. Various alignment layers are possible, but most devices use a

polymer coating to impart either homeotropic (i.e. normal to the surface), planar homogeneous or tilted homogeneous alignment of the director, figure 4. For example, the twisted nematic device includes polyimide coatings rubbed in a direction to impart a homogeneous alignment with a surface pre-tilt  $\theta_s$  of typically  $1^\circ$  to  $2^\circ$ , though a supertwist TN would require a somewhat higher pre-tilt of  $2^\circ < \theta_s < 6^\circ$ . For the simple TN, a  $90^\circ$  twist from the top to bottom surfaces is induced in the device by arranging the rubbing directions on the opposing surfaces to be normal to each other. The prevention of tilt and twist disclinations is ensured by including a small helical twisting power to the nematic through the addition of very low quantities of a chiral nematic, and by matching the sign of the helicity to the two pretilts to minimise bend and splay distortion [58]. Ignoring biaxial surface terms, the orientation of the director at each surface is governed by the surface energy  $G_S$ :

$$G_S = \frac{1}{2} \int_S [W_\theta (\mathbf{n} \cdot \mathbf{s} - \theta_s)^2 + W_\beta (\mathbf{n} \cdot \mathbf{r})^2 + W_p (\mathbf{P} \cdot \mathbf{s})^2] dS, \quad (18)$$

where  $\mathbf{s}$  is the surface normal and  $\mathbf{r}$  is the preferred alignment direction in the plane of the surface, figure 4a). Changes to the surface tilt are related to the zenithal anchoring energy,  $W_\theta$ . Typically,  $10^{-7} \leq W_\theta \leq 10^{-3} \text{ Jm}^{-2}$  and  $10^{-9} \leq W_\beta \leq 10^{-5} \text{ Jm}^{-2}$  [59] though for typical commercial devices the anchoring energies are greater than  $10^{-5} \text{ Jm}^{-2}$  and are usually considered as fixed boundaries. The polar surface term  $W_p$  is insignificant for nematics but is important for ferroelectric liquid crystal devices, where there is often a preferred orientation of the spontaneous polarisation with respect to the surface normal.

Each device is constructed in two stages: the back-end process is done under strict clean-room conditions, and the front-end, wherein the devices are filled with liquid crystal and the associated optical layer and driving electronics added and testing is done. The back-end processes are done in a clean room and consist of producing empty laminates each with the potential to form multiple displays. The factory

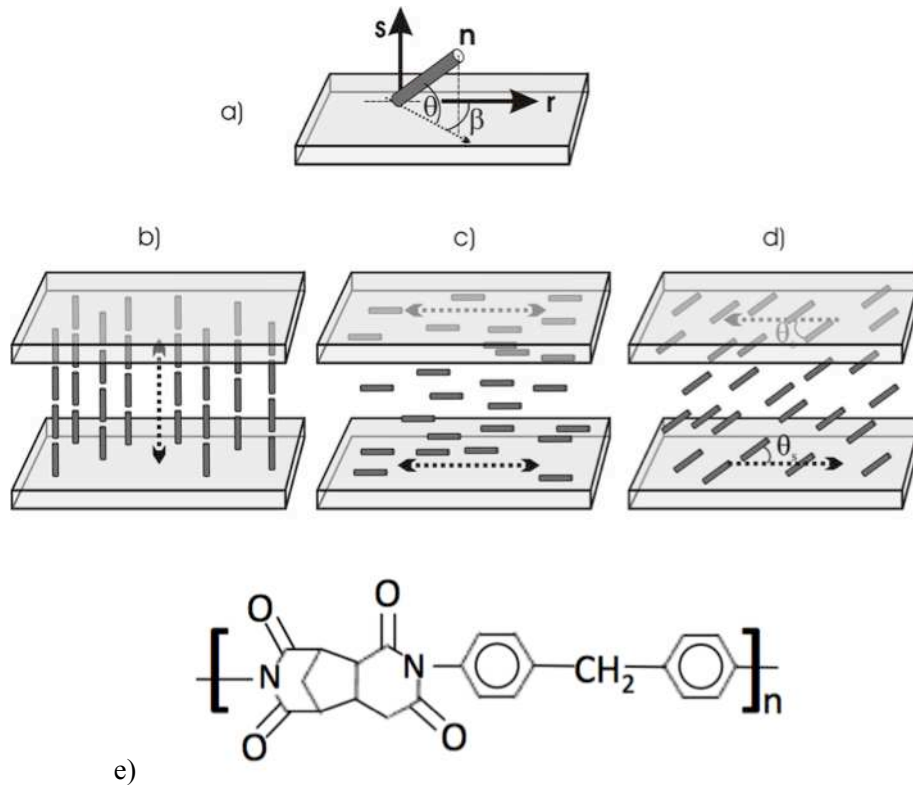


Figure 4. Nematic surface alignment leading to uniform director profile: a) Definition of in-plane azimuthal angle  $\beta$  and out-of-plane zenithal tilt angle  $\theta$ ; b) Homeotropic; c) Planar homogeneous; and, d) Uniform Tilted from anti-parallel surfaces with pre-tilt  $\theta_s$ ; e) Basic structure of the dedicated polyimide AL 1051 from JSR.

equipment dictates the size of the plates used; it is important for high yield and efficiency that the glass is large enough to allow at least six or eight displays to be made on a single laminate. Even 47" diagonal television displays are produced eight per laminate using generation 8 sized glass ( $2,200 \times 2,500$  mm), and large scale associated manufacturing equipment.

The plates are made on a production line preventing the use of many standard laboratory based practices, such as oven baking and spin-coating. Each step occurs within the TAKT time, which is the time that one plate moves from one step to the next; the TAKT time, by definition, must be the same for all of the steps on a given line. Following a brief inspection, the laminate is then sent to the front-end, where it is singulated, filled and the remaining components attached.

The processes for constructing a passive matrix display are shown in figure 5. Many of these processes are common to either passive matrix or TFT driven active matrix devices. Common back end processes include:

1. **Glass Cleaning:** Glass is supplied with the appropriate thickness of ITO deposited onto one side. The plate is washed with de-ionized water, ultra-sound, soaps and sometimes solvents such as IPA (though this is not preferred due to flammability).
2. **Electrode patterning:** This is done using photolithography. A thin layer of positive photoresist is printed onto the substrate, soft baked (to harden) and a mask is placed in contact with the layer. Where exposed to UV, the photoresist is washed-off by developer, but the photoresist remains in contact with

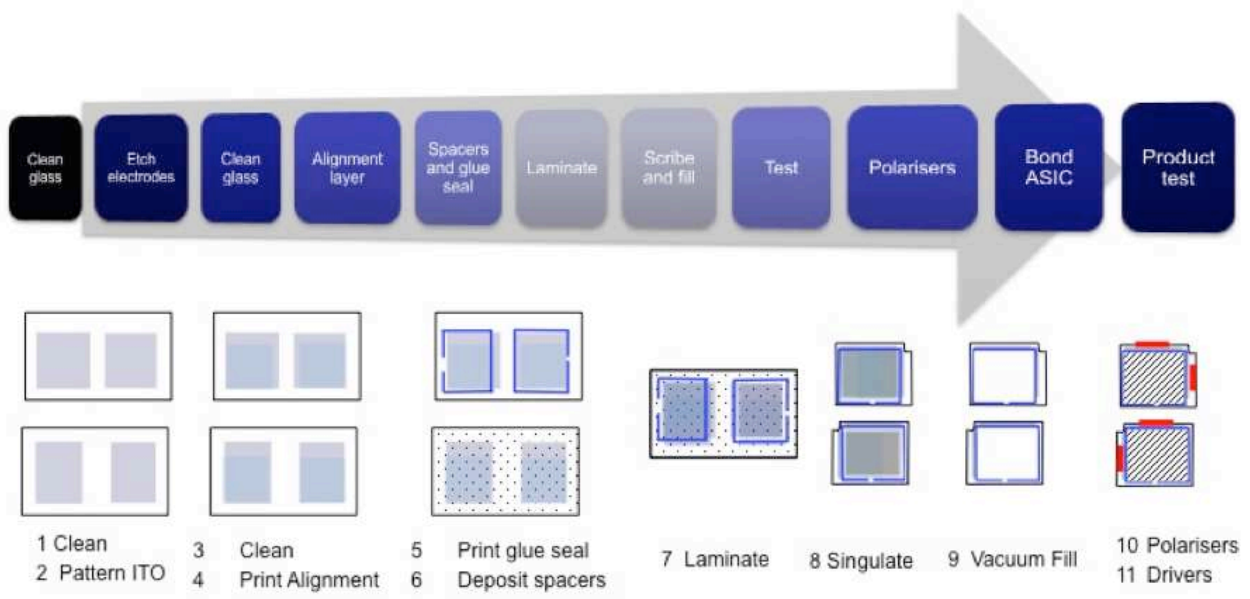


Figure 5 Construction steps for a passive matrix display

the ITO everywhere else. The exposed ITO is then removed by acid and finally the remaining photoresist is stripped from the patterned ITO using an aggressive solvent. It is common for the electrode patterning to be done separately from the standard production process.

3. **Alignment layer.** Following another clean step, the alignment layer is pad-printed onto the patterned glass in the areas that form the viewing area of each display. The alignment layer is patterned to avoid the part of the electrodes where bonding (electrical access) is required, and where the glue-seal will be deposited (to ensure a strong seal). The polyimide is then baked at high temperature (e.g. 180°C) to harden it, and then rubbed using a rayon cloth mounted onto a roller. The resulting pre-tilt is not only dependent on the choice of the alignment polymer, but also on the rubbing strength  $L$ :

$$L = N \cdot l \cdot \left(1 + \frac{2\pi r n}{60v}\right) \quad , \quad (19)$$

where  $N$  is the number of passes of the roller,  $l$  is its contact length (mm),  $n$  is the roller rotation

speed (rpm),  $r$  the roller radius (mm) and  $v$  the speed of the plate (mm.s<sup>-1</sup>). Each of these steps needs to be controlled to minimise display variation.

4. **Spacers.** Polystyrene spheres of the required spacing are either deposited in air or solvent onto one of the glass plates that form the laminate. The density of the spacers depends on the cell gap, but is typically 50 – 100 per mm<sup>2</sup>.
5. **Glue seal.** A thermal epoxy is syringe deposited onto the other substrate to form the boundaries for each individual display. The seal is designed to be as thin as can be reliable, with four edges comprising the sealant but with one edge having a ≈5mm wide hole to allow filling. After deposition, the glue solvent is removed in a soft bake and the plate brought into contact with its opposing, spacer-coated plate. The laminate is then sealed under pressure using a heated press. Usually, the glue seal includes glass rod spacers to ensure the most uniform spacing to the edge of the panel. Often, the glue seal will also include a low density of gold beads, each with a diameter 20% or so higher than the spacers. These gold beads are distorted to near-cylinders under the pressure used

to seal the device. In this fashion, they form multitudinous one-dimensional conductors randomly distributed throughout the sealant, linking the top and bottom substrates. These allow connection from one plate to the other, and thereby allow a single driver to be used to supply the row and column signals. Careful patterning of the ITO electrodes ensures that no unwanted shorts occur, within the alignment tolerance of the plates.

The completed laminate then leaves the high-end clean room for the front-end processes. Common front-end processes are:

6. **Singulation:** Each display is cut from the laminate using a diamond scribe. Each display is cut to give at least one bonding ledge to allow electrical access to the electrodes. The panels are inspected for any non-uniform cell gaps, and tested for shorts.
7. **Filling and sealing:** For small area LCDs, each device is filled in a vacuum chamber, where the cell is initially evacuated, the liquid crystal brought into contact with the sealant's filling hole where it begins to fill by capillary action. Whilst still in contact the vacuum is removed and the air-pressure used to force the liquid crystal into the remainder of the display. Once complete, each display is sealed with a low-ion content UV glue whilst pressure is applied to the cell to ensure that the correct cell gap is obtained on the sealed cell. Large display panels are filled before singulation using a one-drop-fill method [60], which is combined with sealant deposition and vacuum assembly steps. One-drop filling is a major enabling technology that helped LCDs meet the cost requirements for large area applications.
8. **Polarisers:** After cleaning, each cell has polarisers and associated optical films mounted front and back. The films are supplied with an index-matching adhesive to reduce extra reflections from the layers. If a reflective display is required, the rear polariser also comprises a diffusive mirror. Front polarisers too may include lightly scattering

elements that act to remove unwanted reflections, and compensation films for improving viewing angle.

9. **Driver bonding.** Connections are made from the exposed ITO on the bonding ledge to the driving circuitry by one of four methods:
  - a. Surface Mount Technology: Connectors are made directly from the bonding ledge to the Printed Circuit Board (PCB);
  - b. Chip-on-Board: The silicon die is mounted onto the PCB and connected to the panel using gold wires, and protected by adhesive;
  - c. TAB mounted drivers. The driver manufacturers often supply tape-automated-bonded chips. The chip is mounted onto a tape with gold I/O lines etched into it. The tape is adhered to the bonding ledge using a 1D conducting adhesive;
  - d. Chip-on-Glass. COG uses gold-bump soldering to attach the silicon chip directly to the bonding ledge. The chip must be protected from light and handling by embedding in a black epoxy adhesive.
10. **Inspection and test.** Obviously, the degree of testing is minimised to reduce costs, but manufacturers will operate a quality system to determine and minimize the occurrence of optical and electrical defects.
11. **Provision of Colour.** Full-colour LCDs are made in the same way as described above, but the glass plates are pre-patterned with colour filters (for the front plate) and thin-film-transistors (TFT, for the rear plate). Usually, RGB filters are used and aligned over sub-pixels in the column electrodes. A black matrix surrounds each filter to maximise contrast, minimise colour leakage and to optically isolate the TFT (thereby preventing problems with photo-generated charge). The resulting structure has a lower pixel fill factor, typically <50%. Given the losses associated with the low fill factor and absorption of 67% of the light by the colour filters, reflective full-colour LCDs are yet to be successful commercially: the images are too dim in all conditions but the brightest sunshine. Instead of using a reflective rear polariser, colour

panels are combined with a backlight unit (BLU) to provide illumination.

### 3.2 LCD Polarisation Optics

Although liquid crystals can be used to emit light [61], all liquid crystal displays use the liquid crystal medium to modulate light incident on the panel, whether from ambient light or from a built-in source. The anisotropic nature of the liquid crystal presents a number of means through which contrast can be produced, whether by scattering, absorption, selective reflection or changes of optical retardation and hence polarisation state. The great majority of LCDs are sandwiched between film polarisers and use changes of optical retardation to give the required appearance. The state of polarisation of light, as it travels through an optically transparent medium, can be linear, elliptical or circular, depending on the relative magnitudes of two orthogonal polarisation components. As the light goes from one transparent medium to another, light of each of the polarisation components will be refracted, reflected, and the polarisation reoriented. Finding the optical state requires solution of Maxwell's equations at each interface for each polarisation. However, if we ignore the reflections and refractions and just consider the polarisation state, then we can consider the light to be given by a 2x1 Jones vector:

$$\begin{pmatrix} E_x \\ E_y \end{pmatrix} = \begin{pmatrix} A_x e^{-i(\omega t + \delta_x)} \\ A_y e^{-i(\omega t + \delta_y)} \end{pmatrix}, \quad (20)$$

where, A is the amplitude, x,y orthogonal components for light traversing in the z-direction and  $\delta$  represents the phase related to the wavelength  $\lambda$  through the refractive index by:

$$\delta_j = \frac{2\pi n_j t}{\lambda}; j = x, y \quad (21)$$

If the light is incident on a birefringent layer which has refractive indices  $n_e$  and  $n_o$  and thickness  $t$ , then the state of the polarisation of the transmitted light will

depend on the orientation of the incident light with respect to the optic axis, and the phase difference between the x and y components. The maximum retardation due to the birefringence is  $\Gamma$ , given by:

$$\Gamma = \frac{2\pi \Delta n t}{\lambda} \quad (22)$$

Transformation of the Jones Vector requires the operators to be 2 x 2 matrices called a Jones Matrices [62].

Consider a simple uniform planar sample with parallel rubbing directions and a uniform cell spacing  $d$ . Ignoring the reflections and absorption in this fashion is reasonable for thin ( $d < 25\mu\text{m}$ ), well-aligned samples, and it means that the polarisation state may be calculated using the Jones Matrix for a birefringent retarder:

$$\begin{pmatrix} e^{-i\frac{\Gamma}{2}} & 0 \\ 0 & e^{i\frac{\Gamma}{2}} \end{pmatrix} \quad (23)$$

Placing this retarder at an arbitrary angle  $\phi$  between crossed polarisers gives the Jones vector for light transmitted by the device:

$$\begin{aligned} \begin{pmatrix} E'_x \\ E'_y \end{pmatrix} &= \begin{pmatrix} 1 & 0 \\ 0 & 0 \end{pmatrix} \begin{pmatrix} \cos\phi & -\sin\phi \\ \sin\phi & \cos\phi \end{pmatrix} \begin{pmatrix} e^{-i\frac{\Gamma}{2}} & 0 \\ 0 & e^{i\frac{\Gamma}{2}} \end{pmatrix} \\ &\cdot \begin{pmatrix} \cos\phi & \sin\phi \\ -\sin\phi & \cos\phi \end{pmatrix} \begin{pmatrix} 0 & 0 \\ 0 & 1 \end{pmatrix} \begin{pmatrix} 0 \\ 1 \end{pmatrix} \\ &= \begin{pmatrix} -2i\sin\phi\cos\phi\sin\frac{\Gamma}{2} \\ 0 \end{pmatrix} \quad (24) \end{aligned}$$

The transmission T is then given by:

$$\begin{aligned} T &= \frac{E'^* \cdot E'}{E^* \cdot E} = \frac{E'_x{}^2 + E'_y{}^2}{E_x{}^2 + E_y{}^2} \\ &= \sin^2 2\phi \sin^2 \frac{\Gamma}{2} = \sin^2(2\phi) \sin^2\left(\frac{\pi \Delta n d}{\lambda}\right) \quad (25) \end{aligned}$$

where  $E^*$  is the conjugate of  $E$  (which may be complex) and  $t = d$  is used for the spacing of the liquid crystal cell.

Equation (25) suggests that the transmitted light is maximum if the cell gap and birefringence are at the quarter wave plate condition  $\Delta n \cdot d = \lambda/4$ , with the polarisers oriented at  $\pm 45^\circ$  to the alignment direction. The eye is most sensitive to green wavelengths, and setting  $\lambda = 550\text{nm}$  gives broad transmission across the wavelength range such that the device will appear white; for a typical liquid crystal this condition occurs for cells spaced at about 2 – 3  $\mu\text{m}$ .

### 3.3 Basic operation: Electrically Controlled Birefringence Mode

Applying an electric field to the aligned liquid crystal will tend to align the liquid crystal director parallel to the field direction, if the material has a positive  $\Delta\epsilon$ , or perpendicular to the field if negative. Considering the pixel in one-dimension only and the director at the containing surfaces anchored strongly, the total free energy of the liquid crystal  $F$  is given by combining equations (3) and (12) as:

$$F = \frac{1}{2} \int_0^d [k_{11}(\nabla \cdot \mathbf{n})^2 + k_{22}(\mathbf{n} \cdot \nabla \times \mathbf{n})^2 + k_{33}(\mathbf{n} \times \nabla \times \mathbf{n})^2 - \epsilon_0 \Delta\epsilon (\mathbf{n} \cdot \mathbf{E})^2] dz \quad (26)$$

For the simple case shown in figure 6a), the electric field is applied normal to the surfaces such that  $\mathbf{E} = (0,0,V/d)$  and initially  $\mathbf{n} = (1,0,0)$ . As the field is increased, there is a torque on the director acting to increase the tilt angle  $\theta$ :

$$F = \frac{1}{2} \int_0^d \left[ (k_{11} \sin^2 \theta + k_{33} \cos^2 \theta) \frac{d^2 \theta}{dz^2} - \epsilon_0 \Delta\epsilon E^2 \sin^2 \theta \right] dz \quad (27)$$

This integral may be solved using the Euler Lagrange equation

$$(k_{11} \cos^2 \theta + k_{33} \sin^2 \theta) \left( \frac{d\theta}{dz} \right)^2 + \epsilon_0 \Delta\epsilon E^2 \sin^2 \theta = C \quad (28)$$

where the constant  $C$  is found from realising that the maximum tilt  $\theta_m$  must occur at the cell centre  $z = d/2$  because of symmetry, at which point  $d\theta/dz = 0$ , and hence:

$$C = \epsilon_0 \Delta\epsilon E^2 \sin^2 \theta_m \quad (29)$$

Substituting back into the Euler Lagrange equation (28) gives:

$$\frac{d\theta}{dz} = \frac{V}{d} \sqrt{\epsilon_0 \Delta\epsilon \frac{(\sin^2 \theta_m - \sin^2 \theta)}{((k_{33} - k_{11}) \sin^2 \theta + k_{11})}} \quad (30)$$

At low field strengths, the small angle limits to the tilt angles allow equation (30) to be re-expressed as:

$$V \cdot dz = d \sqrt{\frac{1}{\epsilon_0 \Delta\epsilon} \cdot \left[ \frac{k_{11}}{(\theta_m^2 - \theta^2)} + \frac{(k_{33} - k_{11})\theta^2}{(\theta_m^2 - \theta^2)} \right]} d\theta \quad (31)$$

which tends towards:

$$V \cdot dz = d \sqrt{\frac{k_{11}}{\epsilon_0 \Delta\epsilon}} (\theta_m^2 - \theta^2)^{-\frac{1}{2}} d\theta \quad (32)$$

as  $\theta^2 \rightarrow 0$ . Integrating (24) to find the threshold field gives:

$$V_C \int_0^{\frac{d}{2}} dz = \frac{d}{2} \sqrt{\frac{k_{11}}{\epsilon_0 \Delta\epsilon}} \cdot \int_0^{\theta_m} (\theta_m^2 - \theta^2)^{-\frac{1}{2}} d\theta$$

$$V_C [z]_0^{\frac{d}{2}} = d \cdot \sqrt{\frac{k_{11}}{\epsilon_0 \Delta\epsilon}} \cdot \left[ \tan^{-1} \frac{\theta}{\sqrt{(\theta_m^2 - \theta^2)}} \right]_0^{\theta_m}$$

$$V_C \frac{d}{2} = d \sqrt{\frac{k_{11}}{\epsilon_0 \Delta\epsilon}} \cdot \left[ \tan^{-1} \frac{\theta_m}{\sqrt{0}} - \tan^{-1} \left( \frac{0}{\theta_m} \right) \right]$$

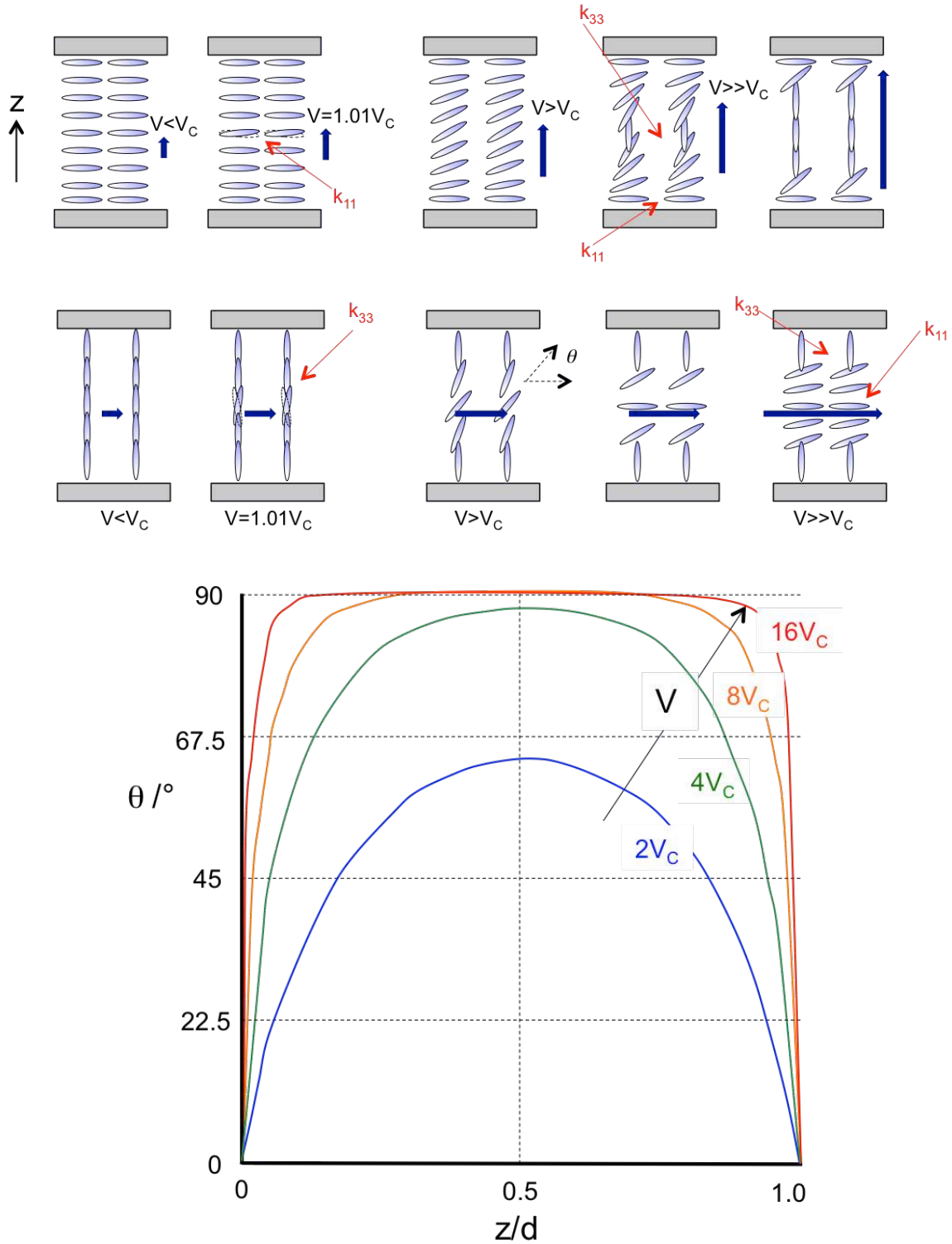


Figure 6. Fréedericksz transitions in a) the planar homogeneous geometry for a positive  $\Delta\epsilon$  nematic, and b) the homeotropic geometry with a negative  $\Delta\epsilon$  nematic. The dominant elastic constants at various field strengths is indicated in red. c) Calculated tilt profile versus  $V/V_C$  for a material with  $\epsilon_{\parallel}=20.25$ ,  $\epsilon_{\perp}=5.36$ ,  $k_{11}=11\text{pN}$ ,  $k_{33}=17\text{pN}$  in a cell of gap  $d=10\mu\text{m}$ , [63].

$$V_C = \pi \sqrt{\frac{k_{11}}{\varepsilon_0 \Delta \varepsilon}} \quad (33)$$

Hence, there is a critical voltage that is independent of cell gap at which the electric field induced distortion begins, a threshold that depends on the root of the ratio of the relevant elastic constant and the dielectric anisotropy. By analogy, the threshold for a negative  $\Delta \varepsilon$  liquid crystal in the homeotropic geometry is:

$$V_C = \pi \sqrt{\frac{k_{33}}{\varepsilon_0 |\Delta \varepsilon|}} \quad (34)$$

Figure 6b) shows the situation where a positive  $\Delta \varepsilon$  material is used, but the field is applied in the plane of the cell; for example using inter-digitated electrodes. Similarly, a planar sample with the preferred alignment direction normal to the applied field will cause the director to twist at the electrode surface. In such instances, the electric field is not uniform, though it may be approximated at the electrode surface to be  $V/l$ , where  $l$  is the separation between the electrodes of opposing voltage. In such cases, the cell gap does not cancel in equation (33) and the threshold depends on both cell gap and electrode spacing:

$$V_C \approx \pi \frac{l}{d} \sqrt{\frac{k_{33}}{\varepsilon_0 \Delta \varepsilon}} \quad ; \quad V_C \approx \pi \frac{l}{d} \sqrt{\frac{k_{22}}{\varepsilon_0 \Delta \varepsilon}} \quad (35)$$

for the homeotropic and planar cases respectively. This latter geometry is utilised with in-plane switching devices, as will be described in section 4.6. If the field is applied normal to a uniform director, the threshold is well defined. In practice, the alignment layers induce a small pretilt, and the director profile of the quiescent state is not uniform, neither is the electric field applied normal to the director. Thus, the threshold is rather second-order in nature, and begins to occur somewhat below the voltage predicted by equations (33) to (35).

Above the threshold, the solution to equation (30) must include the higher angle terms. Again considering the planar aligned case shown in figure 6a), dividing equation through by  $V_C$  gives:

$$\frac{V}{V_C} \cdot dz = \frac{d}{\pi} \sqrt{\frac{\kappa \sin^2 \theta + 1}{(\sin^2 \theta_m - \sin^2 \theta)}} d\theta \quad , \quad (36)$$

where  $\kappa = (k_{33} - k_{11})/k_{11}$ . Immediately above the transition, a reasonable solution is found by integrating (28):

$$\frac{V}{V_C} = \frac{2}{\pi} \int_0^{\theta_m} \sqrt{\frac{1 + \kappa \sin^2 \theta}{(\sin^2 \theta_m - \sin^2 \theta)}} d\theta \quad , \quad (37)$$

using a Fourier analysis to solve the complete elliptical integral of the third kind:

$$\frac{V}{V_C} = \left( 1 + \frac{1}{4}(\kappa + 1) \sin^2 \theta_m + \dots \right) \quad (38)$$

which, has the first order solution:

$$\frac{z}{d} = \frac{1}{\pi} \sin^{-1} \left( \frac{\theta}{\theta_m} \right) - \theta \sqrt{(\theta_m^2 - \theta^2)} \cdot \frac{1 + 3\kappa + \dots}{12\pi \left[ 1 + \frac{1}{4}(\kappa + 1)\theta_m^2 + \dots \right]} \quad (39)$$

where:

$$\theta_m = \sin^{-1} \sqrt{\left( \frac{4}{(\kappa + 1)} \left[ \frac{V}{V_C} - 1 \right] \right)} \quad (40)$$

This indicates that, immediately above the threshold, the tilt of the director increases linearly, with a gradient that is inversely related to the elastic ratio  $k_{33}/k_{11}$ . This is indicated in figure 6a), where the bend elastic constant becomes increasingly pertinent at the centre of the device, and splay is increasingly pushed to the alignment surfaces.

Above the electric field induced Fréedericksz transition, the situation is complicated by the effect of the non-uniform dielectric properties of the distorted director profile on the applied electric field. The electric torque is related to the electric displacement vector  $\mathbf{D}$  and above the transition the director profile is no longer uniform such that  $\mathbf{E}$  has a direction that is dependent on the distortion. That is, the effect of the

field depends on the elastic energy, but conversely, the elastic energy depends on the field. Ignoring the effects of charge,  $\nabla \cdot \mathbf{D} = 0$  and assuming  $\mathbf{D}$  is a function of  $z$  only, solutions to the free energy expression require  $\mathbf{E}$  to be calculated self-consistently with the director profile:

$$D_z = \frac{V}{\int_0^d \frac{1}{\varepsilon_0(\Delta\varepsilon \sin^2\theta + \varepsilon_1)} dz} \quad (41)$$

and thus

$$\frac{V}{V_C} = \frac{2}{\pi} \sqrt{\left(\frac{\Delta\varepsilon}{\varepsilon_1} \sin^2\theta_m + 1\right)} \cdot \int_0^{\theta_m} \sqrt{\frac{1 + \kappa \sin^2\theta}{\left(\frac{\Delta\varepsilon}{\varepsilon_1} \sin^2\theta + 1\right)(\sin^2\theta_m - \sin^2\theta)}} d\theta \quad (42)$$

Solutions to this integral are done numerically. Indeed, display manufacturers use commercial packages, such as “*LCD Master*” from Shintech, “*TechWiz*” from Sanayi or “*DIMOS*” from Autronic Melchers [64], to calculate the director profile as a function of applied field for their devices.

Consider the case of figure 6a) where the cell retardation is set to the quarter-wave-plate condition at 550nm (the peak of the eye’s response,  $\Delta n \cdot d = 550\text{nm}/4 = 137.5\text{nm}$ ) and the alignment direction is set at  $\phi = 45^\circ$ . As the voltage is then applied, the overall birefringence of the cell decreases as the optic axis of the director at the centre rotates to towards the field and viewing direction, and the effective birefringence is reduced to  $\Delta n'$ . Simplistically, we can consider the director to be uniformly at some average tilt angle  $\bar{\theta}$ , the new refractive indices are given by:

$$n'_o = n_o ; \quad \frac{1}{n'_e{}^2} = \frac{\sin^2\bar{\theta}}{n_o{}^2} + \frac{\cos^2\bar{\theta}}{n_e{}^2} \quad , \quad (43)$$

such that the effective birefringence  $\Delta n'$  is:

$$\Delta n' = n'_e - n_o = \frac{n_e n_o}{\sqrt{n_e^2 \sin^2\bar{\theta} + n_o^2 \cos^2\bar{\theta}}} - n_o \quad . \quad (44)$$

From equation (25), the transmission of polarised light (i.e. after the first polariser) becomes:

$$T = \sin^2\left(\frac{\pi \Delta n' d}{\lambda}\right) \quad (45)$$

With sufficient field,  $\Delta n' d \rightarrow 0$  and equation (45) predicts  $T \rightarrow 0$ . Thus, above  $V_C$  the cell changes from white towards black. Figure 7a) shows this decrease in transmission for red, green and blue wavelengths, calculated using equations (40) and (45) for a 0.67mm cell filled with a liquid crystal material with  $n_e = 1.7$ ,  $n_o = 1.5$  and  $k_{33}/k_{11} = 2.0$ .

Figure 7b) shows the behaviour for a sample with a higher initial retardation; the same material but with a 2.5 $\mu\text{m}$  cell gap. Each wavelength has transmission peaks corresponding to odd multiples of the quarter wave plate condition (i.e.  $\Delta n' d/\lambda = 3/4$  and  $1/4$ ); because these peaks occur at different voltages for different wavelengths, the cell appears to change colour as the voltage is increased.

There are a number of reasons why such a simple device is not used as a display effect, illustrating the thinking that the display engineer needs to follow.

- The optimum cell gap is very small, typically less than 1 $\mu\text{m}$ , and always much lower than the cell gap required for a high production yield (typically 4 $\mu\text{m}$  or higher).
- The device cannot be passive-matrix multiplexed, since the saturation voltage is typically several times  $V_C$ . This will be explained in the following section.
- The optical configuration is very sensitive to changes of cell gap. For example, a typical LCD tolerance is  $\pm 0.15\mu\text{m}$ ; such a change would cause a 12% reduction in the transmission and colouration for the ECB device.
- The viewing properties of the device are very poor in both high and low voltage states, as illustrated in figure 8. In the 0V state, the effective birefringence decreases off-axis, the quarter-wave plate condition is lost and the

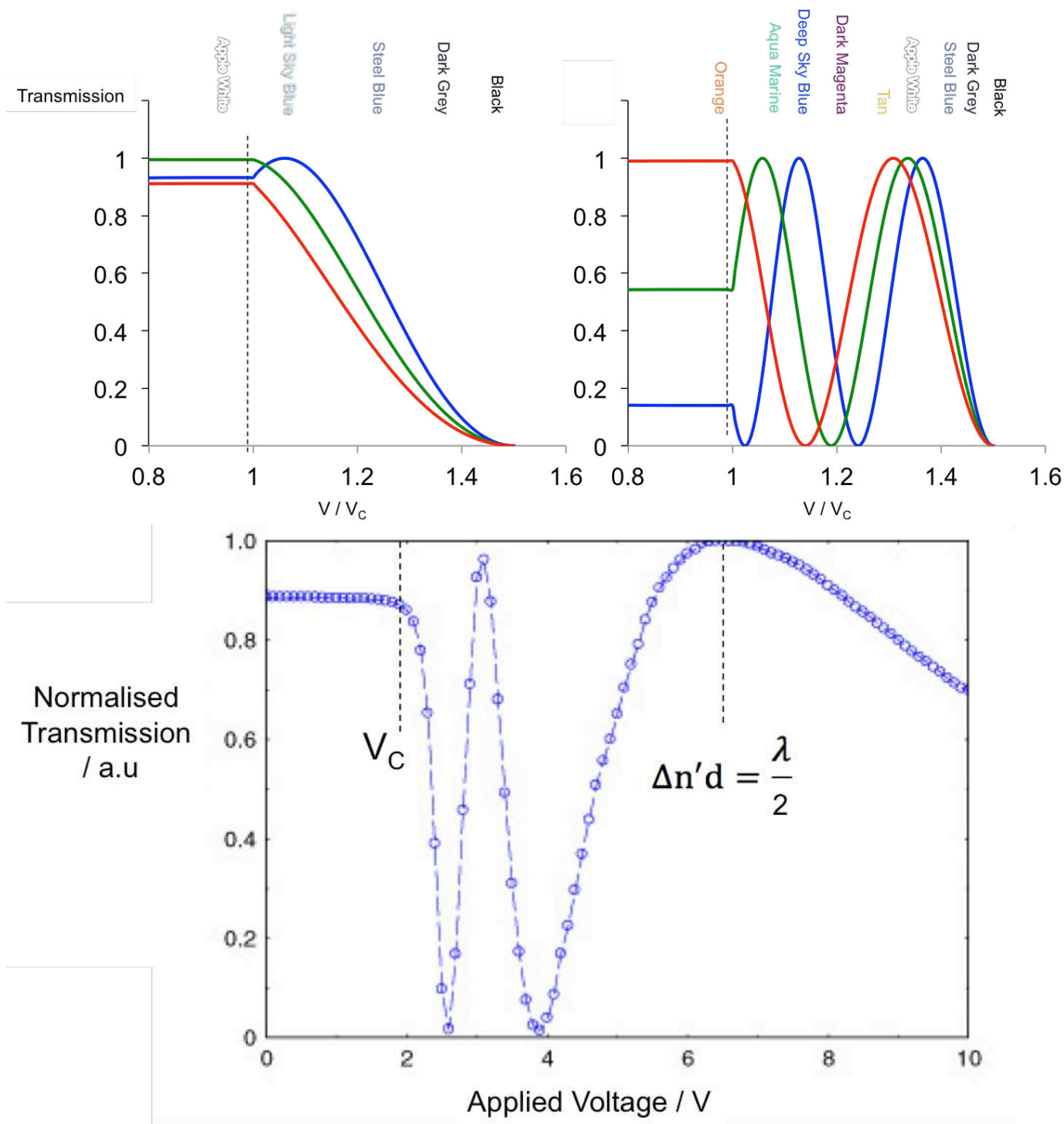


Figure 7 Theoretical transmission characteristic for an electrically-controlled birefringence LCD. a) The retardation at the quarter wave plate condition for green light ( $d = 0.67\mu\text{m}$ ,  $\Delta n = 0.2$ ) ; b) a thicker cell with retardation at the full wave condition for  $\lambda = 500\text{nm}$  ( $d = 0.67\text{mm}$ ,  $\Delta n = 0.2$ ). Other fitting parameters used:  $n_e = 1.7$ ,  $n_o = 1.5$  and  $k_{33}/k_{11} = 2$ . c) Experimentally determined transmission curve for a cell close to the full plate condition. The results are taken for a white light source imaged through an eye-response filter.

device looks dark instead of bright (in the direction orthogonal to this, there is little change and the device still looks white). In the high voltage state, the off axis transmission is even darker than the full ON state when viewed in the direction of the director tilt. When viewed in the other quadrant, the retardation increases rather than decreasing as desired on switching causing contrast inversion, and the device begins to appear coloured.

The response time for even such a simple device is complex, due to the effects of field induced flow and the need for the anisotropic viscosities to be considered. If flow is ignored, the response time depends solely on the twist viscosity  $\gamma_1$  that describes rotation of the director. The Euler-Lagrange equation for the time dependent free energy of equation (28) then becomes:

$$(k_{11}\cos^2\theta + k_{33}\sin^2\theta)\frac{\partial^2\theta}{\partial z^2} + (k_{33} - k_{11})\sin\theta\cos\theta\left(\frac{\partial\theta}{\partial z}\right)^2 + \varepsilon_0\Delta\varepsilon E^2 \sin\theta\cos\theta = \gamma_1\frac{\partial\theta}{\partial t} \quad (46)$$

For simplicity, the elastic anisotropy is discarded, and a single elastic constant  $k$  is assumed:

$$\varepsilon_0\Delta\varepsilon E^2 \sin\theta\cos\theta + k\frac{\partial^2\theta}{\partial z^2} = \gamma_1\frac{\partial\theta}{\partial t} \quad (47)$$

Applying a small angle approximation [65], the characteristic *ON* and *OFF* times are:

$$\tau_{ON} = \frac{\gamma_1}{\varepsilon_0\Delta\varepsilon E^2 - \left(\frac{\pi}{d}\right)^2 k} = \frac{\gamma_1 d^2}{\varepsilon_0\Delta\varepsilon (V^2 - V_C^2)} = \frac{\gamma_1 d^2}{\pi^2 k \left[\left(\frac{V}{V_C}\right)^2 - 1\right]}; \quad (48)$$

$$\tau_{OFF} = \frac{\gamma_1 d^2}{\pi^2 k}.$$

These times are made short by using materials with low viscoelastic ratios  $\gamma_1/k$ , but most effectively by keeping the cell gap  $d$  low. Examples of mixtures providing response times as low as 30ms at  $-20^\circ\text{C}$  and 10ms at  $+20^\circ\text{C}$  in a  $3\mu\text{m}$  cell have been produced [66]. Given the 3-  $4\mu\text{m}$  lower limit on cell gap set by clean-room quality and device uniformity, it would seem advantageous for high  $\Delta n$  materials to be used to enable the required optical effect with a lower cell gap. In practice, however,  $\gamma_1$  tends to increase with  $\Delta n$  and

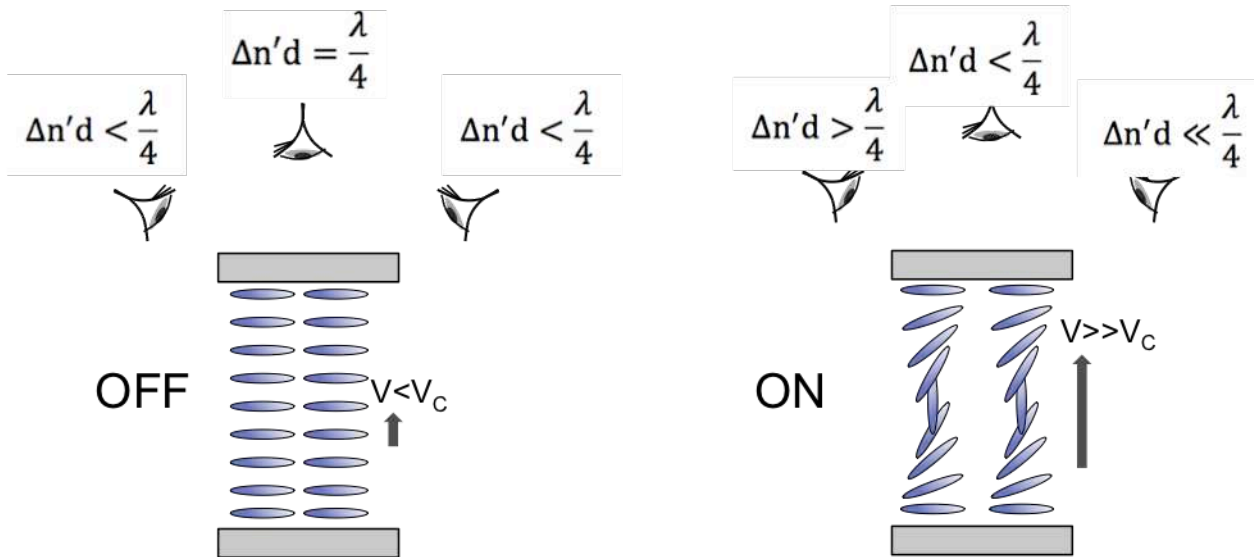


Figure 8 Explanation for the poor viewing angle for the electrically controlled birefringence effect.

so the efficacy of this is limited. Ensuring that the voltage is made high can quicken the ON time significantly. However, it is the sum of the ON and OFF times that is relevant for display applications. Moreover, if the display requires intermediate grey levels or some degree of passive matrix addressing (see section 3.4), the ON voltage is limited, and even the ON time can be slow. For example, switching to the grey level closest to  $V_C$  is inherently slow.

In the case of a passive matrix addressed device, even the OFF pixels have a voltage  $V_d$  applied and the response time is given by [67]:

$$\tau_{OFF} = \frac{\gamma_1 d^2}{\pi^2 k \left[ 1 - \left( \frac{V_d}{V_C} \right)^2 \right]}; \quad (49)$$

In practice, the response is complicated by induced flow of the liquid crystal, and the aligning effect of the director in response to such flows. For example, the OFF response is often slowed considerably by back-flow that tends to initially reorient the director at the centre of the cell in the opposite direction to that which gives the eventual lowest energy state, [68]. Avoiding this “optical bounce” effect is considered further in section 6.2.

### 3.4 Passive Matrix Addressing and the Multiplexing Limit

For low information contents, it is satisfactory to form a display where each pixel is driven directly from the driver. Usually, one of the electrodes is shaped into the desired pattern, such as a pixel for a seven-segment or alphanumeric image, and the other electrode is a common electrode. A display of  $N$  pixels then requires  $N+1$  electrodes. An example arrangement is shown in figure 9a), where a single seven-segment number is displayed using just eight electrodes. Rather than have separate connections to the two plates of the LCD, access to all of the electrodes is through a single bonding ledge: the opposing common electrode is connected through via-electrodes that are connected through the one-dimensional conducting seal. The access electrodes to each segment is kept small, to

minimise overlap with the common electrode. It is essential for such a design that the common plate has only a single point of overlap with ITO on the electrode plate and conducting seal, to prevent unwanted shorting of pixels. A typical transmission versus voltage characteristic for an LCD is shown in figure 9b). With a direct drive scheme, the OFF voltage must be below the threshold  $T_{10}$  (usually 0V), and the ON voltage should be above the saturation level  $T_{90}$ .

A direct drive approach is satisfactory for devices with a small number of pixels. More complex images require some degree of matrix addressing (or multiplexing), where appropriate signals are applied to electrodes on both top and bottom plates. The electrodes may also be shaped into alphanumeric characters and designed for a low level of multiplexing, or indeed into a more complex  $r(\theta)$  arrangement for the display of polar co-ordinates. The most common design, however, is for the electrodes to comprise  $N$  rows and  $M$  columns to form a rectangular  $M \times N$  display. Time division multiplexing is used to apply appropriate signals to the rows and columns, when driven from only  $M + N$  connections.

Consider the simple  $7 \times 6$  matrix display illustrated in figure 10, where each pixel is addressed by sequentially scanning through the 6 rows, whilst the appropriate data is synchronously applied to the columns to discriminate between the ON and OFF states. Figure 10 shows an example instant within the image frame, where the data voltages are being applied to 7 columns and are those for the third row electrode. The data signal on the columns are  $\pm D$  volts, where it is the sign of the signal that discriminates between the ON and OFF states of the pixel on the third row. At this instant, +S volts is being applied to the third row whilst all other rows are kept at ground 0V. The data being applied at this instance is (+---+D). The potential difference at the pixels is defined as Row – Column, such that the third row experiences the voltage:

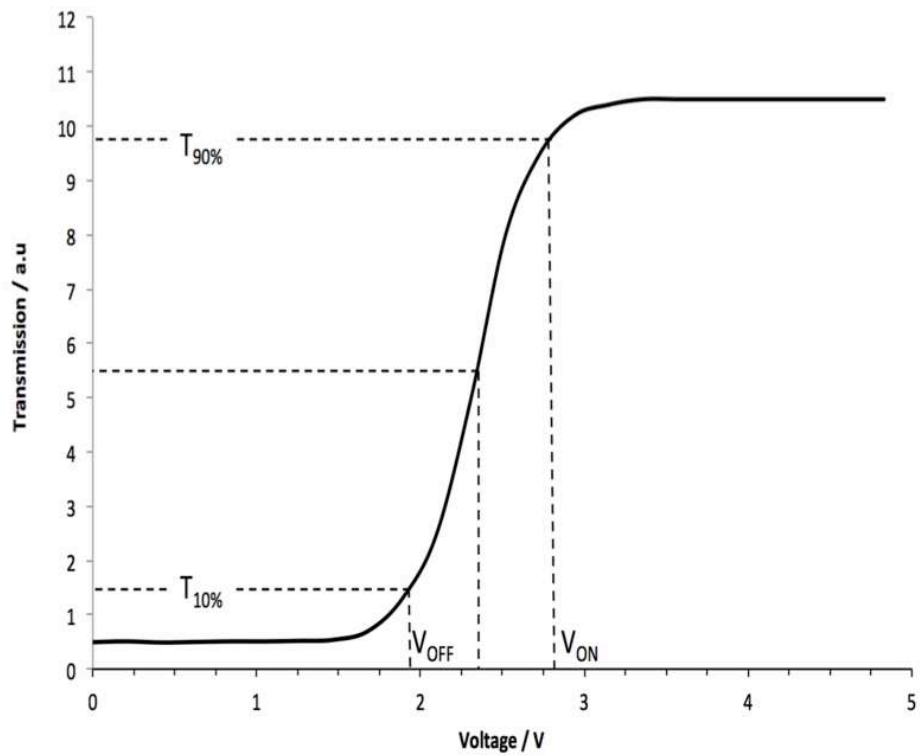
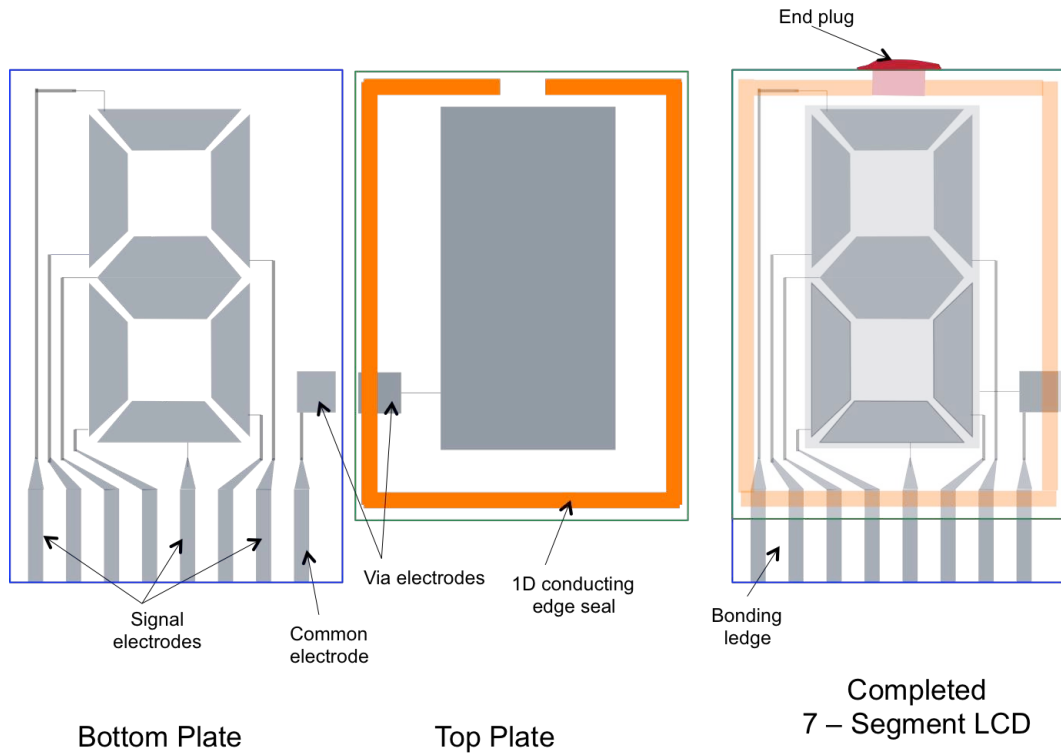


Figure 9 Design of a single element seven-segment LCD, showing front and rear plates face-up, and the completed module. b) A typical Transmission Voltage characteristic for an LCD.

Row 3: +S-D ; +S-D ; +S+D ; +S+D ; +S-D ; +S+D ;  
 +S-D ,

and each of the other rows experiences:

Row 1,2,4,5,6: -D ; -D ; +D ; +D ; -D ;  
 +D ; -D

Once the third row is addressed, the scan signal moves to the fourth row and the data signals change sign appropriately to supply the signal for that row. The aim of the multiplexing scheme is to ensure that the high voltages  $|(S+D)|$  are sufficient to discriminate from the low voltages  $|(S-D)|$ , despite

the fact that each row is only addressed for a  $1/N$  fraction of the frame time, and for the remainder of the frame  $(N-1)/N$  each pixel experiences the data signal  $\pm D$ .

Nematic displays respond to the root-mean-square voltage applied over the whole frame. As soon as the signal has been removed, each pixel starts to relax back to the off state, and so constant refreshing at a frame rate sufficiently fast to prevent this relaxation (*or frame response*) and maintain the image. For a simple scheme, the frame time will equal the slot time for each row  $\tau$  multiplied by the number of rows  $N$ . It is independent of the number of columns, and hence it is common for the rows to be chosen as the lower number in the matrix to ensure the faster frame rate.

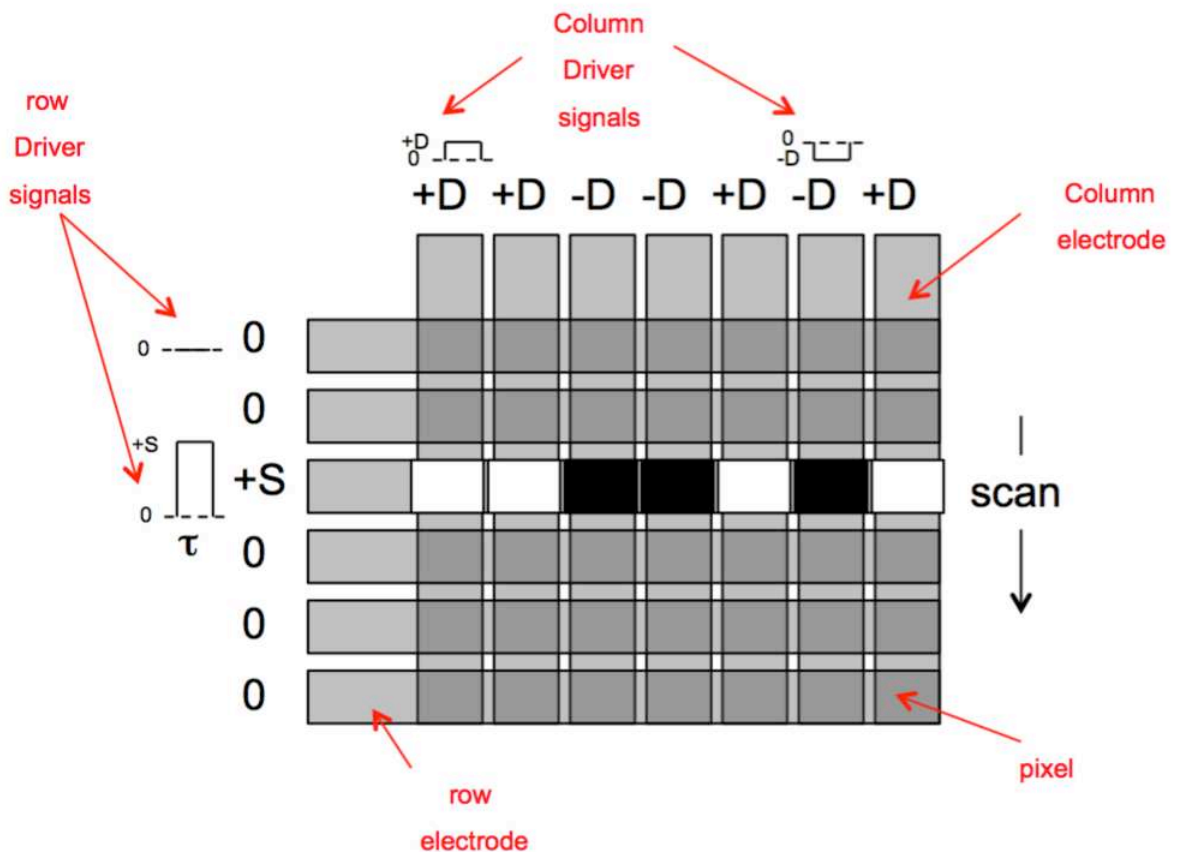


Figure 10 Example of passive matrix multiplexing for a 7x6 pixel graphic display. The row and column signals are for the 1/6 proportion of the frame that corresponds to the 3<sup>rd</sup> row being addressed.

The root mean square of the voltage applied over N rows for the ON and OFF signals are:

$$\overline{V_{ON}} = \sqrt{\frac{(S+D)^2+(N-1)D^2}{N}} \quad ; \quad \overline{V_{OFF}} = \sqrt{\frac{(S-D)^2+(N-1)D^2}{N}} \quad (50)$$

and D and S should be chosen to ensure that  $V_{ON}$  is above the Transmission saturation (i.e.  $> T_{90\%}$ ) and  $V_{OFF}$  below the threshold (i.e.  $< T_{10\%}$ ). The steepness of the electro-optic response is related to  $R = V_{ON}/V_{OFF}$ :

$$R^2 = \left(\frac{\overline{V_{ON}}}{\overline{V_{OFF}}}\right)^2 = \frac{(S+D)^2+(N-1)D^2}{(S-D)^2+(N-1)D^2} = \frac{b^2+2b+N}{b^2-2b+N} \quad (51)$$

where  $b = S/D$  is called the bias ratio. The maximum number of lines that can be driven for a given S and D is found by differentiating:

$$\frac{\partial(R^2)}{\partial b} = \frac{\partial\left(\frac{b^2+2b+N}{b^2-2b+N}\right)}{\partial b} = \frac{4(b^2+N)}{(b^2-2b+N)^2} = 0 \quad (52)$$

This has solutions when either  $b = \infty$  or  $b = S/D = \sqrt{N}$ . Substituting the latter into equation (52) gives the Alt-Pleshko [69] relationships:

$$\left(\frac{\overline{V_{ON}}}{\overline{V_{OFF}}}\right)_{max} = \sqrt{\frac{N+2\sqrt{N}+N}{N-2\sqrt{N}+N}} = \sqrt{\frac{\sqrt{N}+1}{\sqrt{N}-1}} \quad (53)$$

or:

$$N_{max} = \left[ \frac{\left(\frac{\overline{V_{ON}}}{\overline{V_{OFF}}}\right)^2 + 1}{\left(\frac{\overline{V_{ON}}}{\overline{V_{OFF}}}\right)^2 - 1} \right]^2 \quad (54)$$

This relationship suggests that, as N increases, the maximum  $\frac{\overline{V_{ON}}}{\overline{V_{OFF}}}$  must tend towards unity; that is, the threshold characteristic must increase in steepness to allow more lines to be addressed, as shown in figure 11a). The typical TN characteristic shown in figure 9c) has a response suited to up to six levels of time-division multiplexing.

The signal voltages S and D that are required for the N x M display are found by substituting the optimum multiplexing ratio  $S = D\sqrt{N}$  into the RMS voltages of equation (50):

$$V_{OFF} = \sqrt{\frac{(D\sqrt{N}-D)^2+(N-1)D^2}{N}} = D\sqrt{\frac{2(\sqrt{N}-1)}{\sqrt{N}}} \quad (55)$$

$$V_{ON} = \sqrt{\frac{D^2N+2D^2\sqrt{N}+D^2+D^2N-D^2}{N}} = D\sqrt{\frac{2(\sqrt{N}+1)}{\sqrt{N}}}$$

which leads to the following data D and strobe S voltages:

$$D = V_{OFF}\sqrt{\frac{\sqrt{N}}{2\sqrt{N}-1}} = V_{ON}\sqrt{\frac{\sqrt{N}}{2\sqrt{N}+1}} \quad (56)$$

and:

$$S = V_{OFF}\sqrt{\frac{N\sqrt{N}}{2\sqrt{N}-1}} \quad (57)$$

Equations (56) and (57) are plotted in figure 11b); they indicate that, at high N,  $D \approx \frac{1}{\sqrt{2}}V_C$  and  $S \approx \sqrt{\frac{N}{2}}V_C$  so that the maximum voltage that needs to be delivered by the driver chip (S+D) increases with the level of multiplexing N, whilst the discriminating voltage D decreases. For this reason, STN displays with N=240 typically require drivers capable of delivering S+D = 20V.

During the addressing frame, the liquid crystal director for the ON pixels in the addressed row will begin to decay as soon as the strobe voltage moves on to the subsequent rows. Thus, it is important that the slot time of the addressing scheme is arranged to minimise any flicker whilst at the same time the pixels are ready to display new information in the following frame; this occurs approximately where:

$$\tau \approx \frac{\tau_{ON} + \tau_{OFF}}{2N} \quad (58)$$

In practice, the scheme shown above is unsuitable for long-term use, because there is no DC balance to the waveform: this leads to eventual electrical breakdown of the liquid crystal and, if the image does not change,

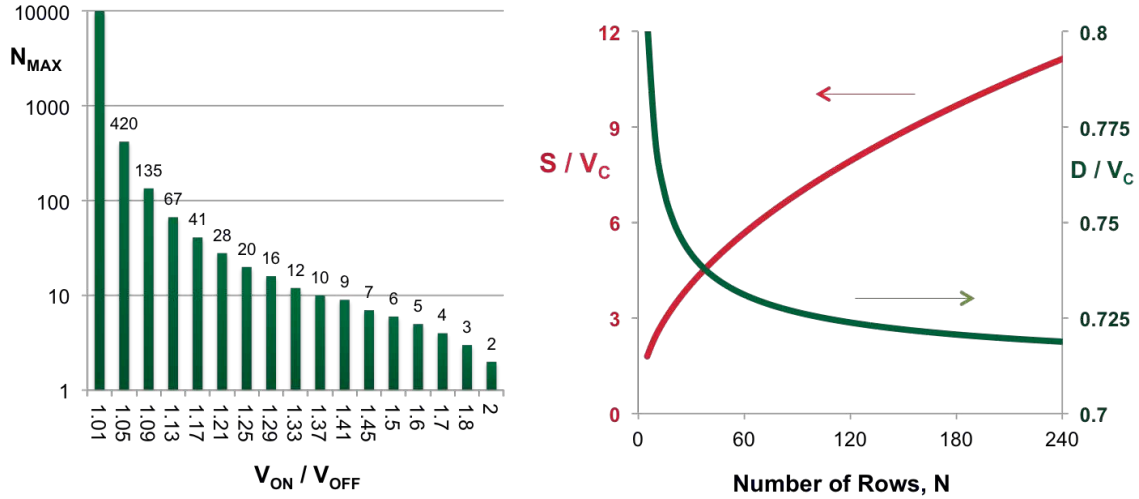


Figure 11 a) The Alt-Pleshko Multiplexing Limit and b) addressing voltages.

can result in image sticking issues associated with ionic conductivity. In practice, therefore, the waveforms will be inverted periodically to maintain a net zero DC voltage. Given the data changes from frame to frame, DC balancing can only be guaranteed if the voltages are inverted twice per frame. That is, if the slot time is halved, and the frame divided into a positive field (+ $S$ ,  $\pm D$ ) and a negative field with (- $S$ ,  $\mp D$ ). The slot time should not be made too short, since the power dissipation of charging and discharging the capacitances each field  $P_f$  is approximately related to:

$$P_f \propto \frac{\epsilon_{av} A}{d} \cdot \langle V \rangle^2 \cdot f \approx \frac{\bar{\epsilon} A}{d} \cdot \frac{D^2}{t} \quad (59)$$

Given that power should be kept low, inversion is usually done only once per frame, often randomly within the frame time to help ensure DC balance regardless of image pattern.

### 3.5 Thin Film Transistors and Active Matrix Addressing

Contrary to the approach taken by *Sharp* who targeted the new market of portable electronic calculators, *RCA* concentrated on replacing the cathode-ray tube for televisual display with an LCD from the outset [2]. The potential application of thin-film transistors as

active elements in displays had been recognised since their invention at *RCA* in the mid 1960s [57]. By 1971, the *RCA* team believed [70] that active components were required to overcome the slow speed and poor electro-optic properties of the dynamic scattering mode device, proposing solutions using dual-diodes, field effect transistors and storage capacitors to ensure that the charge across the pixel remained constant across the frame. It was the team at *Westinghouse* [71] that were the first to implement this in practice, producing a TN 6x6 matrix driven by CdSe TFT. In the UK, the team led by Hilsum at *RSRE* understood the handling, reliability and lifetime issues presented by CdSe and Te, and in 1976 approached Spear and LeComber at the University of Dundee, who were working on the use of hydrogenated amorphous silicon ( $\alpha$ -Si:H) for use in photovoltaic cells. The Dundee team produced  $\alpha$ -Si:H with electron mobility  $\mu_e$  of  $0.4 \text{ cm}^2/\text{Vs}$ , and proved that the material was suited to address LCDs [72]. The Dundee and *RSRE* teams fabricated insulated-gate field effect TFTs onto a glass substrate using photolithography, and fabricated the world's first  $\alpha$ -Si active matrix LCD in 1980 [73]. This was followed in 1982 by a 240 x 240  $\alpha$ -Si TFT TN from *Canon* in Japan [74], and the immense ensuing effort and investment in Asia to bring TFT

LCDs to the dominance of the display market that it enjoys today.

Very high levels of multiplexibility are possible using thin-film transistors fabricated onto the rear plate of the LCD behind each pixel (or sub pixel in a colour display). A 4k UHD television, for example, has  $2160 \times 3840 \times 3 = 24.9\text{M}$  TFT per panel, and is 2160 ways multiplexed. Each TFT supplies charge to a (sub-) pixel to switch the liquid crystal to any of 256 grey levels. The TFT is a field effect transistor (FET) formed from thin metal-insulator-semiconductor layers, as shown in figure 12a). Most LCDs use a bottom-gate configuration, where the amorphous silicon is deposited onto the pre-patterned gate electrodes,  $n^+$  doped with hydrogen, and source

and drain electrodes patterned on top of this. The electrodes are usually made from Aluminium, Chromium or Molybdenum. With a negative-voltage applied between the gate electrode and the drain  $-V_{GD}$ , electrons are depleted from the semiconductor at the interface with the insulator, preventing current between Source and Drain electrodes, figure 12a) ii). When a positive-bias  $V_{GD}$  is applied to the gate, however, electrons accumulate at this interface allowing current flow from source to drain  $I_{SD}$  when the drain is positive, and from drain to source when the drain is negative, figure 12a) iii). Figure 12b) shows the transfer characteristic originally produced by the Dundee / RSRE team in 1981.

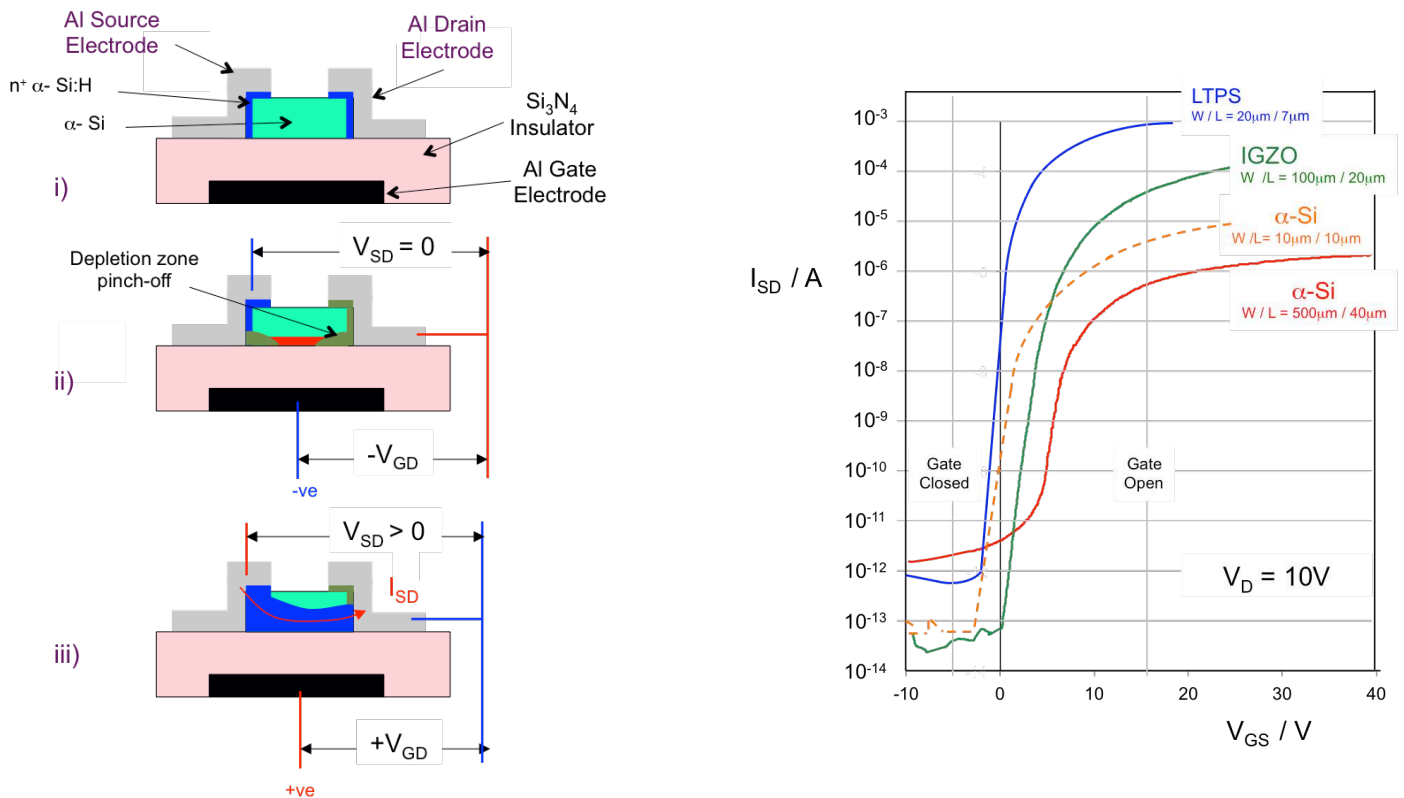


Figure 12 a) Basic construction and operation of a TFT. b) Current-Voltage transfer characteristics for the original Dundee / RSRE  $\alpha\text{-Si:H}$  TFT [72], together with contemporary results for a-Si:H [74], low-temperature polycrystalline silicon (LTPS) [75] and Indium-Gallium-Zinc Oxide (IGZO) TFT [76].

A schematic of how a TFT is used in a typical LCD pixel is shown in figure 13. The LCD has an active matrix back-plane and a front plane with a single common electrode. For backlit colour displays, the front plate will also comprise the colour filters, with a black matrix to ensure sufficiently high contrast, prevent colour leakage, and shield the TFT from incident light and unwanted photo-induced charge generation. The TFT plate has row and column metal bus lines that allow the TFT to be addressed, with the row electrode connected to the transistor gate and the columns the transistor source. The ITO electrodes that form the pixel are connected to the drain electrode. The TFT is also protected using a SiO<sub>x</sub> barrier layer, onto which the liquid crystal alignment layer is deposited. The presence of bus-lines, shielded transistors and storage capacitor reduces the active area of each pixel; aperture ratios as low as 30% to 40% are typical. This reduces the transmissivity of the panel, and necessitates brighter backlighting to provide an attractive appearance. It also negates the use of the colour TFT LCDs in reflective mode, because of the light losses associated with the polarisers, colour filters and the low aperture ratio.

Addressing a TFT matrix is done line-by-line in a similar fashion to that described previously for passive matrix displays, but now the row and column signals are applied to the same substrate, as shown in figure 14a). From the  $\alpha$ -Si:H TFT characteristic of figure 12b) it is clear that applying +15V<sub>GD</sub> to the gate electrode allows current I<sub>SD</sub> to flow between the source and drain due to the signal voltage V<sub>SD</sub> applied to the column, whereas -5V on the gate turns the TFT off and prevents current from flowing. With the scheme of figure 14a), the transistors in each of the un-addressed rows (rows  $n-1$  and  $n+1$ ) are turned OFF by the negative signal applied to the gate bus lines, whilst the transistors in the addressed row (row  $n$ ) are opened using +15V<sub>GD</sub> to the gate electrodes and switched ON. Synchronously, data voltages are applied to the source bus; there is no current for any of the OFF rows, but the pixels on the ON row are charged to the appropriate voltage by the current I<sub>SD</sub>. After sufficient

time for the pixel to charge to the new level  $\tau$ , the gate is reclosed (with -5V<sub>GD</sub>) and the gate pulse (+15V<sub>GD</sub>) scans to the next row and new data on the source columns. The frame is completed when all  $N$  rows have been scanned, after the frame time  $\tau N$ . It is important to ensure that the liquid crystal material is exposed to the minimum net DC over several frames. To help ensure this, the polarity of the data signal is reversed, using frame-inversion, scan-line inversion, column inversion or pixel inversion (shown in figure 14a).

To understand some of the important design rules for a TFT LCD, consider the example of a 16.3” QSXGA monitor. It has 2048 x 2560 pixels at 202dpi, with the RGB sub-pixels on the columns (to maximise the time required to address each row). Such a panel typically has an aperture ratio of 27% and operates at 60Hz ( $\tau = 8.1\mu\text{s}$ ). That is, the sub-pixel dimensions are about 22 $\mu\text{m}$  x 65 $\mu\text{m}$  and a pixel capacitance  $C_{LC}$  of 0.16pF (assuming a cell gap of  $d = 4\mu\text{m}$  and permittivity  $\epsilon_{LC} = 5$ ).

Firstly, the pixel should not fully discharge within the 16.7ms frame time due to the off current of the transistor. Assuming an exponential decay, and a 1% voltage tolerance gives the condition [78]:

$$\tau_{OFF} = C_{LC} \cdot R_{OFF} \approx C \frac{V_{SD}}{I_{SD}} > 200\tau N \quad (60)$$

The  $\alpha$ -Si characteristic from figure 12b) shows I<sub>SD</sub> is 20pA when the TFT is OFF and 10 $\mu\text{A}$  when ON. Hence, equation (60) suggests that the TFT had a sufficiently low OFF current to drive a pixel of capacitance 6pF, easily sufficient for the 40pF pixels used in the original work of reference [74], but is far too leaky to drive the 0.16pF of a modern QSXGA monitor. Simply employing a storage capacitance  $C_S$  in parallel with the pixel, as shown in figures 13 and 14, increases the capacitance to the desired level and ensures that the pixel remains charged throughout the frame. Similarly, I<sub>SD</sub> in the ON condition for the highest signal level V<sub>SD</sub> should be sufficiently high to charge the pixel to at least 99% of that voltage level

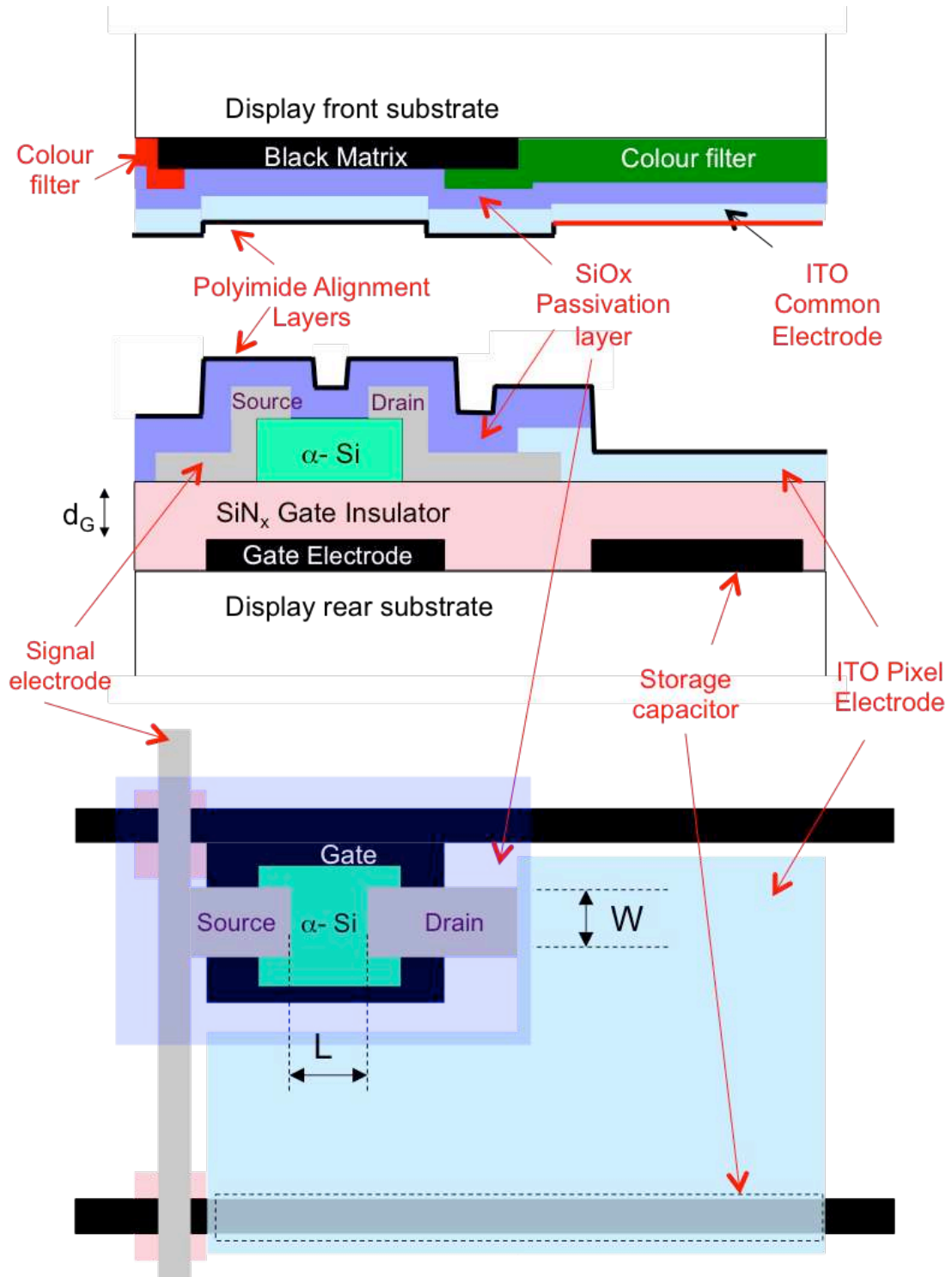


Figure 13 Cross-section and Plan views of a typical TFT driven sub-pixel on a backlit colour LCD.

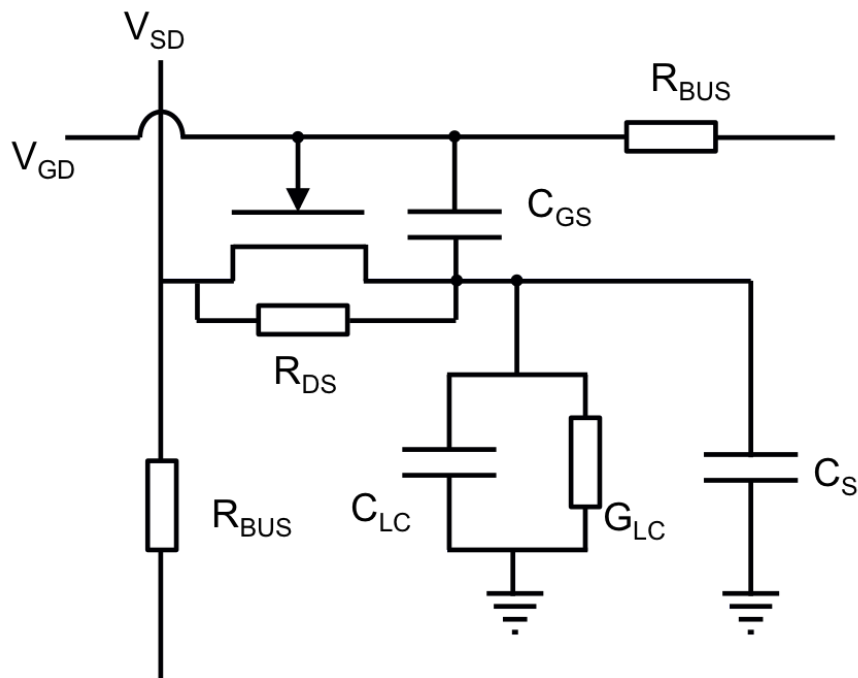
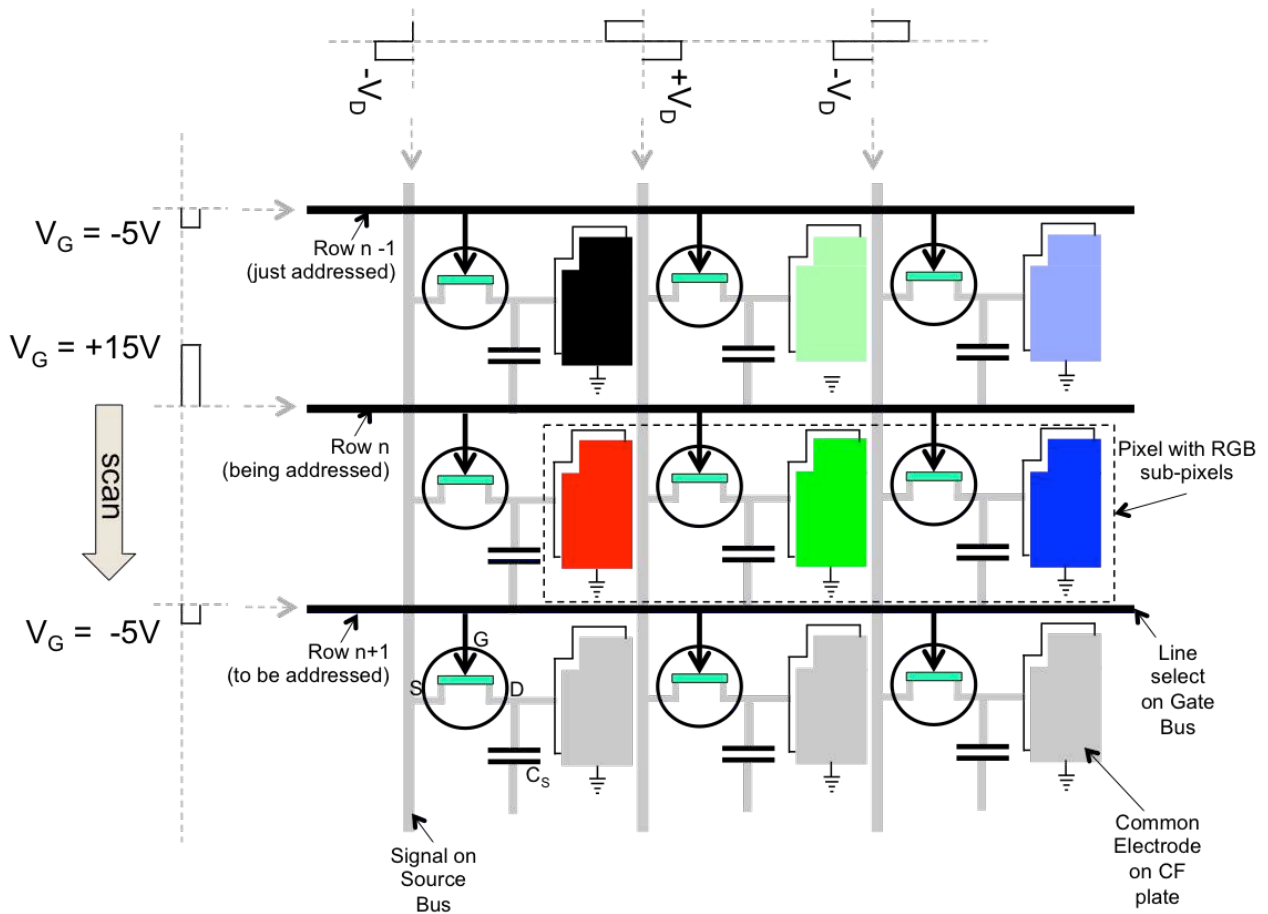


Figure 14. a) Active Matrix addressing of an LCD panel. b) Equivalent circuit for the pixel including the TFT parasitic losses, line losses and the conductance of the liquid crystal.

within the addressing time  $\tau$ , which occurs when  $\tau_{ON}$  is 10% of the addressing time  $\tau$ :

$$\tau_{ON} = C \cdot R_{ON} \approx (C_S + C_{LC}) \frac{V_{SD}}{I_{SD}} < 0.1\tau \quad (61)$$

Equations (60) and (61) can be combined to find the maximum number of lines that can be addressed by a TFT,  $N_{max}$ , with a given ration of ON to OFF currents:

$$N_{max} = \frac{1}{2000} \cdot \frac{I_{SD(ON)}}{I_{SD(OFF)}} \quad (62)$$

The characteristic of reference [73] shown in figure 12b) suggests that the original TFT could address up to 250 lines (as was claimed) but required improvement to address the 2048 rows of the monitor display. Some of the improvements to TFT performance made to achieve such high levels of multiplexing, 256 grey levels and high contrast ratios are outlined in the following discussion.

The equivalent circuit for a more realistic pixel is shown in figure 14b). The TFT includes an inherent resistance for the semiconductor  $R_{DS}$  and the capacitance per unit area of the gate  $C_{GS}$ . Also important is the conductivity of the liquid crystal itself  $G_{LC}$  and the resistance of the bus lines  $R_{BUS}$ . The simplest model for field effect transistors predicts that for sufficiently high gate voltages, well above the transistor threshold  $V_{th}$  and drain voltage  $V_{SD}$ , the current  $I_{SD}$  is given by [78]:

$$I_{SD} = \mu_e C_{GS} \frac{W}{L} \cdot \left( V_{GD} - V_{th} - \frac{1}{2} V_{SD} \right) V_{SD} \quad (63)$$

where  $\mu_e$  is the electron mobility,  $W$  is the width of the TFT channel and  $L$  its length, as defined in figure 13. The TFT threshold is typically about +3V, and is directly related to the charge density of free electrons  $n_0$ :

$$V_{th} = -en_0 \frac{d_G}{C_{GS}} \quad (64)$$

where the gate capacitance per unit area  $C_{GS}$ :

$$C_{GS} = \frac{\epsilon_0 \epsilon_{\alpha Si}}{d_G} \quad (65)$$

and  $d_G$  is the thickness of the  $\text{SiN}_x$  insulator layer, figure 13. The  $\alpha$ -Si leakage resistance dominates the off current:

$$I_{SD} = \frac{W}{L} \cdot \frac{V_{SD}}{R_{DS}} \quad (66)$$

Substituting equations (63) and (66) into (62) gives the relationship:

$$N_{max} \sim \mu_e C_{GS} R_{DS} \quad (67)$$

That is, achieving the low OFF current is achieved by reducing the transistor width to length ratio  $W/L$ , but the high ON to OFF current ratio, and hence maximum number of lines that can be addressed, is achieved by reducing the thickness of the insulating and semiconducting layers, leading to a typical  $C_{GS}$  of about  $0.1 \mu\text{F}/\text{cm}^2$ . A low insulator thickness has the additional benefit of reducing the area of the storage capacitor and correspondingly increases the aperture ratio. Figure 12b) also includes the characteristic of a TFT used for modern LCD panels, such as the QSXGA monitor describe earlier (where  $W/L = 10 \mu\text{m} / 6 \mu\text{m}$ ).

Decay of the voltage across the pixel is not just related to the leakage current of the transistor and equation (60): loss of charge across pixel occurs if the conductivity of the liquid crystal  $G_{LC}$  is too high. This is quantified by the voltage holding ratio (VHR), which represents the time it takes for the pixel voltage to decay to 50% [79]:

$$VHR = \sqrt{\frac{R_{ON}C}{2\tau N} \left( 1 - e^{-\frac{2\tau N}{R_{ON}C}} \right)} \quad (68)$$

Ionic impurities in the liquid crystal must be minimised to maximise VHR, and hence maintain a high display contrast. This cannot be done with nitrogenated compounds, preventing the use of highly polar materials such as the cyano-biphenyls. Instead, per-fluorinated compounds are essential. Although

mixtures produced from such compounds have a much lower  $\Delta\epsilon$ , this is compensated by the low viscosity and hence fast switching speeds that can be achieved with these materials [79].

The pixel aperture ratio and hence the transmission efficiency of the backlight is dictated by the target display resolution, the area of the panel (due to the losses caused by  $R_{BUS}$ ) and the fabrication tolerances. A typical TFT is fabricated as follows [78]:

1. The gate metal, usually Cr or Mo, is sputtered onto clean glass to a thickness of about 200nm.
2. The first set of electrodes are wet-etched: photoresist is printed over the glass area and exposed through a large area chrome mask placed with very high accuracy using a mask-aligner. This is then developed to form the gate electrodes and bus line, and the bottom electrode of the storage capacitor.
3. Plasma-enhanced Chemical Vapour Deposition (PECVD) is used to deposit 400nm of  $Si_3N_4$ , followed by 130nm of intrinsic  $\alpha$ -Si and 50nm of  $n^+$   $\alpha$ -Si:H.
4. The source, drain and storage capacitor electrodes are then formed by sputtering Cr over the surface and wet etching the appropriate patterns, again using a wet etching process and mask aligner.
5. The chrome electrode then acts as a self-aligned mask for plasma etching of the  $n^+$   $\alpha$ -Si:H to complete the source and drain electrodes (often using an etchant stopper).
6. The remaining intrinsic  $\alpha$ -Si:H is plasma etched away using a third mask and mask aligner step, thereby forming the TFTs.
7. The ITO is sputtered and plasma etched to form the pixels using a fourth mask and alignment step.
8. The last step uses PECVD to deposit the 350nm of  $SiNx$  or  $SiOx$  barrier layer, and uses a fifth mask to provide access to the bonding pads. A mask aligner is not usually required for this step that is far less critical than the previous photolithographic steps.

Each of the four critical mask alignment steps needs very high resolution to prevent panel variability. These steps are expensive, and various attempts to reduce the number of mask steps have been attempted, including the use of back-to-back diodes. High tooling costs lowers the design flexibility, and so TFT panels tend to be available only in a range of standard sizes and resolutions. If the requirement is for non-standard size in a niche market, the end-user may need to choose a passive matrix approach, which is why the market for passive matrix displays remains strong despite the poorer performance. For a given display diagonal, the aperture ratio decreases linearly with increasing resolution. Various other pixel designs to that shown in figure 13 have been suggested, often involving alternative placement of the storage capacitor. However, very high display resolutions require a different approach, such as the use of low-temperature poly Silicon (LTPS).

Poly-crystalline silicon (p-Si) was amongst the first semiconductors to be used for LCDs [81], and found in the first applications for TFT by *Canon* as the watch used in the 1983 film *Octopussy*, and *Sharp's* 1991 hang-on-the-wall TV [7]. The material has a high mobility of 200-400  $cm^2/Vs$ , which is intermediate between the 1.5  $cm^2/Vs$  of amorphous silicon and 1400  $cm^2/Vs$  for crystalline. Such high mobilities allow far smaller transistors, higher ON currents (particularly important for Organic Light Emitting Diode OLED displays), and potentially integrating the display drivers onto the glass itself. This latter advantage potentially leads to significant overall cost savings, because the drivers would be produced in the same process steps as the pixel TFT. The problem with producing p-Si TFTs were the very high processing temperatures, requiring those early demonstrators to be produced on quartz substrates. In the mid-1980s [81], low-temperature poly silicon (LTPS) TFTs were fabricated using excimer laser annealing of the  $\alpha$ -Si to form the polycrystalline structure whilst keeping the processing temperature to 260°C, equivalent to that used for  $\alpha$ -Si. Today, many smart-phones benefit from the excellent properties of LTPS, which allows resolutions above 400dpi and better battery life due to the reduction in backlight power that the high aperture

ratio allows. However, the cost of LTPS is high, because the fabrication of the top-gate transistors required uses 9 to 11 critical mask steps: this typically adds about 20% cost to the panels over equivalent  $\alpha$ -Si LCDs.

Together with other disadvantages such as high leakage current, the high production cost of LTPS has driven research into other semiconductors, including various metal oxides. ZnO is particularly interesting, since it retains a high mobility, and combines a very high ON to OFF state current ratio with optical transparency over the visible region. Recently, the 1:1:1 combination of Indium Gallium and Zinc Oxide (IGZO) [82, 77] to form active element has been put into production by *Sharp*. A 50nm amorphous IGZO layer is nitrogenated to form the n+ doped semiconductor with a mobility of  $\mu_e = 10\text{cm}^2/\text{Vs}$ . Figure 12b) includes a comparison of the TFT transfer characteristics for  $\alpha$ -IGZO against both LTPS and  $\alpha$ -Si. Although IGZO has a lower mobility than LTPS, it combines a very high ON/OFF current ratio ( $>10^9$ ) with the same low-cost fabrication designs of  $\alpha$ -Si. It is likely that IGZO will play a leading roll in future display devices, as displays continue to move to ever higher pixel contents, resolutions and power efficiencies.

## 4 Standard LCD Modes

### 4.1 Overview

There is a wealth of different liquid crystals modes possible, some of the important ones being shown in figure 15. Some modes have niche applications, such as the cholesteric temperature sensor or the zenithal bistable display (ZBD) and these will be described in the section 5. Modes that have contributed to the mainstream LCD markets, from the early watches and calculators to today's full colour video rate displays are covered in this section.

The evolution of the modern LCDs used in mobile phones, computer monitors and HDTV has been undertaken in several stages, exemplified by listing the major advances, as in table 4. After the basic principles had been evaluated, as described in the previous sections, the most important step was to

increase the complexity of the display to allow hundreds of lines of information to operate at video-frame rate, with grey-scale and colour. By the mid 1990s, the technological steps to achieve this had largely been satisfied through the adoption of the TFT active backplane. At that point, the race moved from complexity to appearance and in particular improving poor viewing angles. Several new modes were developed, each finding market success for different manufacturers, first allowing LCDs to replace cathode ray tubes (CRT) in computer monitors and in 2007, surpass CRT sales for TV. However, the war shifted to new battle grounds and yet further improvement of appearance, including ultra-high resolution and wide-colour gamut drive the competition in the mobile telecommunications marketplace. Before describing the individual modes, it is apposite to discuss the technological and market forces that dictated each shift in stage.

Following the discovery of the Alt-Pleshko multiplexing limit for passive matrix addressing [69] maximising display content was the key driver for the LCD industry throughout the 1980s and early 1990s. Several approaches were taken:

1. Increasing the gradient of the LC transmission-voltage response, either through material improvement (controlling the elastic constant ratio  $k_{33}/k_{11}$ ) or new LCD modes (supertwist nematic, STN).
2. Designing bistable LCD modes, where pixels no longer responds to the RMS signal over the frame, but are rapidly latched between the ON and OFF states and remains in the desired state after the signals applied.
3. Introducing a non-linear element, such as a TFT, that isolates and delivers the appropriate signal to each pixel.

The first of these approaches was successful for low-cost, black and white STN displays, but was limited by the slow frame time, low number of grey-levels and a maximum of 480 multiplexed lines. Many novel methods for making an LCD inherently bistable were invented at the end of the 1970s and beginning of the 1980s [101]. The most promising bistable technology was the surface stabilised ferroelectric LCD, invented

Table 4 Significant advances on route to LCD market dominance.

Year	Invention	Protagonists	Ref.	Stage
1967	Dynamic Scattering Mode	Heilmeier et al., <i>RCA; US</i>	[3, 4]	Basics
1971	Active Matrix Addressing	Lechner et al., <i>RCA; US</i>	[70]	
1971	Twisted Nematic Mode (TN)	Schadt and Helfrich, <i>BBC; CH.</i> Ferguson, <i>U. Kent; US</i>	[14] [83]	
1971	Vertically Aligned Nematic Mode (VAN)	Kahn, <i>Bell Labs; US</i> Schiekel and Fahrenscho <i>AEG-Telefunken; W. Germany</i>	[84] [85]	
1973	Cyano-biphenyl Nematics	Gray et al. <i>Hull, RSRE, BDH; UK</i>	[15]	
1973	Formulation of Wide temperature range eutectic LCD for TN	Raynes <i>RSRE, UK</i>	[16]	
1973	In-plane switching proposed	Kobayashi, <i>U. Tokyo; JP</i> Soref, <i>Sperry; US</i>	[86] [87]	
1973	First commercial LCD products in calculator and wristwatch	Wada et al., <i>Sharp; JP</i> <i>Seiko; JP</i>	[7]	
1974	Defect-free TN	Raynes and Waters <i>RSRE; UK</i>	[58]	
1979	First amorphous silicon TFT used to address LCD	Spear and Le Coomber, <i>U. Dundee; UK</i> Hilsum, Hughes, <i>RSRE; UK</i>	[72] [73]	
1980	Bistable Surface Stabilised Ferroelectric (SSFLC)	Clark and Lagerwall, <i>U. Göteborg, SE</i>	[88]	
1982	Supertwist Mode (STN)	Raynes <i>RSRE; UK</i>	[89]	
1984	Supertwist Birefringence Effect (SBE)	Scheffer and Nehring <i>BBC, CH</i>	[90]	
1987	Foil compensation for STN	Katoh, <i>Asahi Glass; JP</i>	[91]	
1992	In Plane Switching Mode (IPS)	Baur et al., <i>Merck; DE</i> Kondo et al., <i>Hitachi; JP</i>	[92] [93]	Wide Viewing Angle
1997	Multi-domain Vertically Aligned Mode (MVA)	Koike and Okamoto, <i>Fujitsu; JP</i>	[94, 95]	
1998	Fringe Field Switching Mode (FFS)	Lee et al., <i>Hyundai; KR</i>	[96, 97]	
2000	Patterned Vertical Alignment Mode	Kim et al., <i>Samsung; KR</i>	[98]	
2001	Axially Symmetric Mode (ASM)	Yamada, Ishii et al., <i>Sharp; JP</i>	[99]	
2004	IGZO TFT invented	Nomura et al., <i>Tokyo Institute of Technology, JP</i>	[82]	Improved resolution and colour
2010	QD enhanced colour backlights	Jang, et al., <i>Samsung, KR</i>	[100]	

in 1980 [88], launching an immense worldwide effort for the next fifteen years in a two-way battle between the FLC and TFT approaches. The complexity of TFT fabrication seemed to promise higher costs over the passive matrix bistable approach. However, despite the launch of a colour SSFLC monitor by *Canon* in 1992 (figure 16d), the TFT-driven TN display was already beginning to enable the image quality required for a new market: the laptop. Early laptop screens were black and white only (such as *Apples's MacIntosh Powerbook 100*, released in October 1991) but the sensitivity of SSFLC to shock made the technology unsuited to portable products. Whilst there was no superior alternative to the TFT-TN LCD for laptop displays, the competition for the SSFLC monitor came from the superior performance and much lower cost of the CRT, and well before the end of the 1990s, the

SSFLC development effort targeting mainstream displays was minimal.

Buoyed by early commercial success from laptops, the TFT TN would attract sufficient investment to explore new modes, targeting shifting the incumbent CRT from the monitor, and eventually TV, markets. The use of TFTs brought with it a new and very important advantage: the flexibility of LC mode design. Modes that had previously been impossible to multiplex became potentially useable. In the late 1990s, modes such as In-Plane Switching (IPS) [92, 93] and Multi-domain Vertically Aligned (MVA) nematic [94, 95] offered sufficiently wide viewing angles to displace the CRT. By the beginning of the new millennium, the LCD was dominant from watches and calculators, to large area monitors [102], as shown in figure 16.

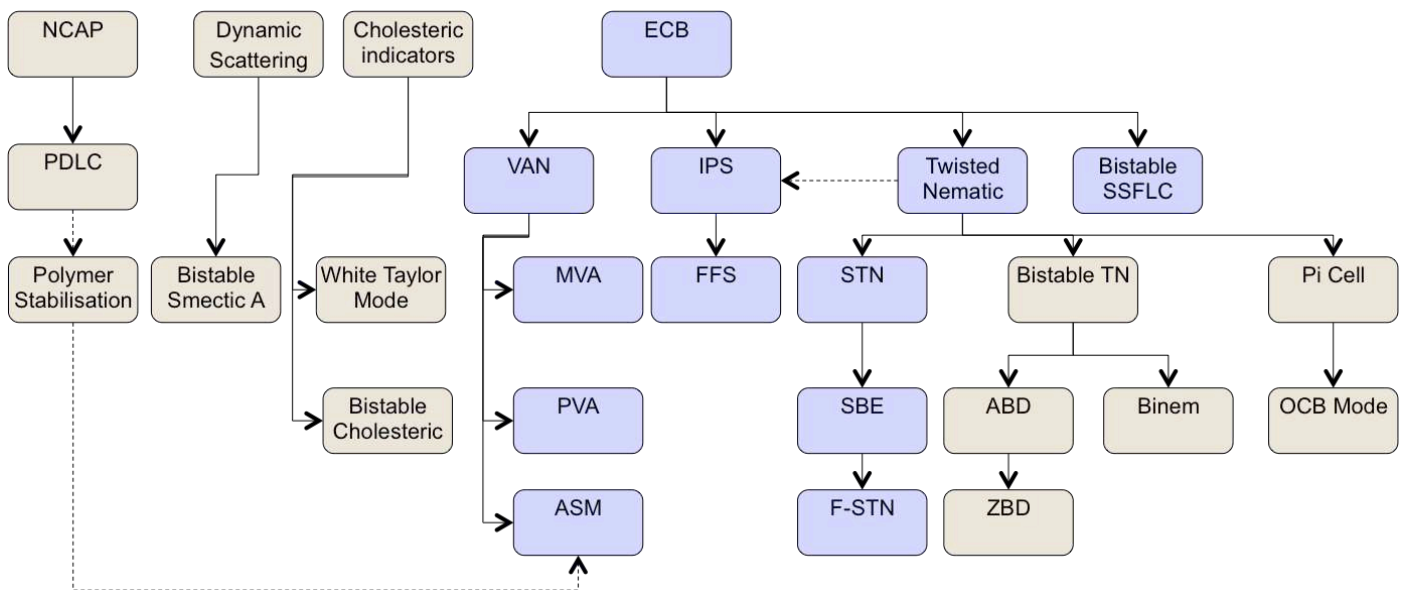


Figure 15 Dendrogram of the important LC modes. The LCD mainstream described in section 4 is indicated by the blue colouration. Abbreviations used are: PDLC: Polymer dispersed liquid crystal; ECB: Electrically controlled birefringence; VAN: Vertically Aligned Nematic; IPS: In-plane switching; MVA: multi-domain vertically aligned; PVA Photo-aligned vertical alignment; ASM: Axially symmetric mode; FFS: Fringe field switching; STN: Supertwist nematic; SSFLC: surface stabilised ferroelectric liquid crystal; SBE: Supertwisted birefringence Effect; F-STN: film / foil compensated STN; ABD: Azimuthal bistable display; ZBD: Zenithal Bistable Display; OCB: Optically compensated bend-mode.

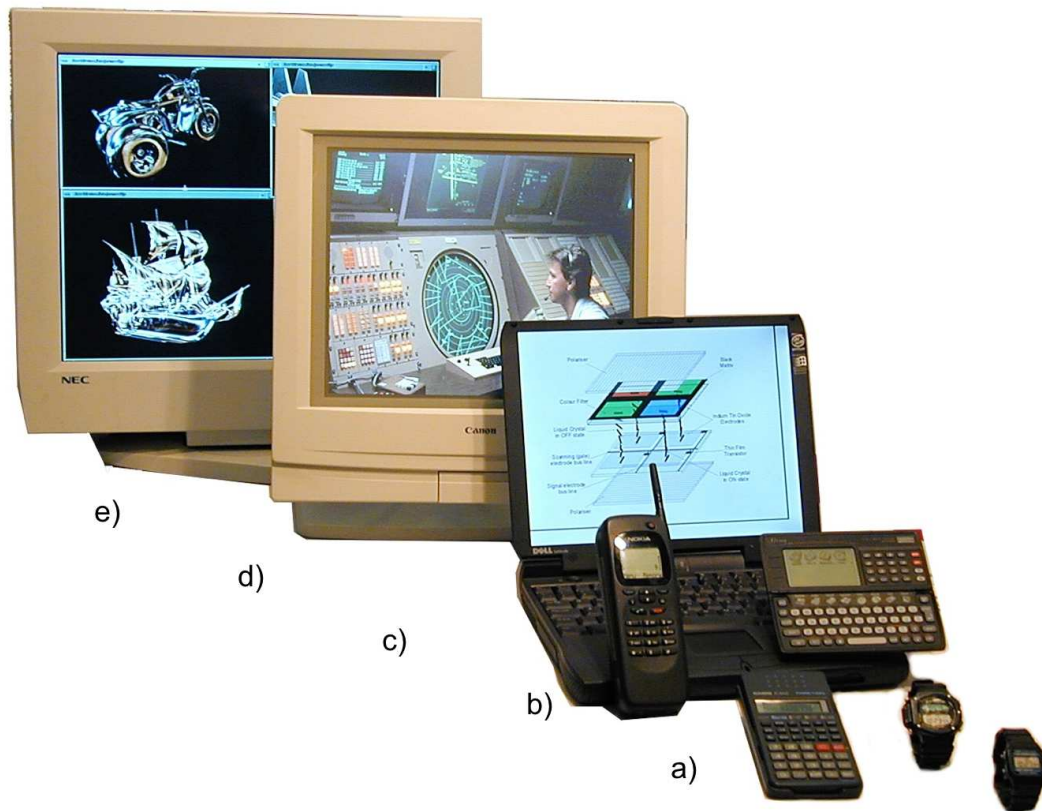


Figure 16: State of the Art LCD at the turn of the Millennium. a) Watches and calculators using the reflective TN; b) A dual display phone and PDA using foil compensated STN; c) a laptop computer with TFT driven TN; d), a 14" monitor display based on bistable SSFLCD; and e), one of the first IPS mode TFT monitors. [100].

The battle for the television market was complicated by another new technology: the plasma display panel (PDP). As an emissive display, the viewing angle and contrast of PDP could not be surpassed by LCDs. This gave PDP an early lead in the flat-panel television market. However, on-going LCD improvements, such as the invention of the fringe-field-switching (FFS) mode [96, 97], and the inability to fabricate high resolution PDP below 40", led to the eventual triumph of LCDs in this most important of markets too.

Coincident with LCD domination of the TV display market, the first i-Phone was launched in June 2007, heralding the age of the smart-phone. The goal of providing resolution at the limit of visual perception helped drive LTPS into the marketplace. However, LTPS also had the advantage of providing higher ON

currents than was possible, thereby meeting the requirement for another emissive display technology: Organic Light Emitting Diodes (OLED). Not only do OLED surpass LCD for contrast and viewing angle, but also for colour saturation. Again, the adaptability of LCD technology provides a solution: replacing the cold-cathode backlights with a blue LED, and adding a film containing red and green quantum dots (QD), provides sharper colours than is possible using colour filters alone [100]. Once more, LCD performance increases to meet the market challenge. Mid-way through the 2010s, OLED is making grounds for portable displays, where features such as form factor and weight also play an important role, but LCDs continues to dominate in all other markets, figure 17. Will OLED eventually replace the LCD altogether? At each stage of LCD evolution, new markets have been

enabled by particular LCD modes. Many of these modes have retained their market share despite more advanced options becoming available. Whether it is the simple twisted nematic in watches and calculators,

the supertwist nematic for instrumentation, or TFT driven TN for low-cost monitors, the successful technologies become difficult to supplant once established.



Figure 17: History of the mainstream of LCD, from the calculator to QD 4k FHD TV.

#### 4.2 Dynamic Scattering mode

The first operating liquid crystal device was an electro-optic shutter, devised by Heilmeyer's predecessor at RCA, Richard Williams, in 1962 [103, 104]. Williams showed that strong turbulence could be induced in a roughly planar sample of a negative  $\Delta\epsilon$

nematic with a DC or low frequency AC field. This turbulence was induced by ionic flow in the liquid crystal disrupting the liquid crystal, thereby causing strong optical scattering in the birefringent medium. Heilmeyer used this switching between scattering and non-scattering states in RCA's first display demonstrators in 1968. Unlike most of the other

modes described, Dynamic Scattering Mode devices did not need polarisers and operating in a 20 -100 $\mu$ m spaced cell at typically 30 – 50V. The onset voltage for scattering is approximately [105]:

$$V_C \sim T \frac{\eta \mu}{\epsilon} \quad (69)$$

where  $\eta$  is the bulk flow viscosity,  $\mu$  is the ion mobility, and  $T$  is a constant typically about 100. For  $\eta = 0.5$  Pa.s and  $\mu = 10^{-4}$  cm<sup>2</sup>/Vs then  $V_C$  is about 5 - 10V. The resistivity of the liquid crystal could be made lower than 10 G $\Omega$ .m through deliberate addition of mobile ionic impurities. The original displays of Heilmeyer used DC fields to induce the ion flow, presumably because of the desire to address the devices using transistors. However, the lifetime was too short due to electrostatic breakdown effects, and so the first commercial devices used low frequency AC instead.

### 4.3 The Twisted Nematic LCDs

#### 4.3.1 Introduction

By 1980, practically all commercial LCDs were based on the twisted nematic. This device set the benchmark for future developments, operating using alignment layers to obtain a uniformly aligned director profile, a cell gap of a few microns sandwiched between polarisers either side. The electro-optic effect is the basic Fréedericksz transition described in section 3.3, wherein the director responds to the RMS voltage coupling to the dielectric anisotropy affecting a change to the birefringence profile through the device, and hence altering the polarisation state of the transmitted light. Each of the remaining devices described in this section uses these principles (although the FLC is a field effect device, with a polar coupling of the field to the ferroelectric spontaneous polarisation). The twisted nematic uses a positive  $\Delta\epsilon$  material, and usually a 90° twist between top and bottom surfaces, with either crossed or parallel polarisers, to operate in normally white (NW) or normally black (NB) modes, respectively. Applying a voltage three or four times greater than the threshold (i.e. applying typically 5V)

causes sufficient reorientation of the director in the bulk of the cell to cause the NW cell to appear dark, and the NB cell bright. TN may be used in transmission, usually driven by TFT and including colour filters, or may be used as a two-polariser reflective mode. In this latter device, the rear polariser incorporates a diffusive reflector so that light incident from the front of the panel is reflected back through the device for a second pass. This leads to a much higher contrast ratio, since any light leakage in the dark state from the first pass is dramatically reduced on the second. However, it also means that the colouration of the white state is more important. Also possible are single-polariser reflective modes, as described at the end of this section.

A key part of any display design is to ensure uniformity of texture for the ON and OFF states. For a 90° TN this means ensuring that degeneracy of both twist and tilt are removed [58]. For twist alone this is simply done using slightly uncrossed alignment directions or, preferably, by inducing a natural sign of twist with the addition of a small amount of cholesteric to give a pitch of a few hundred micron. Removing tilt degeneracy requires that there is pre-tilt on both alignment surfaces. However, it remains essential that the pre-tilt and sign of twist are matched, so that there is minimal splay from one surface to the other when undergoing the correct twist. Otherwise, reverse tilt and twist domains may still form as the director relaxes to the quiescent state after switching.

#### 4.3.2 The OFF State and TN Design

The polarisation optics from a uniformly aligned birefringent liquid crystal cell was calculated in section 3.2. It was shown that the polarisation state after transmission through multiple elements is calculated simply by multiplying the appropriate Jones matrices together. The twisted nematic has a director twist angle that varies linearly from one surface to the other. Thus, it can be described as a series of very thin birefringent retarders, each with a slightly different orientation angle. Slicing the device into  $N$  layers, the retardation and orientation of each is given by:

$$\frac{\Gamma}{N} = \frac{2\pi\Delta n d}{\lambda N} ; \phi_{j+1} = \phi_j + \frac{\Phi}{N}, j = 0, 1, 2, \dots, N-2 \quad (70)$$

where  $\Phi$  is the total twist angle. The overall Jones matrix  $M$  is the multiplicative sum of each of these elements  $M_j$ :

$$\begin{aligned} M &= \prod_{j=1}^N \left( R(\phi_j) \cdot M_j \cdot \overline{R(\phi_j)} \right) \\ &\equiv \prod_{j=1}^N \left( R(-\phi_j) \cdot M_j \cdot R(\phi_j) \right) \\ &= R(-\Phi) \left[ \begin{pmatrix} e^{-i\frac{\Gamma}{2N}} & 0 \\ 0 & e^{i\frac{\Gamma}{2N}} \end{pmatrix} R\left(\frac{\Phi}{N}\right) \right]^N = \\ &R(-\Phi) \left[ \begin{pmatrix} \cos\frac{\Phi}{N} e^{-i\frac{\Gamma}{2N}} & \sin\frac{\Phi}{N} e^{-i\frac{\Gamma}{2N}} \\ -\sin\frac{\Phi}{N} e^{i\frac{\Gamma}{2N}} & \cos\frac{\Phi}{N} e^{i\frac{\Gamma}{2N}} \end{pmatrix} \right]^N \quad (71) \end{aligned}$$

As  $N$  tends to infinity, then each retarder becomes infinitesimally thin, and [106]:

$$M = \begin{pmatrix} \cos\Phi & -\sin\Phi \\ \sin\Phi & \cos\Phi \end{pmatrix} \begin{pmatrix} \cos X - i\frac{\Gamma \sin X}{2X} & \Phi \frac{\sin X}{X} \\ -\Phi \frac{\sin X}{X} & \cos X + i\frac{\Gamma \sin X}{2X} \end{pmatrix} \quad (72)$$

where:

$$X = \sqrt{\Phi^2 + \left(\frac{\Gamma}{2}\right)^2}$$

Solving for the transmission:

$$T = \left\{ \cos X \cos(\Phi + \phi_1 - \phi_2) + \frac{\Phi}{X} \sin X \sin(\Phi + \phi_1 - \phi_2) \right\}^2 + \left\{ \left[ 1 - \left(\frac{\Phi}{X}\right)^2 \right] \sin^2 X \cos^2(\Phi - \phi_2 - \phi_2) \right\} \quad (73)$$

where the input and output polariser directions with respect to the input director are  $\phi_1$  and  $\phi_2$ , respectively. As expected, equation (73) reduces to the transmission of a retardation plate, equation (25) if the

overall twist  $\Phi = 0$ , and crossed polarisers are used ( $\phi = \phi_1$  and  $\phi_2 = \phi_1 + 90^\circ$ ).

For the Normally White mode twisted nematic TN with  $\Phi = 90^\circ$ , the polarisers are crossed ( $\phi_2 = \phi_1 + 90^\circ$ ) and oriented with either  $\phi_1 = 0^\circ$  or  $90^\circ$ . The transmittance from equation (73) then simplifies to the Gooch – Tarry expression [107]:

$$T = 1 - \frac{\sin^2\left(\frac{\pi}{2}\sqrt{1 + \left(\frac{2\Delta n \cdot d}{\lambda}\right)^2}\right)}{1 + \left(\frac{2\Delta n \cdot d}{\lambda}\right)^2}, \quad (74)$$

and the value of  $\Delta n \cdot d$  is chosen to ensure that the right-hand term is zero for  $\lambda \approx 550\text{nm}$ , so that the TN appears white. If the polarisers are kept parallel instead, then the transmittance becomes:

$$T = \frac{\sin^2\left(\frac{\pi}{2}\sqrt{1 + \left(\frac{2\Delta n \cdot d}{\lambda}\right)^2}\right)}{1 + \left(\frac{2\Delta n \cdot d}{\lambda}\right)^2}, \quad (75)$$

and the TN is Normally Black at the same retardation conditions. Equations (74) and (75) are plotted versus retardation in figure 18. There is minimum with NB, maximum with NW, where the twisted structure of the birefringent material transmits linearly polarised light that is orthogonal to the input polarisation and perpendicular (for NB, parallel if NW) to the output polariser. This occurs at a series of conditions, given by:

$$\frac{\Delta n \cdot d}{\lambda} = \sqrt{m^2 - \frac{1}{4}}, \quad m = 1, 2, 3 \dots \quad (76)$$

including the first minimum at  $\Delta n \cdot d = \frac{1}{2}\sqrt{3} \lambda$  and second at  $\Delta n \cdot d = \frac{1}{2}\sqrt{15} \lambda$ . At any one of these minima (or maxima for the NW, although the term minima is used conventionally regardless of the polariser orientations), the transmission is least sensitive to changes in retardation (including viewing angle and cell non-uniformity) and polariser orientations. As the retardation is increased (i.e., for high cell gaps) successive minima are increasingly less sensitive to retardation changes until the Mauguin condition is

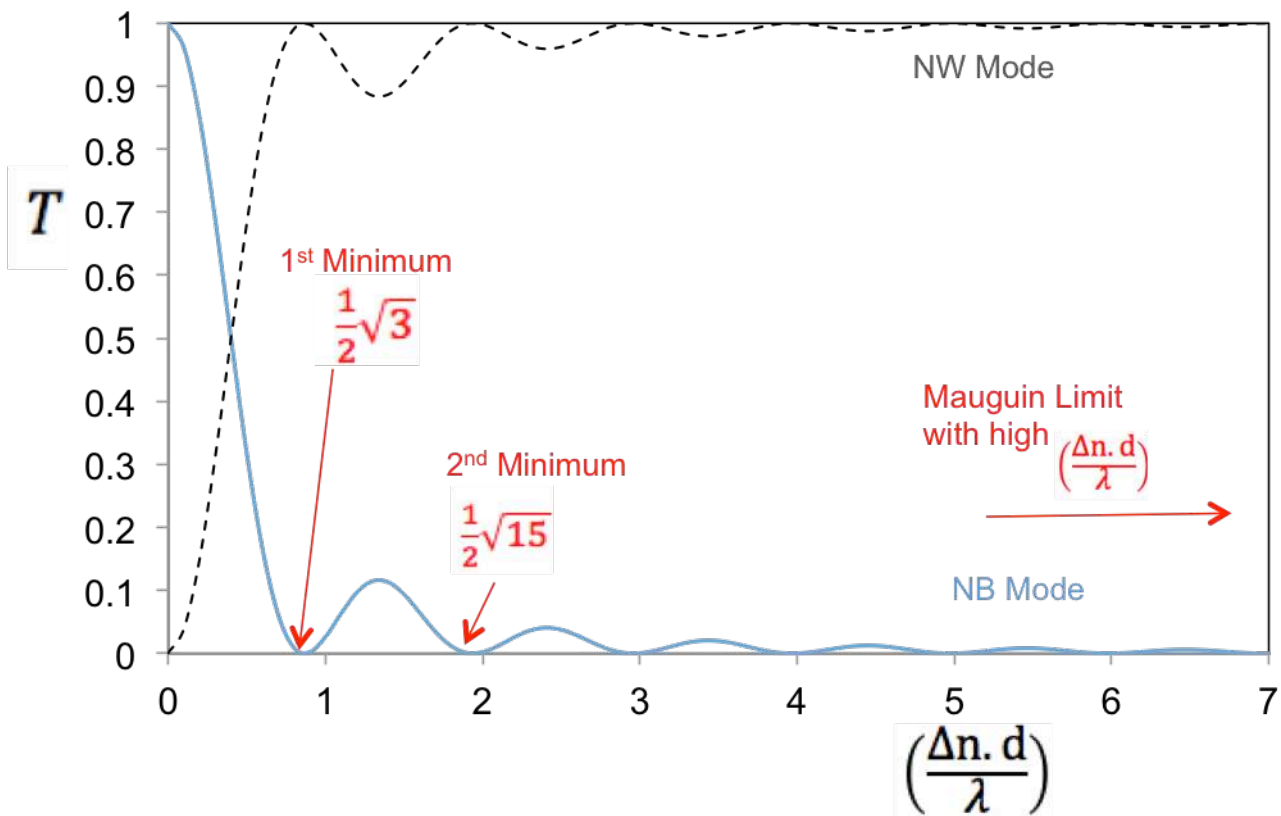


Figure 18 The Gooch-Tarry curve for the quiescent transmission of a 90° Twisted Nematic Display versus retardation, for normally black (NB) mode (parallel polarisers) and normally white (NW) mode (crossed polarisers).

approached at the high retardation limit [45], where polarised light transmitted by the cell is rotated through 90° regardless of cell gap, wavelength, temperature or polarisation angle.

The choice of retardation is dictated by fabrication limitations on cell gap, the operating speed that is required, the colouration of the white state and the required contrast. Response times depend on the square of the cell gap, through equation (48). This usually limits practical operation to either the first or second minimum condition. The wavelength dependences for 1<sup>st</sup> min. and 2<sup>nd</sup> min. devices are shown in figure 19. Again, choosing the wavelength to occur at the peak eye response of  $\lambda=550\text{nm}$ , the first and second Gooch – Tarry minima for a TN filled with 5CB are  $2.6\mu\text{m}$  and  $5.9\mu\text{m}$ , respectively. Most TFT LCDs operate at the first minimum, using lower birefringence materials,  $\Delta n \approx 0.1$  and  $d \approx 4.5\mu\text{m}$ ,

because this cell spacing is conducive to a high manufacturing yield and the switching speed is satisfactory. If switching speed is the priority, rather than use higher birefringence materials with the concomitant increases of viscosity, an alternative approach is to use a 75° twist, [67]. The first minimum peaks at a lower transmissivity than for a 90° cell (98.4%), but this can be corrected by reorienting the polarisers through -7.5°, as shown for the results in figure 19. Typically, the cell gap for the 75° TN mode is 80% that of the standard 90° TN, potentially leading to a 50% speed increase, provided the reduced cell gap remains suitable for manufacture.

For each of the modes, it is important to consider the colouration of the white state. For a backlit colour TN, this is less important than for a black and white reflective device, because any loss of white colour balance can be compensated in the

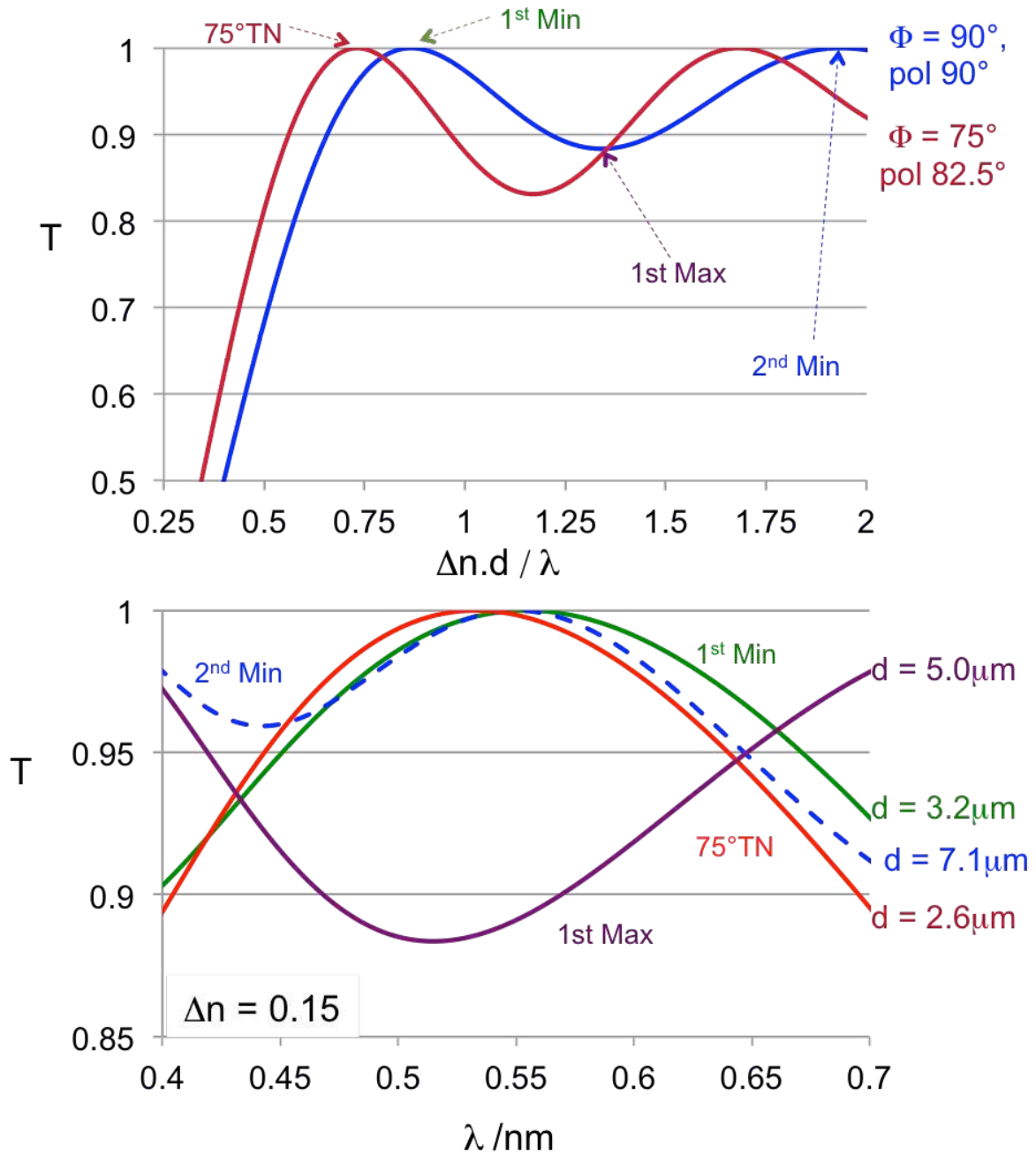


Figure 19 Choices of white state and cell gap for the TN. a) The Gooch Tarry curve for the 90° and 75° twist angle TN. b) Theoretical wavelength dependences of the transmission for a material with a typical birefringence ( $\Delta n = 0.15$ ) for 90° TN cells operating at the first minimum, first maximum and second minimum and for a 75° TN with uncrossed polarisers at 85°. The cell gaps are also indicated.

addressing signals, back light spectrum and colour filters. For a dual-polariser reflective display, the second pass of the light through the cell exaggerates any unwanted colouration.

Figure 19b) shows the theoretical wavelength dependences in transmission for four TN modes. Converting these spectra to CIE 1931 x and y colour co-ordinates, as shown in figure 20, gives a locus of

white hues depending on the retardation and the colouration of the polarisers [108]. Two loci are plotted, corresponding to a standard polariser centred on green and a slightly bluer variety. These polarisers represent the range of colours that can be targeted whilst retaining a black OFF state; narrower spectrum polarisers can also be used to modify the ON state colouration, but with a noticeable colouration of the dark state too. Also shown on the chart are the coordinates for the D65 standard, representing a target for the ideal white state. Operating at the first minimum tends to give a greenish hue to the white, state whereas, the second minimum gives an improved white, due to the increased blue transmittance shown in figure 19b). Thus, a second minimum TN is preferred for applications where the response time is unimportant (being five times slower than the equivalent first minimum mode) but the attractive bluish white is preferred. Alternatively, an intermediate retardation close to the point of the first maximum (i.e. at  $\Delta n.d/\lambda = \frac{2}{7}\sqrt{22}$ ) has been used [108] to produce a neutral white as close to the D65 standard as possible, particularly when combined with the

slightly blue tinged polariser. The optimum cell gap for this is:

$$d \approx \frac{1}{4\Delta n} (0.45\sqrt{15} + 0.68\sqrt{3}) \quad , \quad (77)$$

where the blue light is close to the second minimum and red wavelengths close to the first minimum, and the green transmittance is decreased somewhat, figure 19b).

The other important consideration for the OFF state is viewing angle. Figure 21a) shows a polar plot of transmissivity for the azimuthal and zenithal directions for a normally white 1<sup>st</sup> minimum TN operating in transmission. The OFF-state viewing angle is good: light at any azimuthal angle experiences the same retardation profile due to the twisted structure, and deviations of zenithal angle away from the display normal (shown as the central point) represent reduction of the effective retardation, to which devices operating at the Gooch-Tarry minima are insensitive.

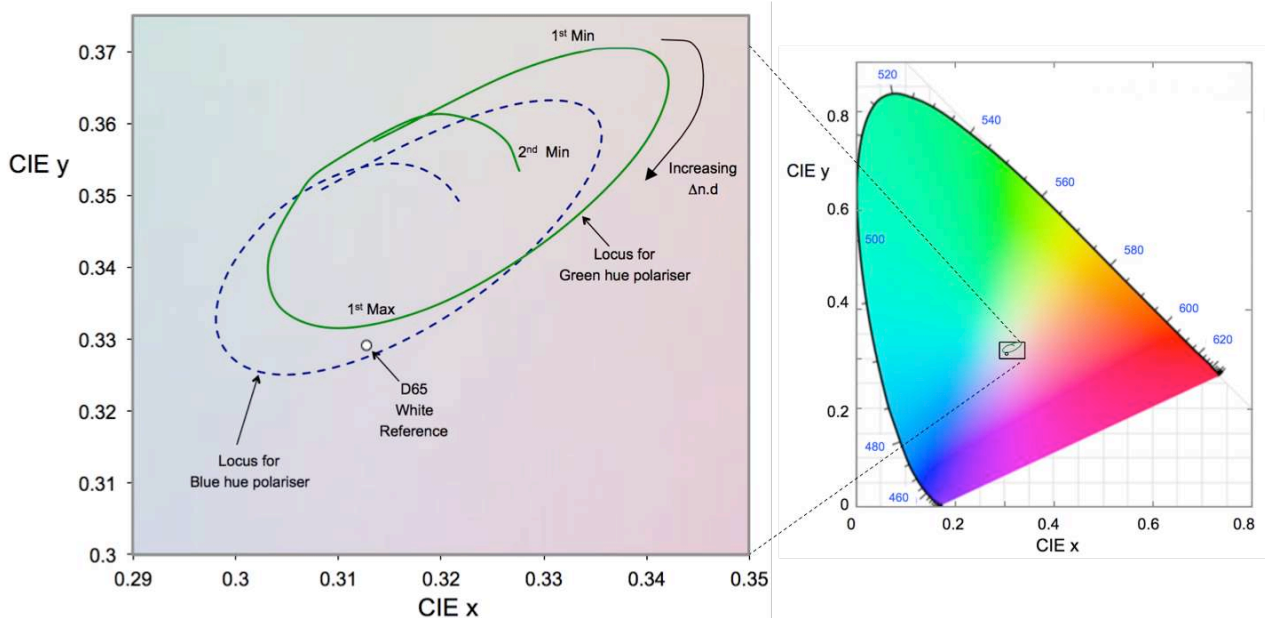


Figure 20 Central region of the CIE colour chart (shown in full on the right) indicating the region of white transmission for a dual-polariser reflective mode TN. Two loci are shown, corresponding to polarisers with a slightly green tint (continuous line) and a slightly blue tint (dashed). The D65 white state reference is shown as a target for pure white. The location on the colour chart of the 1<sup>st</sup> min, 2<sup>nd</sup> min and 1<sup>st</sup> maximum are indicated.

### 4.3.3 The ON State and Optical Compensation

The ON state transmission is very viewing angle dependent. This is evident from the contrast ratio of OFF / ON transmission shown in figure 21b) since contrast is dominated by the dark ON state transmission. The blackest ON state occurs when the light is transmitted parallel to the liquid crystal optic axis, the direction where the liquid crystal behaves as an isotropic medium and any light transmitted is due to leakage of the polarisers. Contrast is highest for on-axis light, since this is the direction of the applied field towards which the director reorients, although it remains affected by the distorted regions close to the surface. Off-axis light experiences a retardation with a direction dependence that is related to the director profile through the cell, which in turn depends on the applied voltage.

The Fréedericksz threshold voltage for a TN is given by:

$$V_C = \sqrt{\frac{\pi^2 k_{11} + \Phi^2 (k_{33} - 2k_{22})}{\varepsilon_0 \Delta \varepsilon}} \quad (78)$$

which simplifies to:

$$V_C = \pi \sqrt{\frac{k_{11} + (k_{33} - 2k_{22})/4}{\varepsilon_0 \Delta \varepsilon}} \quad (79)$$

for a standard  $\Phi = 90^\circ$  TN. Often,  $k_{22} \approx k_{33}/2$  in practice, and so the Fréedericksz threshold is similar to that of the ECB mode, and typically around 1V. Figure 21c) shows schematically what happens as the voltage is increased above  $V_C$ , and numerical calculations of the response for typical elastic constants are given in figure 21d). As the voltage increases, the initially linear twist from one surface to the other becomes increasingly concentrated into the centre of the cell where the director approaches the vertical condition, whereas regions of splay and bend are increasingly pushed towards the surfaces. Thus, the director profile approaches a vertically aligned central region, with twist-free splay-bend regions oriented at  $90^\circ$  to each other close to the two surfaces. The optical transmission through the cell is complex and requires numerical modelling. The voltage

dependence of the normal incidence transmittance can be estimated by considering the mid-plane tilt of the director  $\theta_m$  [109, 110]. Immediately, above  $V_C$  this is:

$$\theta_m^2 = 4 \left( \frac{V}{V_C} - 1 \right) / \left( \frac{k_{33} - \left( \frac{\Phi}{\pi} \right)^2 \left[ \frac{k_{33}^2}{k_{22}} + k_{22} - k_{33} \right]}{k_{11} + \left( \frac{\Phi}{\pi} \right)^2 [k_{33} - 2k_{22}]} + \frac{\Delta \varepsilon}{\varepsilon_{\perp}} \right) \quad (80)$$

which becomes, for the  $90^\circ$  TN cell:

$$\begin{aligned} \theta_m^2 &= \\ 4 \left( \frac{V}{V_C} - 1 \right) &/ \left( \frac{5k_{33} - \left[ \frac{k_{33}^2}{k_{22}} + k_{22} \right]}{4k_{11} + [k_{33} - 2k_{22}]} + \frac{\Delta \varepsilon}{\varepsilon_{\perp}} \right) \\ &\approx 4 \left( \frac{V}{V_C} - 1 \right) / \left( \frac{5k_{33}}{8k_{11}} + \frac{\Delta \varepsilon}{\varepsilon_{\perp}} \right) \end{aligned} \quad (81)$$

for the reasonable approximation  $k_{33} \approx 2k_{22}$ . Given the surface pre-tilt is small, this expression represents the linear part of the transmission - voltage characteristic above  $V_C$  shown in figure 9b). The multiplexibility of the TN is related to the steepness of this characteristic through the Alt-Pleshko expression, equation (54). Thus, to ensure the highest number of lines that a passive-matrix TN can be multiplexed, the denominator of equation (81) should be kept low. This is done in practice using hybrid mixtures of polar and non-polar compounds [111], in which  $k_{33}/k_{11}$  is lowered due to short-range order effects, offered a route to multiplexing of up to 20 lines.

Off-axis calculations of the transmissivity for the ON state certainly require numerical modelling. However, the form of the contrast ratio curve shown in figure 21b) is anticipated by considering the director profile of the high voltage state as a vertically aligned nematic in the bulk, with two orthogonal hybrid aligned states in the surface regions. The director in these two regions are oriented parallel to the polarisers, at azimuthal directions  $45^\circ$  and  $135^\circ$  in figure 21b), and hence appears dark at all angles. This understanding led to pronounced improvements of transmissive mode TN viewing angles through optical compensation. Discotic liquid crystals are similar to the standard rod-like calamitic mesogens used in displays but exhibit negative birefringence.

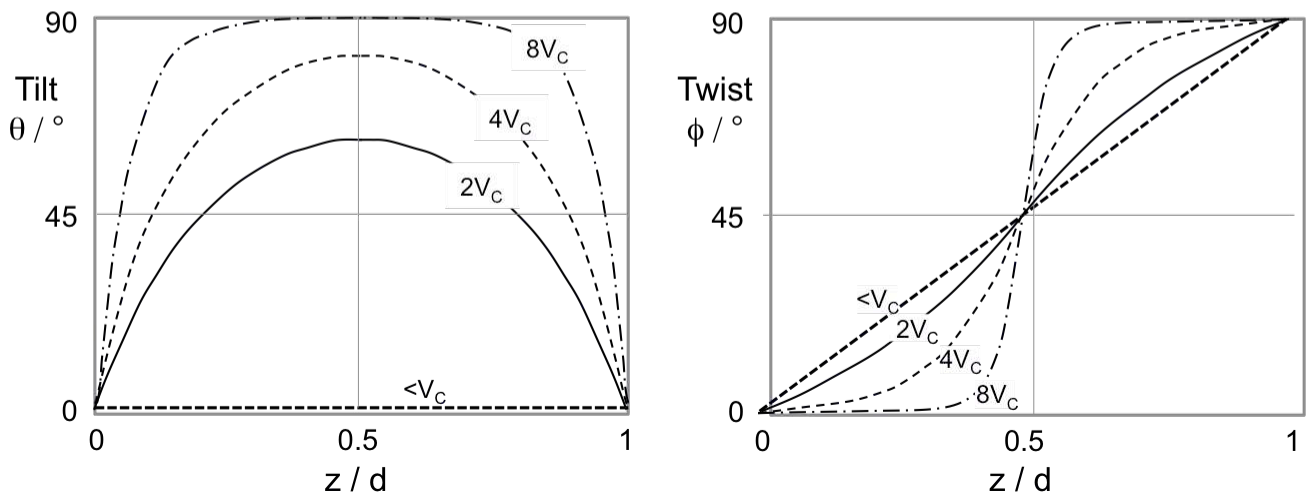
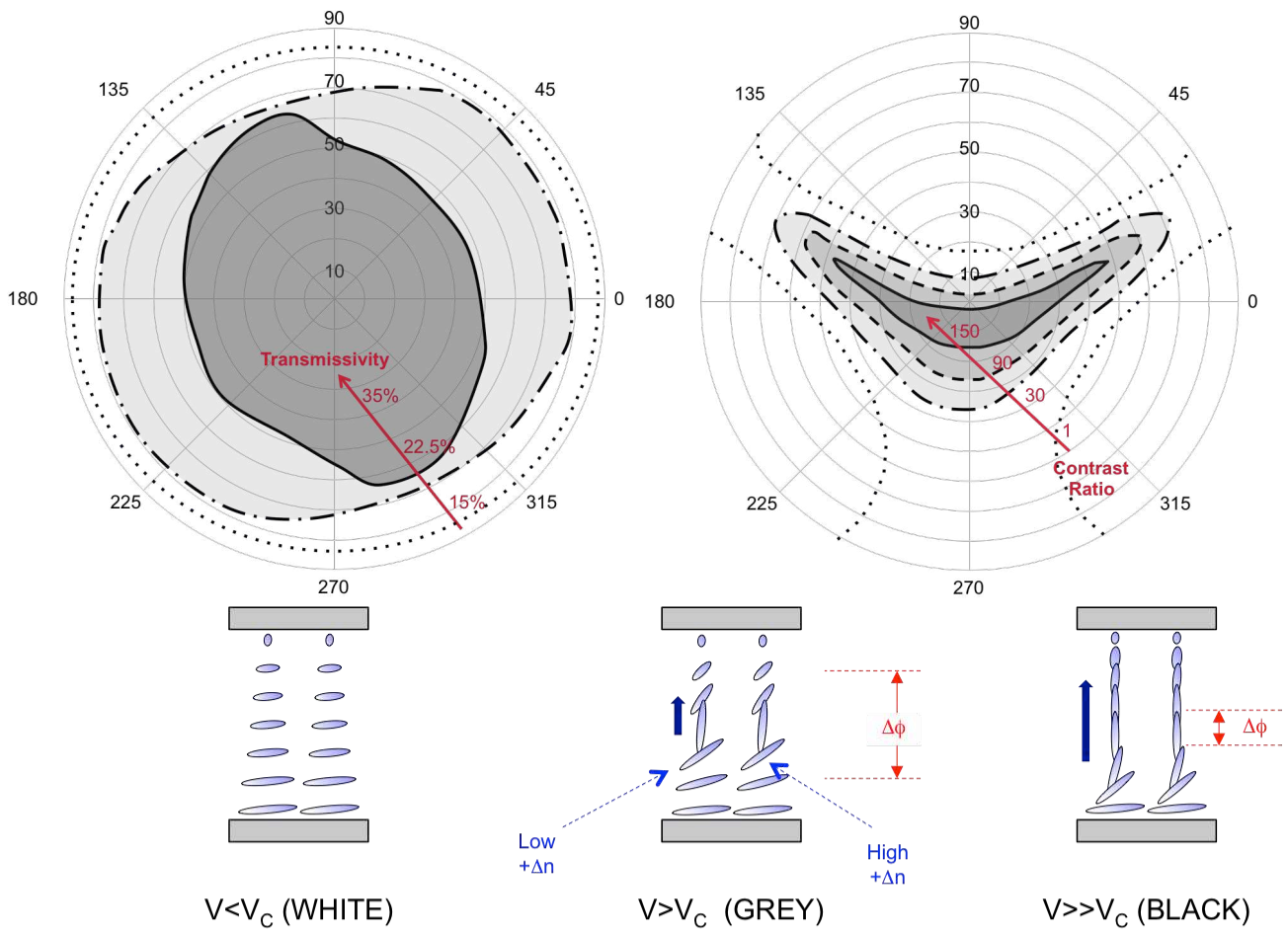


Figure 21 Measured viewing angle characteristics of a first minimum NW TN operating in transmission, showing polar plots of a) ON state transmissivity and b) ON / OFF contrast ratio. c) Schematic of the TN with low, intermediate and high voltages. d) Twist and tilt director profiles for the TN versus voltage.

Combining discotic and calamitic layers with equal but opposite retardations leads to a net optically isotropic medium, black at all angles when between crossed polarisers. Figure 22 shows how this works in practice [112, 113]. Polymer film fabricated from a hybrid aligned discotic are laminated either side of the LCD with the optic axes parallel to the fully ON state director at the adjacent surface, and the splay anti-symmetric. This leads to a greatly improved off-axis contrast ratio, as shown in figure 22b), and helped lead to sufficiently good performance for TN displays to be used in laptops and monitors.

Two-polariser reflective mode TN devices are usually used in low cost applications such as watches and calculators where the cost of extra optical compensation layers is prohibitive. However, the viewing angle characteristic of such devices is far more symmetrical than that of the transmissive device shown in figure 21b), due to a self-compensating effect. Off axis light that experiences a lower  $\Delta n$  from the director tilted towards it on the first pass through the device, experiences a correspondingly higher  $\Delta n$  when traversing in the other direction on the second pass after reflection.

With all reflective displays, it is important to consider the illumination conditions; in particular the colour balance of the incident light and its degree of diffusivity. Indeed, the viewing angle characteristic can be considered both as an optical output for diffuse illumination, or as means for ensuring the maximum light input. In practice, the LCD reflectivity is controlled to some extent by the diffusivity of the reflector and / or front polariser. Indeed, adaptations of the reflective layers can be used to deliberate trade-off viewing angle and reflectivity. The appearance of the display can be remarkably different when viewed by the diffuse light of a cloudy day or by the highly directional light on a sunny day or in a dark room with a single light source. In the former case, the appearance of a scattering mode display will easily surpass that of the polarised LCD, but the situation is reversed for directional lighting and viewing closer to the specular angle.

#### 4.3.4 Single Polariser Reflective Mode TN

Conventional two-polariser reflective TN and STN LCDs have two further optical limitations. Parallax caused by the separation of the rear reflecting polariser from the image plane by the thickness of the rear plate, leads to shadowing of the image when viewed off axis. This can be distracting for black and white devices, but is severely detrimental to reflective colour devices due to colour leakage between sub-pixels. Secondly, the optical efficiency of the white state is relatively low because the light passes four times through the polarisers. The transmission of the highest quality LCD polariser is 43%. However, a further 5% is absorbed on each pass so that the maximum reflectance possible with a two-polariser reflective display is less than 28%, typically 23%. This is also a severe limitation for pixelated reflective colour LCDs, where the colour filters and decreased aperture ratio then lead to prohibitively low 7% reflectivity.

Single polariser reflective TN reduces these optical losses by using a front polariser only and using an internal reflector on the inside surface of the rear substrate of the display to remove the parallax. The reflector is made slightly diffusive to scatter the reflected light in different directions, so that the OFF state has an attractive appearance and good viewing angle even when lit by a point source. The reflector can form the rear electrode, as shown in figure 23a). Single polariser operation requires that the liquid crystal profile is designed to rotate the input polarised light through  $90^\circ$  after both passes through the liquid crystal, thereby being absorbed by the single front polariser and appearing black. That is, the polarisation is elliptically polarised after the first pass, the indicatrix is rotated on reflection and the light becomes linearly polarised after the second pass orthogonal to the input polariser: the display appears dark. For a positive  $\Delta \epsilon$  material, this will always correspond to the OFF state, since in the ON state the director approaches the vertical condition and appears optically isotropic: no change to the polarisation occurs on either pass and the light is transmitted. The theoretical curves shown in figure 23 ignore losses: in

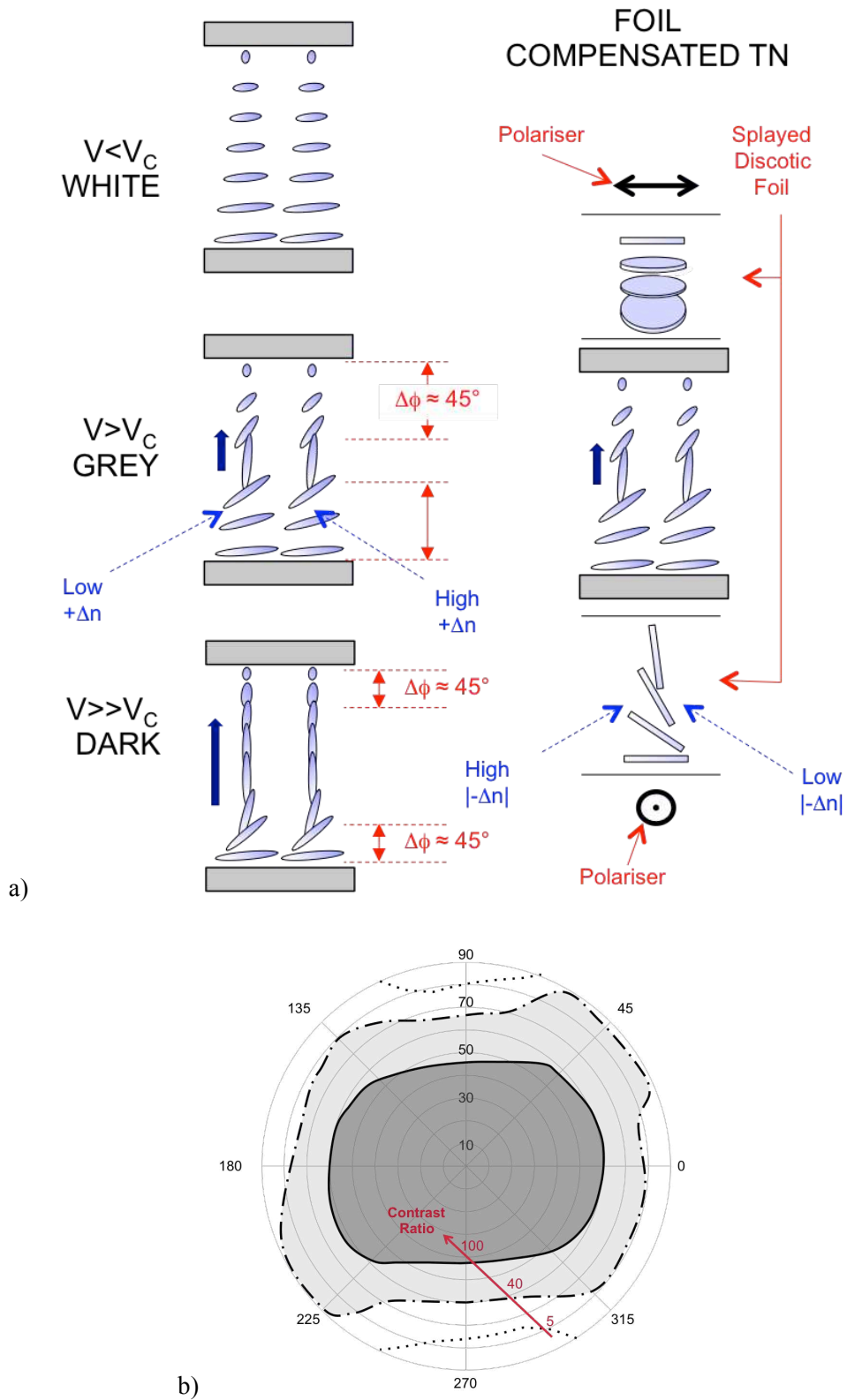


Figure 22 Foil Compensated TN. a) Use of discotic foils to compensate the viewing angle of the OFF state for a transmissive TN LCD; b) and experimental measurements for the resulting viewing angle.

practice the reflectivity may reach up to 35% in the single polariser modes. The image may be inverted and Normally White operation achieved by the addition of a quarter-wave plate between the polariser and the liquid crystal, as shown in figure 23a).

Consider a single polariser display using the simplest LCD geometry, the ECB mode of section 3.3. Here, the liquid crystal acts as a switchable wave-plate. Multiplying the Jones matrices for a polariser, wave-plate with optic axis at angle  $\phi_1$  to the polariser, and the same wave-plate and polariser after reflection gives:

$$R = 1 - 4\sin^4\Gamma\sin^2 2\phi_1 \quad , \quad (82)$$

where the retardation is approximately:

$$\Gamma = \frac{\pi\Delta n.d}{\lambda}\cos^2\bar{\theta} \quad , \quad (83)$$

and  $\bar{\theta}$  is the average director tilt and  $\phi_1$  is the polariser orientation measured from the input director. The OFF state appears dark ( $R = 0$ ) if  $\Gamma = \phi_1 = m\pi/4$  ( $m = 1, 3, 5, \dots$ ). That is, at the quarter wave-plate condition light is circularly polarised with one handedness, which is swapped to the other handedness after reflection and no longer transmitted by the retarder. This mode suffers from poor dark state leakage and colouration, due to wavelength and angular dispersion away from the quarter-wave condition. As for transmissive state devices, improved performance is achieved using the twisted nematic geometry.

There are several options for single polariser reflective TN operation [67], including twist angles ranging from  $60^\circ$  to  $90^\circ$ . Replacing the wave-plate with the Jones matrix for a TN in the derivation above gives [114]:

$$R = \left(1 - \frac{2\alpha^2}{1+\alpha^2}\sin^2\gamma\right)^2 + \left(\frac{2\alpha\sin\gamma}{1+\alpha^2}\right)^2 [(\sqrt{1+\alpha^2})\cos\gamma.\cos 2\phi_1 - \sin\gamma.\sin 2\phi_1]^2 \quad (84)$$

where  $\alpha = \Gamma/\Phi$  and  $\gamma = \Phi\sqrt{1+\alpha^2}$ . This gives dark state solutions ( $R = 0$ ) when the following two conditions are met simultaneously:

$$\Phi = \frac{1}{\sqrt{1+\alpha^2}}\sin^{-1}\sqrt{\frac{1+\alpha^2}{2\alpha^2}} \quad (85)$$

$$\phi_1 = \frac{1}{2}\tan^{-1}(\sqrt{\alpha^2-1})$$

These solutions represent the cases where the liquid crystal is at the quarter-wave condition, rotating the polarisation through  $90^\circ$  over the two passes, and tend to those of equation (82) as  $\Phi$  tends to zero ( $\alpha \rightarrow \infty$ ), with  $\phi_1 = \pm\pi/4$  and  $\Delta n.d/\lambda = (2\pi+1)/4$  for  $m = 0, 1, 2, \dots$ . Figures 23b) and c) show the solutions to equation (85) for the first three orders.

Consider the solution for  $\phi_1 = 0$ , shown in figures 23d) and e): equations (85) predicts  $R=0$  occurs when  $\alpha = \pm 1$ , for which  $\Phi = \pi/(2\sqrt{2}) = 63.64^\circ$  and  $\Delta n.d/\lambda = 0.353$ . This is a rather low retardation; even if a commercial liquid crystal with the lowest birefringence available ( $\Delta n \approx 0.09$ ) is used, this LCD mode requires a  $2.2\mu\text{m}$  cell gap, potentially lowering production yield and increasing cost. Second and third order examples are also listed in table 5. Although the cell gap becomes more typical, the colouration of the dark state is far too high for use in a conventional display. Such modes, however, are useful for liquid-crystal-on-silicon (LCOS) projection systems, where three panels are tuned to operate at the RGB wavelengths.

The  $63.6^\circ$  single-polariser TN [114] was successfully deployed in Nintendo's *Color Game Boy* games console, from 1998 – 2003. The display was manufactured by *Sharp*, who included achromatic retarders to invert the display to Normally White operation. This minimised dark state leakage, which is essential for any colour display, whereas the resulting wavelength dependence of the white state was readily compensated through the colour filters. Although the design gives the highest reflectivity possible with a

polarised light mode LCDs, the introduction of colour filters still leads to a maximum reflectance of less than 10%. The approach taken by *Sharp* was to introduce prismatic elements into the back reflector, thereby directing off-axis light into the viewing direction; the reduced viewing angle display was considered suitable for this single viewer application. The adoption of better performing backlights and high aperture ratio LTPS back-planes eventually led to transmissive displays only becoming acceptable for colour portable applications. Interestingly, full colour reflective and transmissive displays remain an area where no technology, liquid crystal or otherwise, has yet met the performance required for market success.

#### 4.4 Supertwist Nematic LCDs

The TN device usually includes a trace amount of cholesteric dopant, simply to impart a natural handedness and prevent domains impairing the appearance. Increasing the cholesteric content so that

the natural pitch of the chiral nematic P is much lower allows twists of greater than 90° to be reached [115]. The range of conditions for such “supertwist” states is [89]:

$$\frac{\Phi}{2\pi} - \frac{1}{4} \leq \frac{d}{P} \leq \frac{\Phi}{2\pi} + \frac{1}{4} \quad (86)$$

or:

$$\left(1 - \frac{\pi}{2\Phi}\right) \leq \beta \leq \left(1 + \frac{\pi}{2\Phi}\right) \quad (87)$$

where  $\beta = 2\pi.d/P\Phi$ . The STN range of twist angles is  $90^\circ < \Phi \leq 270^\circ$ , which corresponds to differences in the rubbing direction  $\varphi_1 - \varphi_2$  of:

$$\varphi_1 - \varphi_2 = \Phi - \pi \quad (88)$$

where it is important to ensure that the sign of the liquid crystal helix matches the pre-tilt of the two surfaces, in the same fashion as the TN. In practice, higher pre-tilts are needed for STN, typically  $2^\circ \leq \theta_s \leq 8^\circ$ .

Table 5 Examples of normally Black Solutions for Single Polariser TN

Order of Minimum	Director Twist $\Phi / ^\circ$	Polariser Angle $\varphi_{\square} / ^\circ$	$\Delta n.d / \lambda$	Cell gap $d / \mu\text{m}$ ( $\Delta n = 0.09$ )
1 <sup>st</sup>	63.6	0 (or 90)	0.353	2.2
2 <sup>nd</sup>	45	56.4 (or -33.6)	0.683	4.2
	60	63.6 (or -26.4)	0.606	3.7
3 <sup>rd</sup>	90	32.7 (or -57.3)	1.175	7.2

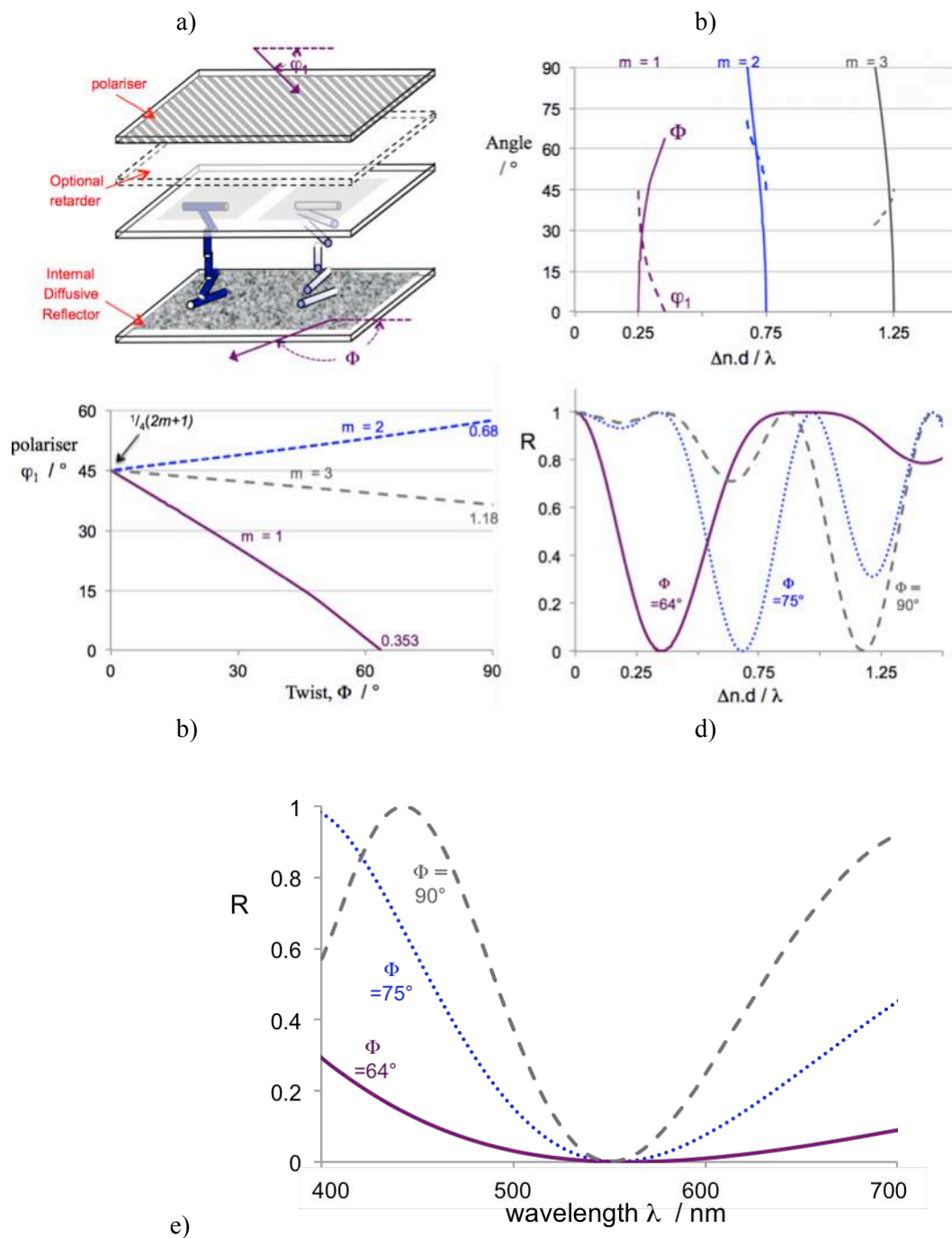


Figure 23 Options for single polariser TN modes. a) Schematic of single polariser TN with internal diffusive reflector. b) Solutions for the Normally Black mode single polariser TN. Continuous lines show the twist angle  $\Phi$  for the first three solution sets to equations (85), and the dashed lines the corresponding polariser angles  $\phi_1$ . c) The data of b) re-plot as twist and polariser orientations. The numbers indicated represent the retardation with  $90^\circ$  twist, whereas the untwisted cells give  $\Delta n \cdot d / \lambda = 0.25, 0.75$  and  $1.25$ , for each mode respectively, each with  $\phi_1 = 45^\circ$ . d) Calculated reflectivity for  $\Phi = 64^\circ, 75^\circ$  and  $90^\circ$  twists, with polariser angles set to give  $R = 0$  for  $m = 1, 2$  and  $3$ , respectively. e) Dark state transmission for  $\Phi = 64^\circ, 75^\circ$  and  $90^\circ$  for a low  $\Delta n$  materials (0.09).

Figure 24 shows the transmission characteristics for a set of devices with twist angles operating across the supertwist range [110]. As the twist increases, both the Fréedericksz threshold voltage and the steepness of the curve increase, the latter allowing an increase of the number of lines that can be passive-matrix addressed [89].

The inherent twist of the chiral nematic effectively reduces the twist elastic constant by the term  $(1-2\pi/P)$ , and the Fréedericksz threshold becomes:

$$V_C = \pi \sqrt{\frac{1}{\varepsilon_0 \Delta \varepsilon} \left[ k_{11} + \left(\frac{\Phi}{\pi}\right)^2 \{k_{33} - 2k_{22}(1 - \beta)\} \right]} \quad (89)$$

Hence,  $V_C$  increases with twist angle  $\Phi$ . Similarly, the voltage dependence of the mid-plane tilt angle is also affected, with equation (80) now given by [110]:

$$\frac{\theta_m^2}{4\left(\frac{V}{V_C} - 1\right)} = \frac{1}{\left( \frac{k_{33} - \left(\frac{\Phi}{\pi}\right)^2 \left[ \frac{k_{33}^2}{k_{22}} + k_{22}(1 - 4\beta + \beta^2) - k_{33}(2\beta - 1) \right]}{k_{11} + \left(\frac{\Phi}{\pi}\right)^2 [k_{33} - 2k_{22}(1 - \beta)]} + \frac{\Delta \varepsilon}{\varepsilon_{\perp}} \right)} \quad (90)$$

As for the TN case, it may be assumed that  $k_{22} \approx \frac{1}{2}k_{33}$  such that the denominator becomes:

$$\frac{k_{33} - \frac{1}{2}\left(\frac{\Phi}{\pi}\right)^2 k_{33}(7 - 8\beta + \beta^2)}{k_{11} + \left(\frac{\Phi}{\pi}\right)^2 k_{33}\beta} + \frac{\Delta \varepsilon}{\varepsilon_{\perp}} \quad (91)$$

Assuming that the chiral doping is chosen to be in the central range for the given twist ( $\beta=1$ ), then the denominator of (82) becomes zero, and the  $\theta_m(V)$  gradient infinite when that twist is set to  $\Phi_{\infty}$ :

$$\Phi_{\infty} \approx \pi \sqrt{\frac{\varepsilon_{\perp}}{\Delta \varepsilon} + \frac{k_{11}}{k_{33}}} \quad (92)$$

Low  $V_C$  requires highly positive  $\Delta \varepsilon$ , for which typically  $0.3 \leq \varepsilon_{\perp}/\Delta \varepsilon \leq 0.5$ . Ensuring that  $\Phi_{\infty}$  is maintained at an attainable twist then necessitates  $k_{33}/k_{11}$  is as low as possible, contrary to the requirement for the standard TN. For example, a typical mixture suitable for STN may have  $\varepsilon_{\perp}/\Delta \varepsilon \approx 0.4$  and  $k_{33}/k_{11} \approx 0.85$  [79] such that the gradient is highest for  $\Phi_{\infty} \approx 200^\circ$ . Equation (92) only acts as a guide for material design, but it shows that keeping both  $k_{11}/k_{33}$  and  $\Delta \varepsilon/\varepsilon_{\perp}$  low is likely to give the highest degree of STN multiplexing. Therefore, the material scientist targets a high  $k_{33}$ ,  $\Delta \varepsilon$  and  $\varepsilon_{\perp}$  whilst keeping  $k_{33}$  low, to combine a low threshold voltage with a high multiplexibility. Where the gradient exceeds  $\Phi_{\infty}$  the voltage response becomes hysteretic, as shown for the  $270^\circ$  STN in figure 24. This is unusable in RMS addressed displays, and so typically twists of  $\Phi = \frac{4}{3}\pi = 240^\circ$  are used in practice. Even then, switching can be disrupted through the formation of stripe domains, electro-hydrodynamic instabilities that cause the helical axis to rotate into the plane of the cell [116]. These require a lower  $d/P$  to be used than the  $\beta = 1$  condition, together with ensuring the pre-tilt is high.

For a  $240^\circ$  STN,  $\frac{5}{8} \leq \beta \leq \frac{11}{8}$  and the range of Fréedericksz thresholds is:

$$\pi \sqrt{\frac{1}{\varepsilon_0 \Delta \varepsilon} \left[ k_{11} + \frac{10}{9} k_{33} \right]} < V_C < \pi \sqrt{\frac{1}{\varepsilon_0 \Delta \varepsilon} \left[ k_{11} + \frac{22}{9} k_{33} \right]} \quad (93)$$

For the typical STN mixture with  $k_{33}/k_{11} \approx 1.2$ ,  $V_C$  is 20% to 70% higher than for the equivalent TN operation, with the higher threshold more practical if  $\beta$  is kept low and the stripe voltage is to be avoided.

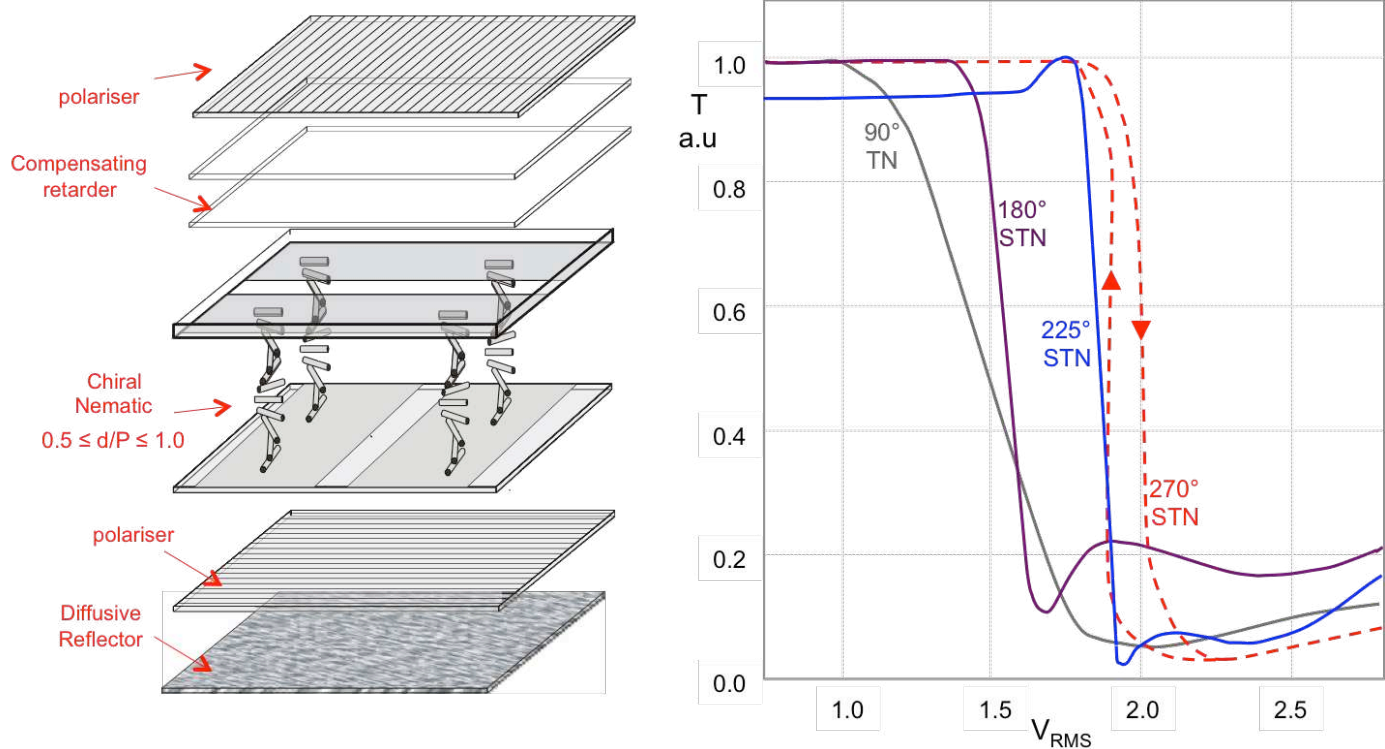


Figure 24 a) Schematic of a typical Two-polariser Reflective Supertwist Nematic, STN. b) STN transmission characteristics for increasing twist angle.

Also, the elastic term that appears in the square brackets of equation (89) is applicable to the response times: inserting into equations (48) show that the STN response compared is inherently quicker than the TN. However, this is rarely found in practice, since the STN is usually highly multiplexed, and the response much slower due to the much smaller changes of RMS voltage.

The first STN demonstrators used a Guest-Host mode, in which anisotropic pleochroic dyes give contrast between the ON and OFF states [89]. However, optical contrast could also be achieved using optical retardation effects, in what is called the Supertwist Birefringence Effect (SBE), [90]. STN also have a Gooch-Tarry type dependence of the polarisation optics, with the first minimum mode occurring at increasing  $\Delta n \cdot d / \lambda$  with twist, as shown in figure 25, and the crossed polariser angles set to  $\varphi_1 =$

$\frac{1}{2}(\Phi - \frac{\pi}{2})$ . The retardation for the first minimum is double that of the TN, potentially decreasing the speed of the device by a factor of four. Even when high birefringence materials are chosen, the effect is too slow for animation, with  $>100\text{ms}$  response times typical. However, the most significant drawback from the original technology were the optical properties: the OFF state is a prominent shade of yellowy-green, or blue if the NB polariser orientations are chosen, the viewing angle is poor, and the contrast is much lower than that of the TN, because the twist remains more evenly distributed through the cell in the STN case as the field is applied [117]. Various attempts were made to improve the appearance, such as the use of blue polarisers to give a White on Blue display with high transmissivity, but the most successful were in the late-1980s, when optical compensators were added.

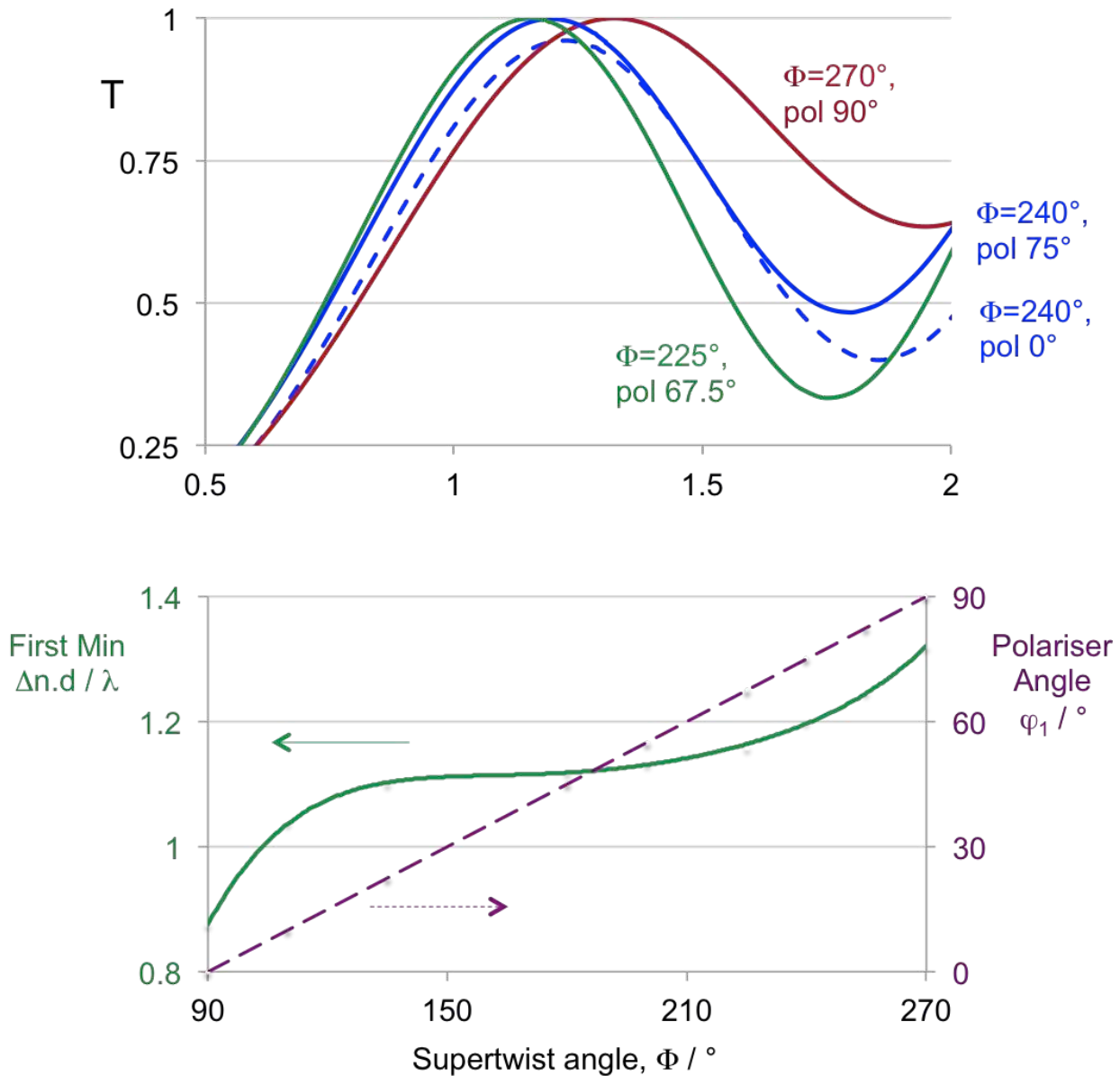


Figure 25 Optics of the Supertwist Birefringence Effect mode.

The first method was to mount an inactive dummy STN panel onto the front of the LCD, equivalent to the active panel but with the opposite handedness [91]. This corrected both the colouration and the viewing angle, and would do so across the whole temperature range. However, the additional cost and weight prohibited this approach commercially, and polymer film retardation plates are now used instead [118]. The

best colour compensation is achieved through the use of two polymer films [7], as indicated in figure 24.

Even where the transmission characteristic is made infinitely steep, the effect of non-uniformities, including electrode resistive losses and temperature variations, prevents multiplexing much beyond 240 lines. Driving alternate rows from opposite sides of the panel doubles the maximum number of rows. Such

high degrees of multiplexibility represents a considerable improvement to the passive matrix TN, and for that reason the STN continues to find a market where there is demand for a high Black and White image content combined with low cost. However, the lack of grey-scale and slow response speed prohibits video applications, and it was these factors that fed on-going research efforts for highly multiplexed displays.

#### 4.5 Ferroelectric Liquid Crystal Displays

Although making only a small commercial impact, Ferroelectric Liquid Crystals commanded major R&D efforts through the 1980s and 1990s, immediately after the publication by Clark and Lagerwall of the Surface Stabilised Bistable FLC mode [88], SSFLC. Companies across Europe and the Far East each produced demonstrators to rival the nascent TFT technology [119]. However, the only panel to receive notable sales in the mainstream displays market at that time was the 15" 1280 x 1024, 16-colour monitor produced by *Canon*, figure 16.

Unlike the other mainstream LCDs described in this section, FLC do not use nematic liquid crystals but rather a particular type of smectic, the tilted smectic C phase, denoted SmC. Unlike the nematic case, reorientation of the director for smectics is constrained by the presence of the smectic layers. The smectic C phase is constrained in this fashion too, but the director is relatively free to reorient about the layer normal in an imaginary cone of possible orientations. The component of the director in the layer plane is described by the unit director  $\mathbf{c}$ , which acts as a two-dimensional nematic. It is reorientation of the  $\mathbf{c}$ -director in response to applied electric fields that yields the potential for electro-optic effects suited for display operation. However, what makes the SmC so interesting is the inherent ferroelectricity allowed by the reduced symmetry of the chiral smectic C phase (SmC\*). Whereas the nematic phase has cylindrical symmetry, the SmC is monoclinic: there is a single  $C_2$  symmetry axis corresponding to the direction orthogonal to the layer normal  $\mathbf{a}$  and director  $\mathbf{n}$ . Such symmetries are inherently biaxial, meaning that they

have two optic axes and three principal permittivities. The difference between the two directions orthogonal to the  $\mathbf{n}$  director is called the biaxiality. The refractive index biaxiality is negligible and FLC are best treated as optically uniaxial materials, with a single optical axis along the director. Thus, the polarisation optics can be treated in the same way as a conventional nematic. However, the dielectric biaxiality  $\partial\epsilon = \epsilon_1 - \epsilon_2$  is significant [120, 121] and, in essence, acts in a similar fashion to the nematic  $\Delta\epsilon$ , dictating the RMS response of the  $\mathbf{c}$ -director. Reflections of the SmC molecules in the tilt plane do not disrupt the phase symmetry: molecular dipoles aligned along the  $C_2$  axis have equal probability of being parallel or antiparallel.

If the phase is chiral, this mirror symmetry is lost and there is a net dipole in the direction of  $\pm C_2$ : the ferroelectric spontaneous polarisation  $P_S$ . This unique feature provides a polar switching torque many times greater than that possible in nematic liquid crystals, resulting in switching times that can be faster than 10 $\mu$ s.

For simplicity, a single elastic constant  $B$  and the flow-free viscosity  $\gamma_1$  are used, although the effect of the elastic anisotropy and the uniaxial dielectric anisotropy  $\Delta\epsilon$  are important too [122, 123]. The switching torque of the FLC is then given by:

$$\gamma_1 \sin^2 \theta_C \frac{\partial \phi_C}{\partial t} = B \cos^2 \delta_C \frac{\partial^2 \phi_C}{\partial z^2} + P_S E_z \cos \delta_C \sin \phi_C - \epsilon_0 \partial \epsilon \cdot E_z^2 \sin \phi_C \cos \phi_C \cos^2 \delta_C \quad (94)$$

The ferroelectric torque differs from the dielectric having a linear dependence on the applied field  $E$ , rather than the RMS  $E^2$ . This means that the torque depends on the field polarity as well as its strength. A typical FLC may have a  $P_S = 50 \text{ nCcm}^{-2}$  and dielectric biaxiality  $\partial\epsilon \approx +0.5$ . For a typical  $\pm 10 \text{ V}$  signal applied across a  $2 \mu\text{m}$  spaced cell, the ferroelectric torque is fifty times greater than the dielectric, dominating the electro-optic behaviour. Assuming the material has a positive  $P_S$ , then  $+E$  will tend to reorient the  $\mathbf{c}$ -director on one side of the cone (towards  $\phi = 0$ ) and  $-E$  to the other ( $\phi = \pi$ ). Simplistically, if these two

conditions equate to the  $\mathbf{n}$ -director being oriented  $\pi/4$  apart, and the device has a spacing set to give the quarter wave-plate condition and crossed polarisers parallel and perpendicular to the director in one of the states, equation (25) predicts that the device will switch between minimum and maximum transmissivity.

A second important aspect of the SSFLC is bistability. As for any LCD, the starting point is to achieve the desired alignment, uniformly over the whole sample [124]. There are several steps to consider for ferroelectric LCDs. The usual SSFLC device geometry relies on the  $N^* - \text{SmA} - \text{SmC}^*$  sequence, as shown in figure 26a). The device requires parallel alignment with the required pre-tilt  $\theta_s$ . The cell gap must be sufficiently low to unwind the cholesteric helix and provide an almost uniform nematic texture, as shown: devoid of twist and with only a slight splay and bend associated with the surface pre-tilt. Furthermore, the helicity of the SmC  $\mathbf{n}$ -director must also be suppressed in a similar fashion. This uniform nematic texture should be retained on cooling into the SmA phase, where the layers will align uniformly perpendicular to the cell walls in what is termed “bookshelf” geometry. On cooling into the SmC\* phase, the director tilts from the layer normal by the cone angle  $\theta_C$ , which grows continuously from  $0^\circ$  at the second-order SmA to SmC\* phase transition to typically  $22^\circ$  to  $25^\circ$  at ambient temperatures, figure 26b). The smectic layer spacing contracts as the director tilts from the layer normal, causing the layers to tilt by an angle  $\delta_C$  and form a symmetric chevron-like structure. The layer tilt remains a constant fraction of the cone angle, typically  $\delta_C \approx 0.85\theta_C$ , so that the director remains continuous across the sharp chevron interface at the cell centre. It is this interface that gives the SSFLC its bistability. The  $\mathbf{c}$  director can be at either of two orientations,  $\phi_i$  and  $\pi - \phi_i$  in one arm, and  $-\phi_i$  and  $\pi + \phi_i$  in the other. These correspond to just two orientations of the  $\mathbf{n}$  director, as shown in figure 26b). Application of a DC field couples to the ferroelectric polarisation, eventually causing such a high torque at the chevron interface that latching from one state to the other

occurs. After the pulse, the director remains in that state, with the director relaxing back to one of the two quiescent states.

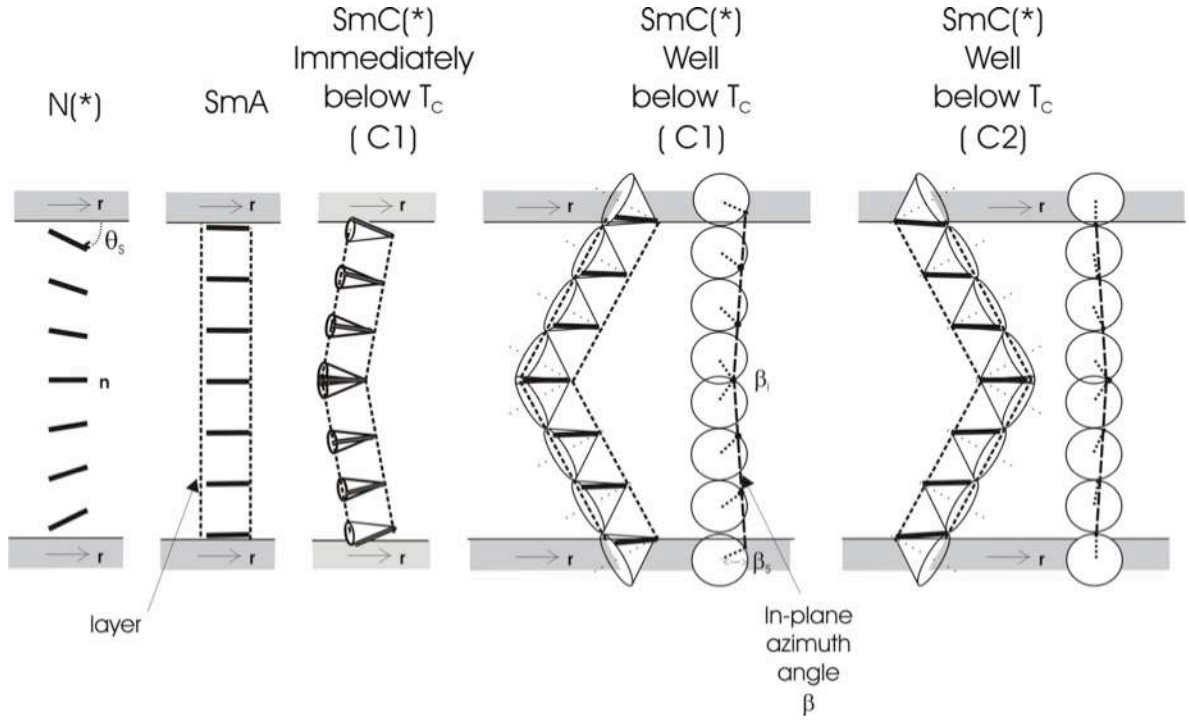
The surface pre-tilt and anchoring energies play fundamental roles in SSFLC devices. Conventional polyimides for nematic alignment are used. These have azimuthal and zenithal anchoring energies in the range of 0.3 to  $1\text{mJcm}^{-2}$ ; high enough to be considered infinite for nematic LCDs, but insufficient to cause changes to the layer orientation or SmC\* cone angle in FLC. Immediately below the SmA to SmC\* transition, the layers always tend to tilt in the direction favoured by the surface pre-tilts. This is the C1 state, shown in figure 26a). As the temperature is cooled further,  $\theta_C$  and  $\delta_C$  increase, forcing the surface director to lie further from the rubbing direction and pre-tilt angle. Close to the temperature where the difference between the cone and layer tilt angles ( $\theta_C - \delta_C$ ) approaches the surface pre-tilt  $\theta_s$ , the tilt of the layers swaps direction to form the C2 layer structure. For low surface tilt angles ( $0.1^\circ \leq \theta_s \leq 2^\circ$ ) samples usually form a mixture of both C1 and C2 states. The lack of uniformity and zigzag defects that separate the regions of opposite layer tilt severely damages the device appearance. However, with intermediate pre-tilts ( $2^\circ \leq \theta_s \leq 8^\circ$ ) the layers form the C2 state completely and uniformly, whereas for higher pre-tilts still ( $12^\circ \leq \theta_s \leq 35^\circ$ ) the layers do not undergo the alignment transition at all and the sample is uniformly C1. Both layer geometries have been used in SSFLC devices [119, 101], though the Canon monitor used the high pre-tilt C1 approach.

The out-of-plane tilt of the director  $\theta$ , and in-plane tilt angle of the projection of the  $\mathbf{n}$ -director into the cell plane are shown in figure 26b). They are given by the expressions:

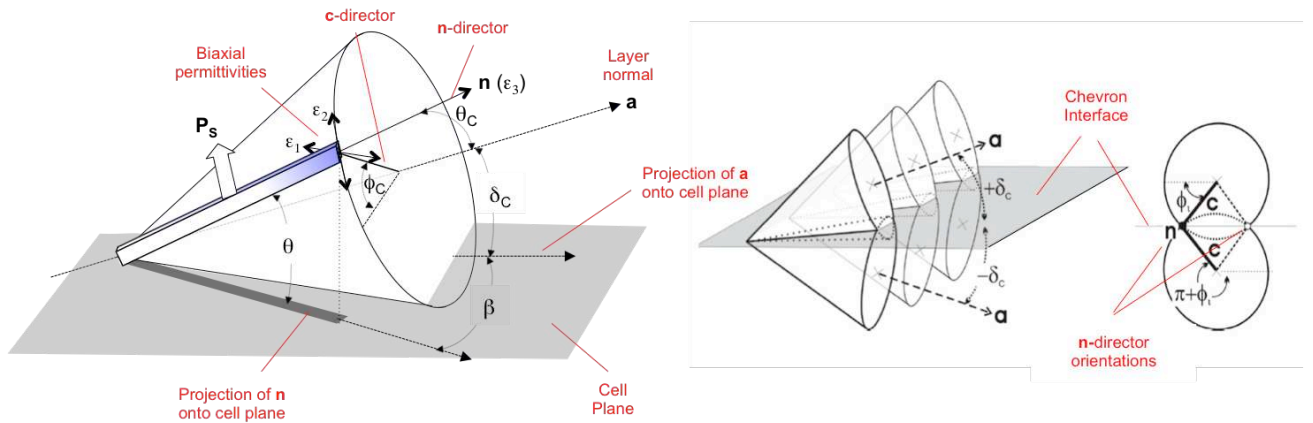
$$\beta = \tan^{-1} \left( \frac{\cos \phi_C \sin \theta_C}{\sin \phi_C \sin \delta_C \sin \theta_C + \cos \delta_C \cos \theta_C} \right)$$

$$;$$

$$\theta = \sin^{-1} \left( \frac{\sin \phi_C \cos \delta_C \sin \theta_C}{\sin \delta_C \cos \theta_C} \right) \quad (95)$$



a)



b)

Figure 26. a) Ferroelectric Liquid Crystal alignment on cooling through the sequence  $N^* - S_A - S_C^*$  for parallel aligned surfaces. C1 and C2 chevron layer textures with low and high tilt and triangular director profiles are shown. b) Definition of angles for  $S_C^*$  devices, and the source of bistability from the chevron interface.

At the chevron interface, there is no out-of-plane tilt and the director has an in-plane twist angle  $\beta_m$  given by:

$$\beta_m = \pm \cos^{-1} \left( \frac{\cos \theta_c}{\cos \delta_c} \right) \quad , \quad (96)$$

which is typically about  $8^\circ$ . For the C1 layer geometry, the surface tilt is chosen to be high, typically  $25^\circ$ . For typical values of  $\theta_c = 25^\circ$  and  $\delta_c = 22^\circ$ , equations (95) give an in-plane tilt of  $\beta_s \approx 27^\circ$ . Thus, the director twists from  $27^\circ$  at one surface to  $8^\circ$  in the cell centre and back out to  $27^\circ$  at the other surface. Assuming that

the twist is approximately linear then the director profile is triangular [125], as shown in figure 26a). The transmission of polarised light through such a cell is similar to that of the reflective TN mode given by equation (84), except the opposite polariser is crossed to the input polariser in the FLC case, rather than being parallel. This has the simple solution for the angle to align the polarisers with respect to the rubbing direction,  $\beta_{ext}$ :

$$\tan 2(\beta_{ext} - \beta_s) = \frac{\tan\left[(\beta_m - \beta_s)\sqrt{1 + \frac{1}{4}\alpha^2}\right]}{\sqrt{1 + \frac{1}{4}\alpha^2}}, \quad (97)$$

where;

$$\alpha = \pi \frac{\Delta n \cdot d}{\lambda(\beta_s - \beta_m)}, \quad (98)$$

as before. Equation (97) suggests that the device will appear highly coloured in its quiescent state for retardations close to the full wave-plate condition. However, if the cell spacing is reduced to the half wave-plate condition, the device appears black with the polarisers aligned at the angle:

$$\beta_{ext} = \pm \frac{\beta_m + \beta_s}{2}. \quad (99)$$

The example above gives  $\beta_{ext} \approx \pm 18^\circ$ . Thus, if the polarisers are placed at  $+18^\circ$  and  $+108^\circ$  to the rubbing direction, the cell will appear black for one state, and transmit most of the light when in the other domain, where the optic axis is about  $36^\circ$  from the polarisers. Approximating the structure to a uniform retarder, and setting the retardation to be at the half-wave plate condition for green light, then the FLC switches between states with the optic axis either parallel or at  $2\beta_{ext}$  to the polariser. Equation (25) suggests that the transmittance should be 91%. This could be maximised so that  $\beta_{ext} = 22.5^\circ$  (and the director reorients through  $45^\circ$ ), for example by using a material with a higher SmC\* cone angle  $\theta_c$ . However, this also causes a decrease in switching speed, and so *Canon* used the lower optical efficiency to help achieve a fast, flicker-free frame for their monitor.

FLCD panels are addressed in a similar fashion to most passive matrix displays, and in the same line-scanning method described in section 2.4. However, the response is no longer to the RMS over the frame, but rather the signal applied to each row must be sufficient to latch the pixels into a new state within the line-time. In this fashion, the information is built up line-by-line. The row waveform has one particular sign of operation, allowing only one set of states to be selected appropriately. Both states are addressed, either using two sub-frames of opposite polarities (with a cost of increasing overall frame time) or by preceding each addressing pulse by a blanking pulse that selects the black state regardless of the data being applied to the previous lines, and then latching selectively or not in the addressing line (with the cost of reduced brightness for pixels that should remain white in consecutive frames). Various addressing schemes are possible [126], influencing speed, operating window and appearance.

A second approach to operating the SSFLC was also attempted jointly by *RSRE* (then *DERA*) and *Sharp* Corporation. This maximised device speed by using the C2 geometry, and multiplexability using a lower  $P_s$  ( $\approx 10 \text{ nCcm}^{-2}$ ) and higher dielectric biaxiality  $\partial\epsilon$  ( $\geq +1$ ), [120, 122]. Equation (94) predicts that the dielectric and ferroelectric terms become equal at about 32.5V for such high biaxiality, low  $P_s$  materials. If the field has the correct polarity to reorient the director from one side of the cone to the other, the dielectric biaxiality suppresses switching and, above the voltage where the torques balance ( $\approx 32.5\text{V}$  for these values), the director will remain unswitched indefinitely. In fact, electrical pulses at about 70% of this voltage [121, 122] start to slow the response rapidly, creating a minimum in the switching characteristic ( $\tau V_{MIN}$ ). Operating close to this voltage (i.e. about 23V, for the high biaxiality SmC\* material in this example) gives a highly non-linear response, thereby enabling thousands of lines to be addressed with a high degree of insensitivity to temperature variations and line losses. Using this  $\tau V_{MIN}$  mode, *Sharp* created a prototype colour  $\frac{1}{4}$  HDTV, operating

with a  $12\mu\text{s}$  line address time, to give 256 grey levels and a 60Hz frame rate [101].

By the mid-1990s, the key advantages of the SSFLC over TFT TN were its perceived lower cost and excellent viewing angle. The good viewing angle was inherent to the SSFLC mode due the fact that the director remains in the same plane for both switched states, as shown in figure 27. Such in-plane switching gives excellent viewing properties, surpassing that of the foil compensated TN of figure 27. However, in the mid-1990s, SSFLC lost the war with TFT driven nematics, because of two reasons. Firstly, the number of critical mask steps grew with FLC complexity. To

achieve microsecond pulses across a passive matrix required metal bus lines to be prepared. Moreover, smectics are fundamentally sensitive to shock, since any flow in the panel disrupts the carefully aligned layers irreparably. To prevent mechanical damage to the LC alignment, polymer walls were defined photolithographically, again introducing a critical mask step. Together with the poorer yield associated with achieving perfect alignment, any cost advantage was severely eroded. The final battle came with the introduction of in-plane switched TFT nematics that matched, and eventually surpassed, the viewing angle of even the SSFLCD, figure 16.

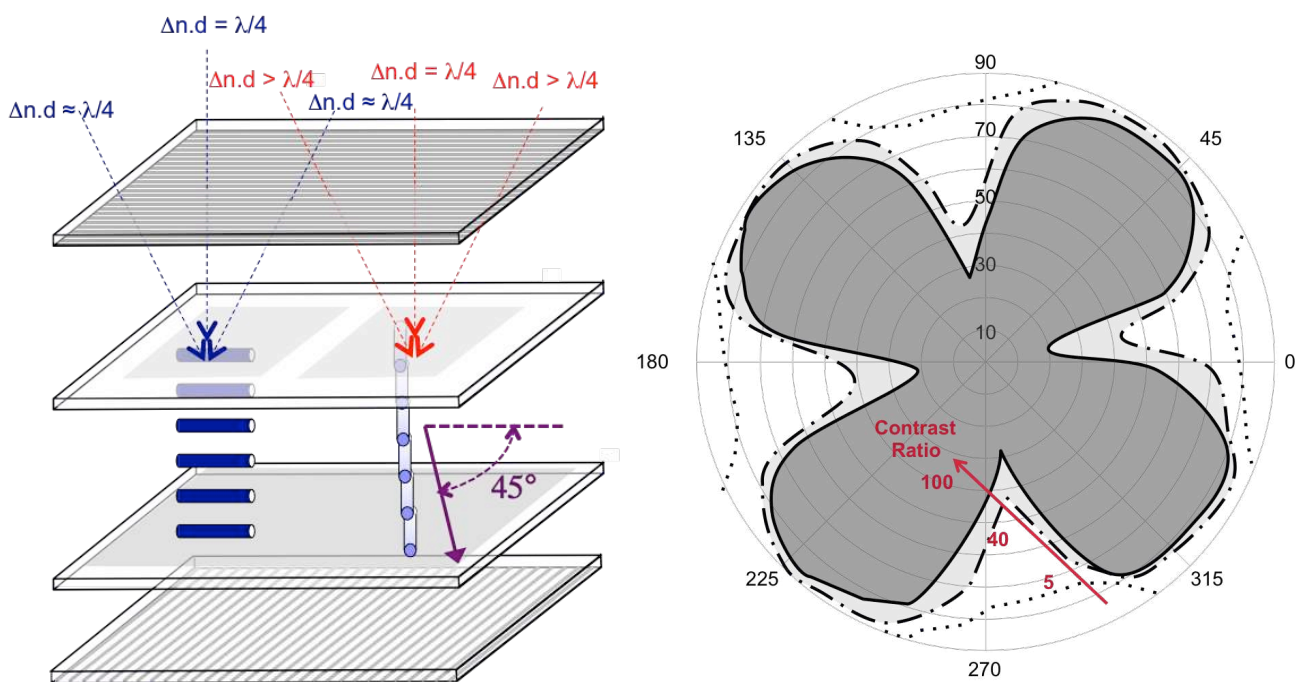


Figure 27 Schematic representation of a switchable quarter wave-plate with in-plane switching. One direction of viewing self compensates the change reduction of birefringence with the increased optical path. The increase in retardation in the other direction (usually set to be the horizontal direction for the white state) is relatively small, and easily compensated. A polar plot for the contrast is sketched on the right.

## 4.6 In-plane Switching LCDs

### 4.6.1 Introduction

Operating with TFT removes steepness of the electro-optic transition as a critical design issue. This enables

LCD modes to be chosen that meet the more stringent optical requirements for large area monitor and televisual displays. The crucial weakness of TN LCDs was viewing angle, even with optical compensation. Viewing angle is particularly important for large area displays, where images must appear uniform from the

centre of viewing to the corners. The viewing angle target is harsher still if the image is to satisfy multiple viewers. The television market also requires fast response times, not just for black to white transitions but also between adjacent grey levels. Extremely high contrast ratios are needed to compete with emissive technologies such as CRT, PDP and, most recently, OLED.

Achieving pixel contrasts in excess of 10,000:1 and  $>160^\circ$  horizontal viewing angles requires

cylindrical symmetry of the director profile in both of the ON and the OFF states. Two approaches were developed during the late 1990s and early 2000s: in-plane switching (IPS) and vertical aligned (VA) modes, as shown in figure (28). Different manufacturers championed each mode, and numerous modifications were tried. This section will concentrate on the IPS mode, and its derivative fringe-field-switching, whereas VA modes are dealt with in the following section.

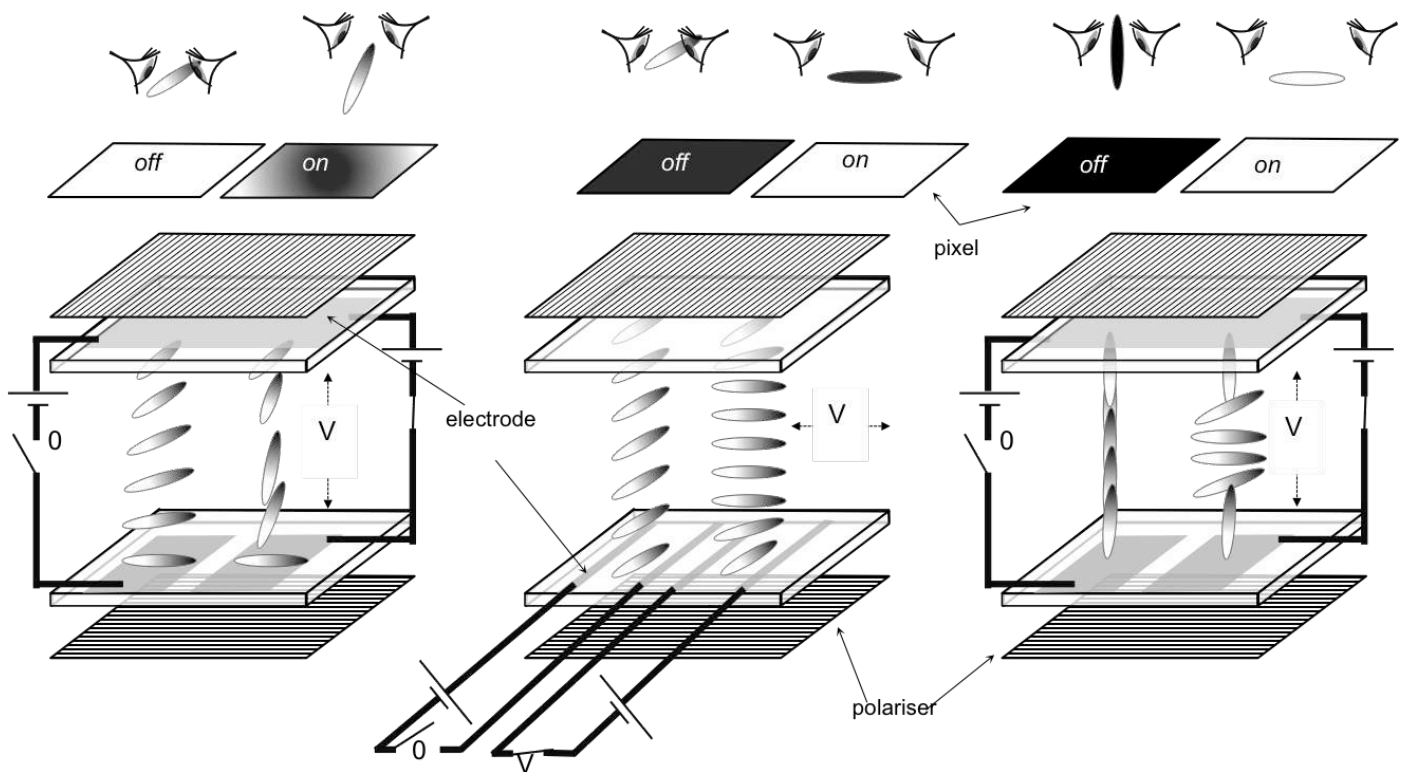


Figure 28. Improvement of viewing angle using IPS or VAN modes.

#### 4.6.2 Basics of IPS Operation

In-plane fields are impractical for passive matrix displays but are readily achieved with Active Matrix LCDs by moving the common electrode to the active

plate (in addition to the Source and Gate lines), in-plane electrodes are etched onto the active back-plane in either a comb-like structure, as shown in figure 29a), or more commonly a zigzag configuration. The field produced by comb-like electrodes is complex,

varying both in the plane of the cell in the direction normal to the electrodes. Ignoring the effect of the liquid crystal permittivity, and taking the first Fourier component only, the field has components [127]:

$$E_y \sim \frac{V}{l} \sin\left(\frac{\pi y}{l+w}\right) \exp\left(-\frac{\pi z}{l+w}\right) ; E_z \sim \frac{V}{l} \cos\left(\frac{\pi y}{l+w}\right) \exp\left(-\frac{\pi z}{l+w}\right) \quad (100)$$

That is, the electric field components have a periodic form in the plane of the cell, but decay exponentially across the bulk of the cell. Rather unsatisfactorily, most treatments ignore the complex field behaviour and assume that, if the cell gap and electrode width are sufficiently low, the field is uniform and restricted to the cell plane. If the quiescent state of the nematic is aligned with the rubbing direction orthogonal to that of the applied field, the IPS mode has a Fréedericksz threshold field that is approximately given by equation (34), although the errors for this can be severe in practice [127]. Assuming a uniform in-plane field, the Euler-Lagrange equation for the elastic distortion above the threshold is [128]:

$$k_{22} \frac{\partial^2 \phi}{\partial z^2} + -\varepsilon_0 \Delta \varepsilon E_z^2 \sin \phi \cos \phi = 0 \quad , \quad (101)$$

which has the simple solution:

$$\phi = \phi_m \sin\left(\frac{\pi z}{d}\right) \quad , \quad (102)$$

for fixed boundary conditions. Aligning the polarisers parallel and crossed to the rubbing direction, the first order solution for the optical transmission is given by that of a wave-plate, equation (25). Approximating the sinusoidal dependence in equation (102) to the triangular form of equation (97) [125] and setting the device thickness at the half-wave retardation gives an effective in-plane tilt of the director of  $\langle \phi \rangle \approx \phi_m / 2$ , and the transmission approaches 50% with increasing voltage. At fields higher than that which gives  $\phi_m = 90^\circ$ , the twist deformation becomes increasingly concentrated towards the surfaces. Thus, the effective twist angle  $\langle \phi \rangle$  exceeds the optimum

$45^\circ$ , thereby causing the transmission to decrease, as shown in figure 29b).

The IPS mode can operate with either positive or negative  $\Delta \varepsilon$  materials, figure 29c), depending on the orientation of the rubbing direction with respect to the electrodes  $\phi_0$ . In this diagram, it is assumed that the anchoring on the surfaces is strong and director reorientation occurs in the bulk of the cell, although somewhat closer to the electrode plate due to the transverse decay of the field. Clearly, the director in the positive mode will tend to orient in the field direction. For the negative mode, the director reorients to be orthogonal to the applied field, either remaining in the cell plane or tilting out of that plane. In-plane switching is always favoured in this case, since the elastic energy associated with the twist elastic constant is lower than the splay-bend that would be induced by the tilt (i.e.  $k_{22} < k_{11} < k_{33}$ ). Although the early demonstrators used negative  $\Delta \varepsilon$ , positive mode is now more common because the materials combine higher  $\Delta \varepsilon$  with lower viscosity, and hence give lower operating voltages and faster response times.

With the TN, STN and SSFLC modes, analytical calculations for the on-axis optical and electro-optic behaviour are reasonably accurate. Optimisation of viewing angle required numerical solutions, due to the importance of off-axis refractive and reflection effects. However, with the adoption of the IPS mode and the variety of multi-domain VAN modes covered in the following section, both the electric field and the director profile vary in two or even three dimensions. This necessitates numerical simulation to optimise the LCD [31, 64]. For example, figure 29b) shows the calculated transmission for a 2D simulation of the IPS mode [129]. Above the electrodes, the field is almost vertical and the director either reorients vertically for positive  $\Delta \varepsilon$  or remains unaffected by the field if negative  $\Delta \varepsilon$ ; in either instance the electrodes appear as unwanted dark bands in the pixel. This necessitates that the gap should be much larger than the width of the electrodes  $l \gg w$ . If too high, the field is reduced and the switching voltages become higher. Typically, the electrodes are  $l = 3 \mu\text{m}$  wide, and have a gap  $l = 6 - 8 \mu\text{m}$ . Therefore,

the banding represents a major reduction in the optical efficiency of IPS mode.

Ideally, the transmission–voltage characteristic should approach linearity across the voltage range, readily giving grey levels. The response of the IPS mode is strongly dependent on the angle of the rubbing direction with respect to the electrodes,  $\phi_0$  [129]. For positive mode IPS,  $\phi_0 \approx 30^\circ$  is used typically [130], not only leading to suitable transmission characteristic and near linearity of the grey scale response times, but also significantly improving the response time, which decreases linearly with increasing  $\phi_0$ .

The viewing angle characteristics of the IPS mode exceed even that of the SSFLCD, shown in figure 27. The first improvement was to orient the electrodes in a small-angled zigzag, to help widen the

viewing cone. However, the stringent requirement to maintain very high contrast well off-axis still necessitates the use of optical compensators. For example, the crossed polarisers themselves leak at the high angles in the four quadrants centred at  $\pm 45^\circ$  and  $\pm 135^\circ$ . A typical IPS mode LCD used in television achieves pixel contrast ratios in excess of 2000:1 for direct viewing, and contrast in excess of 1000:1 over  $175^\circ$  horizontal and vertical viewing. The lowest pixel contrasts still surpass 200:1 at  $140^\circ$  viewing in the  $45^\circ$  quadrants. Such impressive viewing angle figures are achieved using a front uniaxial wave-plate with its axis oriented crossed to the rubbing direction (and input polariser) combined with a negative uniaxial wave plate formed from a homeotropic discotic liquid crystal polymer [131].

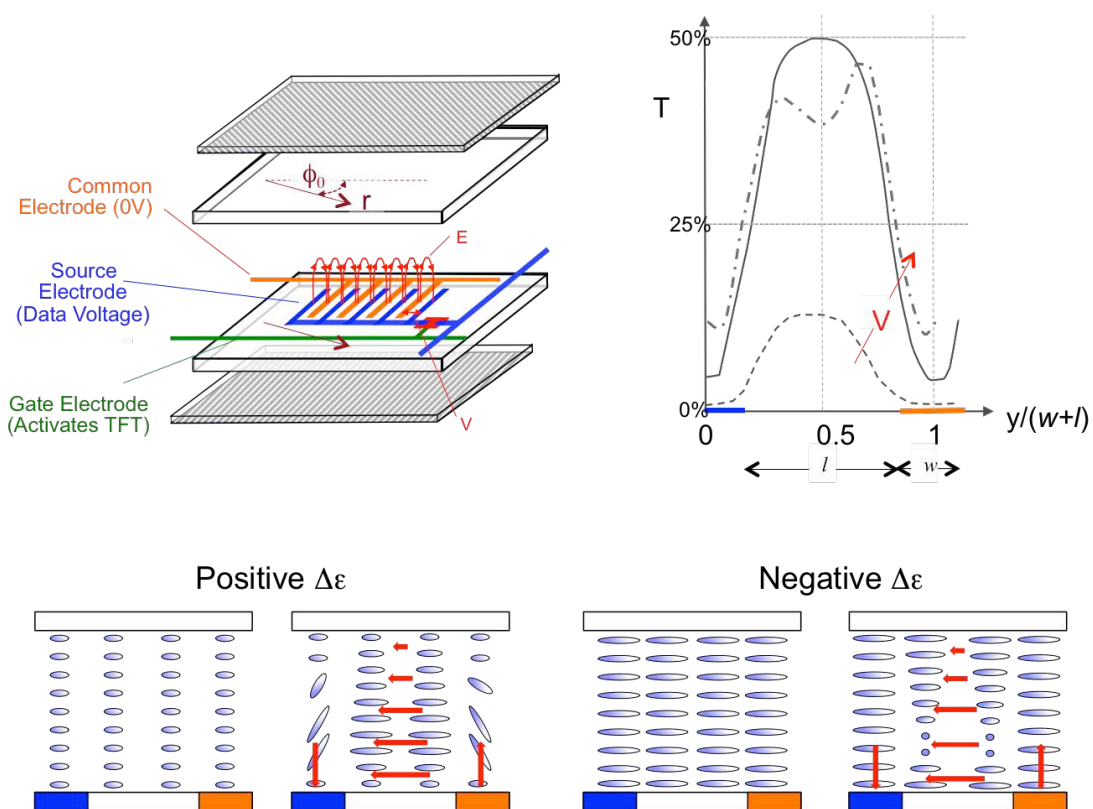


Figure 29 IPS Principles. a) Schematic of the TFT in-plane electrode arrangement; b) Theoretical transmission calculated for low and high switching voltages for one electrode period [125]. c) Mode choices associated with positive  $\Delta\epsilon$  and negative  $\Delta\epsilon$  materials.

### 4.6.3 Fringe-Field Switching mode.

Despite the impressive performance of IPS, the mode suffers from poor optical efficiency due to the banding structure caused by lack of director switching above the electrodes. For high-resolution portable display applications, this is very important because increasing the output from the backlight to compensate for optical inefficiency is too costly for battery life. Many mobile phones and tablets deploy fringe-field-switching mode LCD [96, 97]. This is a modification to IPS mode, where a uniform counter electrode is placed beneath a dielectric layer with the interdigitated electrodes on top. The pitch of the electrodes is much smaller than the cell gap, figure 30. There is little electric field directly above the central line of the data electrodes, but immediately either side of this there is an in-plane field component that causes the director to reorient. This arrangement greatly reduce the transmission loss caused by the banding, and can be operated with electrodes that are closer together, therefore allowing lower operating voltages to be used. The fringing fields break the symmetry sufficiently to allow operation without alignment pre-tilt, again helping to improve viewing angle towards the limit. This is difficult with conventional rubbed polymers but can be achieved using photo-alignment.

Typically, the dielectric layer is 500nm thick, providing much higher fields close to the electrode surface than typical for the IPS mode [132]. Together with the reduced electrode spacing, this lower operating voltages, and hence power. The dielectric layer acts as the storage capacitor for the pixel, thereby increasing the aperture ratio and concomitantly increasing optical efficiency still further. Typically, FFS mode has double the optical efficiency of the IPS mode, with the only disadvantage being that two transparent electrodes need to be deposited and etched onto the rear plate during fabrication process. The success of FFS mode can be measured by its adoption for many portable products, notably the *Apple iPad* from 2011.

## 4.7 Vertically Aligned Nematic Modes

As for IPS, the invention of vertically aligned nematic (VAN) occurred early in the history of LCDs [85], but was reinvigorated with the widespread adoption of TFT and the need for wide-viewing angle technologies in the mid-1990s. Homeotropic alignment gives a near perfect black state at normal incidence, and a viewing angle easily compensated using a negative uniaxial retardation plate. Being dominated by the dark state, the contrast of VAN mode devices is generally exceptional at all angles and is independent of temperature or cell gap variations. The director is switched into the plane of the cell when a negative  $\Delta\epsilon$  liquid crystal is used. The direction of tilt will be degenerate and form scattering domains unless some preferred orientation is imparted to the cell. For example, if one of the homeotropic surfaces is rubbed, it gives a pre-tilt of typically  $89.8^\circ$ , and the director will tilt uniformly in this direction with increasing field. However, this will give a poorer viewing angle for the white state, as indicated in figure (8). To overcome this limitation, *Fujitsu* invented the multidomain vertically aligned mode in 1997 [94, 95], termed MVA mode. The aim of the invention was to maintain the vertical cylindrical symmetry as the director reorients with applied voltage, using domains of opposing tilt. Typically each pixel is subdivided into two or four areas with orthogonal tilt directions for each. Different area ratios may be used for the horizontal and vertical directions, provided that the area for opposing pairs is equivalent.

Initial attempts to produce multi-domain alignment used the rather impractical approach of dual rubbing, where a rubbed surface was protected during a second antiparallel rubbing by a photolithographically defined mask that was subsequently removed. The approach that *Fujitsu* took was to arrange dielectric protrusions onto the electrodes and underneath the homeotropic alignment layer, as shown in figure 31a). Each protrusion has a convex shape with sidewalls angled to the surface, but is sufficiently small and rarefied to have negligible effect on the overall pixel alignment. When the voltage is applied, the slight field fringing around the protrusion causes

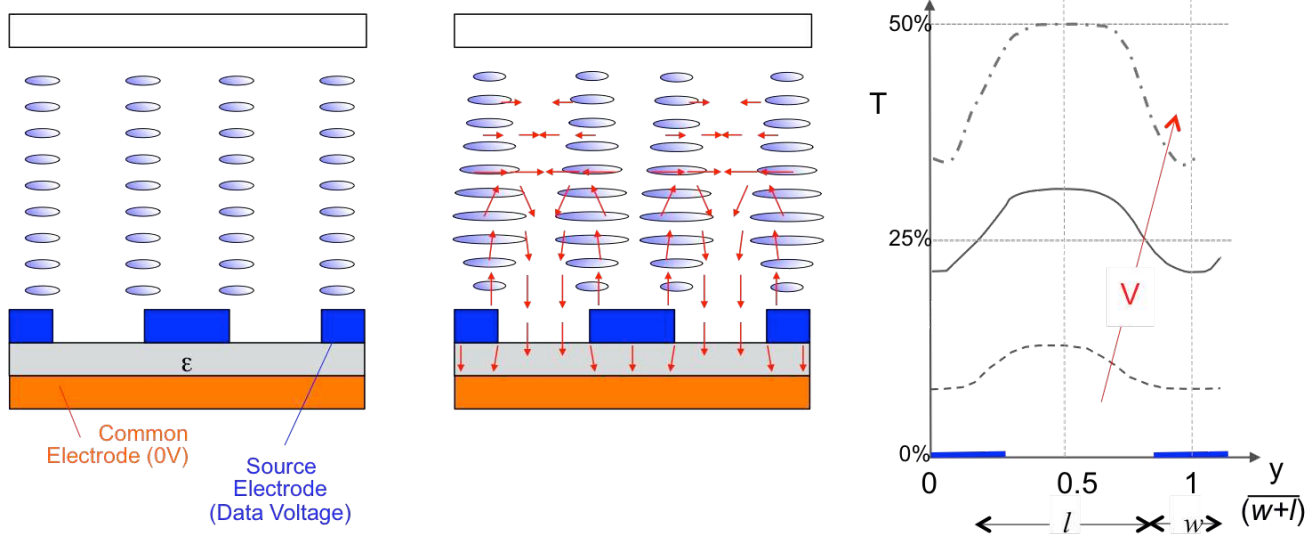


Figure 30 Fringe-Field Switching mode. a) Basic structure and operation, and b) typical transmission distribution with varying voltage within a period of the data electrodes, shown in blue.

tilting in opposite directions on either side of the protrusion, thereby breaking the symmetry and automatically causing domains of the opposite tilt sense. Early modules included protrusions on both inner surfaces, as shown in figure 31, but including the protrusion on a single surface only saved additional photolithographic steps, and was found to give satisfactory performance.

*Samsung* made a further advance for the VAN mode in 2000. Similar to the MVA mode, the patterned vertically aligned mode (PSA) replaced the protrusions with slits in the electrodes to create the fringing fields, figure 31b) [98]. *Sharp* [99] designed the axially symmetric micro-cell (ASM) mode LCD, where polymer walls surround the nematic, forming a microcell container for the liquid crystal, figure 31c). The walls are formed by photo-induced phase separation of a monomer during the polymerisation that occurs on UV exposure of a grid like pattern. A chiral dopant is added to the nematic with the correct

pitch to ensure a twisted orientation of  $90^\circ$  for the given cell gap. Unlike the MVA and PVA modes, disclinations are avoided altogether because the director forms a mono-domain whilst retaining the axial symmetry that results in the exceptional viewing angle.

These VAN modes share the properties of wide viewing angle, very high contrast, and fast operation. High switching speeds are common to each of the vertically aligned modes because the field induced distortion is dominated by the bend elastic constant  $k_{33}$ , which is usually significantly higher than both  $k_{11}$  and  $k_{22}$ , equation (48). The mode also has the advantage of not requiring the rubbing step during fabrication, which can give improved yield and costs. However, the mode is slower than modern IPS mode panels, because full switching is needed to obtain the bright state, whereas IPS switches the director through a lower angle if  $\phi_0 \gg 0$ .

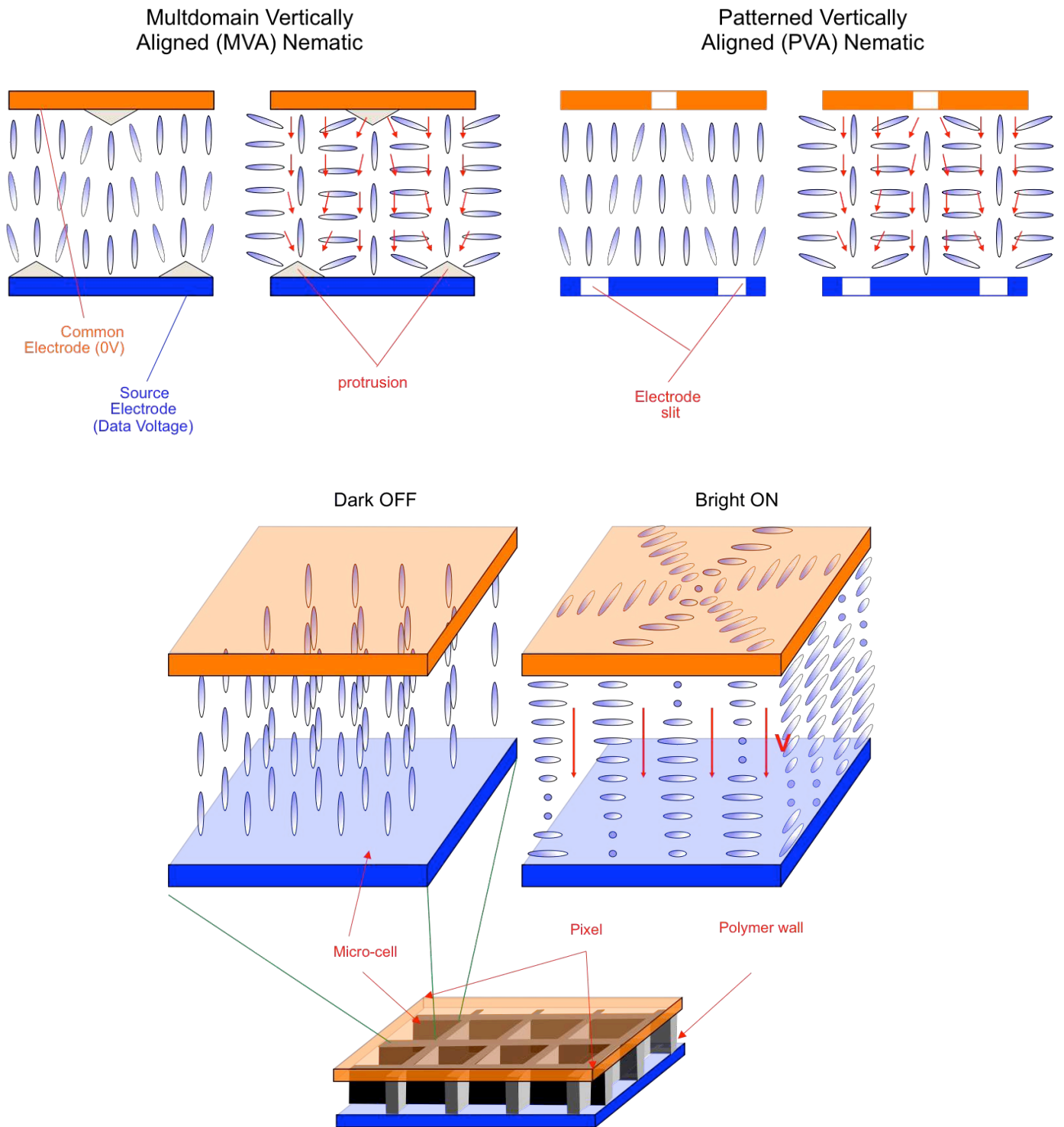


Figure 31 Vertical Aligned Nematic Modes. A) Multi-domain Vertical Aligned (MVA) mode; b) Patterned Vertical Aligned (PSA) Mode; c) Axially symmetric multi-cell (ASM) mode.

## 5 LCDs for non-mainstream and Niche Markets

### 5.1 Introduction

The wealth and diversity of different device modes that exploit liquid crystals is a measure of both the variety of phases and behaviours exhibited by these organic materials, and by the ingenuity of the scientists, engineers, inventors and innovators working in this field over the past half century. The path to providing flat screen monitors and FHD television displays is littered with unsuccessful attempts. However, many of those technologies found, or indeed created, niche markets, offering unique selling points in other applications. A selection of some of the more important LCDs used outside the conventional direct view displays are summarised in this section.

### 5.2 Cholesteric LCDs

#### 5.2.1 Temperature, Strain and Gas Sensors

From the first discovery of liquid crystals by Reinitzer in 1888 [18], the bright colours of cholesteric liquid crystal textures have fascinated observers. Indeed, the first liquid crystal application was not an electronically addressed display, but rather as sensors that deployed this colouration. In the early 1960s, prolific inventor James Fergason observed that the peak wavelength of cholesteric selective reflection depended strongly on both temperature and trace amounts of chemical vapour [133], envisaging device applications. His work inspired many applications, from detecting minute temperature changes on human skin due to the influence of nicotine or underlying tumour, to visualisation of faulty electronic circuitry. Photographer Henry Groskinsky, inspired by the vivid colours of the cholesteric, recorded these applications for *Life Magazine* in 1968 [134]. The article also mentioned that the liquid crystal could be encapsulated into a polymer, another of Fergason's inventions that will be described in section 5.5. That was used by *NCR* to detect the mechanical strain within a loaded spring, an application that was later extended to aeronautical testing of planes, rockets and turbine

blades [135]. Indeed, it was encapsulation that eventually led to mass production of liquid crystal thermometers that remain popular today.

The cholesteric has a natural helical structure shown in figure 1. Light travelling along the helical axis undergoes Bragg reflection due to the repeating nature of the optic axis. This occurs for circular polarised light with the same handedness as the cholesteric pitch  $P$  and at a band of wavelengths centred on  $\lambda_0$  given by:

$$\lambda_0 = \bar{n}.P.\cos\theta \quad , \quad (103)$$

where  $\theta$  is the angle of incidence with respect to the helical axis and  $\bar{n}$  is the average refractive index ( $= \frac{1}{2}n_e + \frac{1}{2}n_o$ ). Strong colouration occurs when  $\lambda_0$  matches a visible wavelength, from 400nm to 700nm. The width of the reflection band  $\Delta\lambda$  is approximately:

$$\Delta\lambda \approx \Delta n.P \quad . \quad (104)$$

The colour is therefore made more vivid by using weakly birefringent cholesteric materials. Light of wavelengths outside the band of selective reflection is transmitted through the sample, as is all light of the opposite handedness. Optical contrast then requires the liquid crystal layer to be mounted on to a dark backing material, to absorb the transmitted light. Tuning of the temperature range over which the pitch varies in the visible regime usually requires two or more components with different pitches and temperature dependences. The pitch diverges as the second order cholesteric to smectic phase transition is approached, leading to rapidly changing colour from red to blue with increasing temperature. Varying the concentration of components with strong smectic local ordering in the cholesteric mixture provides control over the operating temperature range for the thermometer.

#### 5.2.2 Bistable Cholesterics

Selective reflection of coloured light from cholesteric liquid crystals can be used for electronic displays too.

Moreover, the cholesteric electro-optic characteristic can be arranged to be bistable, allowing unlimited multiplexibility using low cost passive matrix addressing. Amongst the first optical switching modes to be studied at *RCA* was the bistable cholesteric [136], the switching mechanism for which was elucidated during the 1970s [137, 138]. However, the success of the bistable cholesteric is largely due to the team at Kent State University headed by Doane [139], and the many innovations made by the engineers at the spin-out company *Kent Displays Inc. (KDI)*, [140, 141].

The basic operation of the display is to switch the cholesteric liquid crystal between the Grandjean texture, where the axis of the helix is largely normal to the display which therefore appears reflective, and the focal conic texture, where the helix lies in the plane of the cell and light is forward scattered to be absorbed by the rear (black) substrate. Latching between the states is done via an intermediate homeotropic state, where the field is unwound by a high electric field coupling to the positive  $\Delta\epsilon$  of the liquid crystal, as shown in figure 32a). If the field is switched off immediately, the helix forms with its axis vertical to the pixel, thereby appearing coloured due to selective reflection. If the field is reduced more gradually through an intermediate level, the helix forms in the plane of the cell, in the focal conic state, and the pixel appears dark. The degree of hysteresis and the sensitivity of the device to mechanically induced damage is controlled using polymer stabilisation.

Most displays are designed to be monochrome, using materials with high birefringence to give the broadest reflectivity. The highest practical levels of  $\Delta n$  give yellowish-green colouration against black, though some customers prefer the inverted optics of white and blue when a blue background is used. Together with the slow response speed, high voltage and sensitivity to shock, the poor appearance means that the devices are not commercially successful, and have been largely superseded by other choices. However, bistable cholesterics remained of interest for full colour bistable reflective displays. Lower birefringent materials are used to give individual layers with sharp red, green and blue

reflection bands. Stacking three layers in series then allows full reflective colour. This type of technology was successfully applied to large area signage by the company *Magink*, providing bright billboards for advertising purposes [142]. As a reflective display, the panels were ideal for bright sunlit conditions, where they could outperform LED electronic signage. *KDI* also used a triple stack to produce full colour reflective displays for portable products. Parallax between the layers was minimised through polymer stabilisation of the individual active layers mounted directly onto a backing foil [141], as shown in figure 32b). Not only did this enable good optical performance, but also the resulting display was very flexible indeed, as is apparent from the demonstrator shown in figure 32c). Although not successful commercially, this also remains true of all other reflective colour display modes, and remains an important gap for future developments.

The technical advances made by *KDI* for flexible colour plastic displays promised new applications outside the display field, such as electronic skins, figure 32d), and electronic writing tablets, figure 32e). The *Boogie board* is an electronic writing pad that uses mechanical pressure to induce the reflective Grandjean texture, on a black background. When the image needs to be refreshed, an electrical blanking pulse is applied to erase the page. This product continues to be successful in a niche market that the technology has created.

### 5.3 Bistable Nematic LCDs and ZBD

Bistable operation of an LCD allows many lines of information to be passive matrix addressed, where each frame is written line by line and each line retains its information until it receives the next addressing signal. Before the large-scale adoption of TFT back-planes and active matrix addressing, various bistable nematic modes were invented, complementing the contemporary efforts to develop bistable cholesteric and ferroelectric liquid crystal displays. Few of these modes made it even to demonstrator stage. However, in the late 1990s, there was a resurgence of interest in bistable nematics [127],

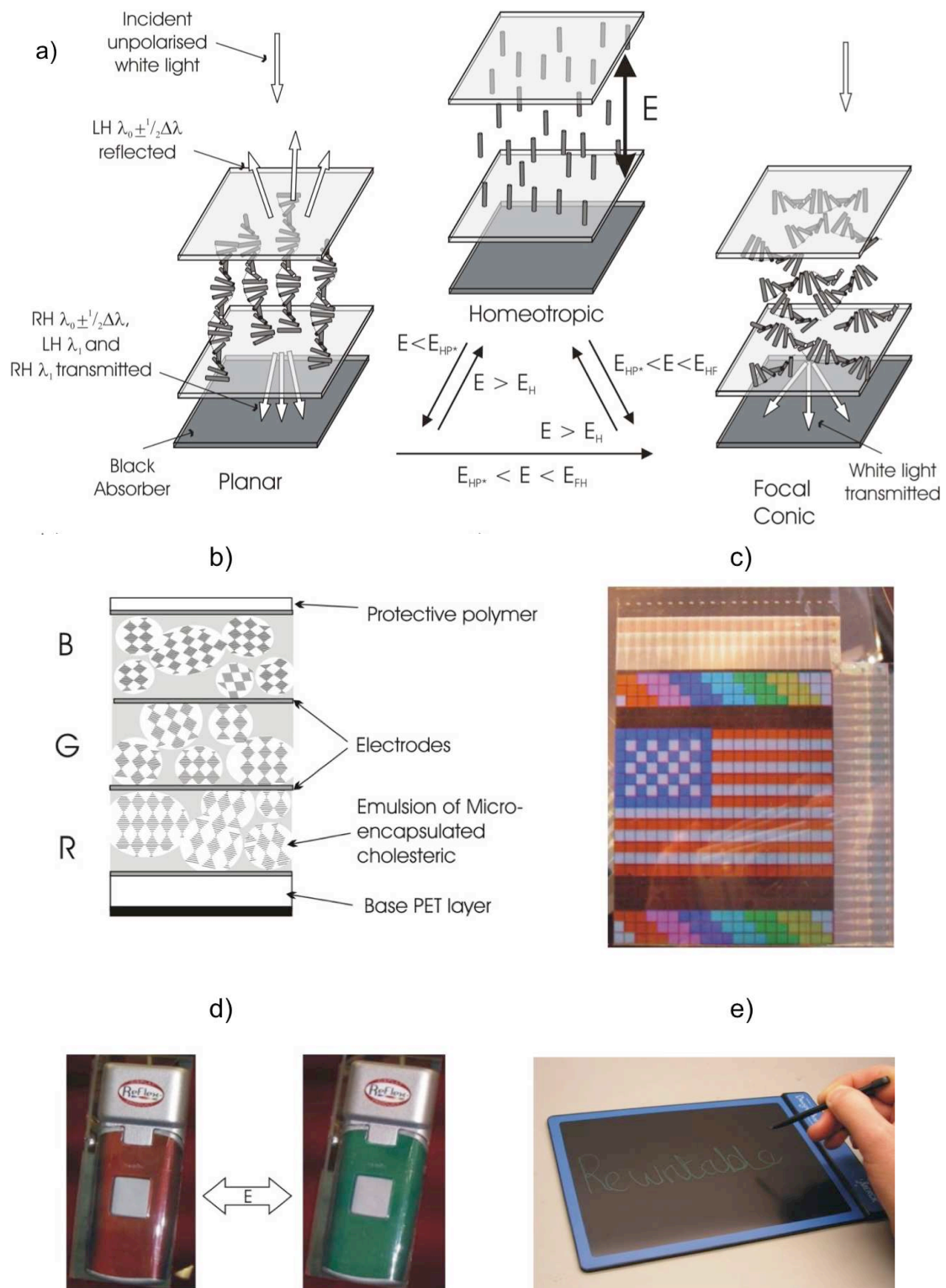


Figure 32 Bistable Cholesterics. a) operating principle; b) tri-layer stack for full colour; c) Prototype of the film backed triple N\* stack; d) Switchable electronic skin using a single layer cholesteric; e) The successful Boogie-Board product from KDI, using bistable cholesteric to form a writing tablet.

notably the work at *Seiko-Epson* on the Bistable Twisted Nematic (BTN) Mode, the 180° BTN or *Binem*<sup>TM</sup> developed by *Nemoptic*, and the Zenithal Bistable Device (ZBD) by *ZBD Displays Ltd.*, (now *Displaydata*). Several factors drove this renaissance:

- Simple passive matrix displays based on TN and STN did not lose market share with the introduction of TFT; rather, the markets that they had created, such as watches, calculators, instrumentation, etc., continued to need low cost, usually reflective displays. Whereas new, high investment production plants in Japan, Korea and Taiwan developed TFT LCDs for high end applications, a plethora of manufacturers in China continued to serve what remained a \$1B passive matrix market well into the 2000s.
- Bistability promised to create new niche LCD markets, particularly where ultra-low power was required. Markets included electronic shelf-edge labels with high information content, electronic book readers, smart-card displays, secondary displays for mobile phones, and an enormous range of indicator displays, from car key-fobs to razor blades. Indeed, the image storage offered by bistability continues to be a unique selling point for many applications associated with the Internet-of-things, where displays can be updated automatically using radio frequency (RF) signals, rather than rely on costly batteries and associated circuitry.
- Bistable displays often have good potential for plastic displays. TFT on plastic remained a challenge to fabricate through the 2000s, due to the difficulties of registering high-resolution patterns on a flexible backplane, and the low fabrication temperatures required for plastic substrates. Bistable nematics offered the possibility of high image content based on simple, low temperature, low cost fabrication on plastic.

However, these drivers, were also attractive to other, non-liquid crystal display modes, such as Janus colloids from *Gyricon*, interference mode MEMS from *Iridigm / Qualcomm*, electrowetting from *Liqua-vista / Amazon* and *Gammadynamics*, and electrophoretics from *Bridgestone* and *E-ink*. In 2005, *Amazon* selected *E-ink* displays for its *Kindle* e-Book readers, based largely on the appearance of its white state and despite the significantly higher cost due to the active matrix. This created demand for scattering mode devices, and many new markets chose electrophoretics over LCDs. One bistable LCD technology that survived was the Zenithal Bistable Display, marketed by *ZBD Displays Ltd*, now *Displaydata*. This spinout from *R.S.R.E* (then *DERA*) in the UK targeted the retail signage market, and in particular electronic shelf-edge labelling. For a retailer to replace tens of thousands of electronic labels per store, cost was paramount, and the bistable LCD has a significant advantage over electrophoretics, whilst offering superior performance and higher image content than the incumbent directly addressed segmented TN LCD. The company's success was not only due to the bistable LCD, but also by development of a novel RF communications protocol [126], that allowed small to mid-sector retailers to take advantage of the labelling, whereas only hyper-stores had been able to afford the infrastructure required for previous labelling systems. The company has sold several million labels worldwide, and now offers a combination of the ZBD LCDs alongside *E-ink* for higher-end application.

Bistability results where a device has two stable states with similar free energies that are separated by an energy barrier, wherein transitions from one state to the other are discontinuous, or first order. An early approach was the Bistable Twisted Nematic (BTN) mode [143], which followed similar principles to that of the STN, but set the d/P ratio of the chiral nematic to lie halfway between states of low and high twist angles  $\Phi$ . For example, setting d/P = 0.5 with parallel surface alignment should give a  $\pi$  twist state. However, if the pre-tilt on both surfaces is sufficiently high, the cost of the induced splay energy becomes greater than that for twist. Thus, the chiral

nematic may either unwind to a uniform  $0\pi$  state to match the surface condition, or may wind further to form the  $\Phi = 2\pi$  twist state, figure 33a). Switching from one state to the other then relies on whether or not flow is induced immediately after a high electrical pulse coupling to a positive  $\Delta\epsilon$ . If the pulse returns to 0V via an intermediate voltage, there is little induced flow and the  $0\pi$  state is formed, whereas a direct transition to 0V induces flow that encourages director twist at the cell centre and the  $\Phi = 2\pi$  state is formed. The two states are metastable, so the texture relaxes back to the intermediate  $\pi$ -state after a second or two on removal of power. This means the device was not suited to zero power applications. Rather, *Seiko Epson* used it as the display for Hi-Fi Graphic Equalizer displays, due to its very fast optical response [144].

A similar approach was taken by *Nemoptic*, who also used a BTN configuration, but with  $d/P = 0.25$  to give either 0 or  $\pi$  twist states, figure 33b). In

this instance, the director cannot change its twist from one state to the other without breaking the anchoring at one of the surfaces, requiring that one of the surfaces be deliberately weakly anchored [145]. Switching of the device again utilised back-flow depending on the trailing shape of the addressing pulses. Marketing the device under the trade name *Binem*<sup>TM</sup>, *Nemoptic* produced various demonstrators [146], including full colour reflective displays, TFT driven panels and, intriguingly, a pixelated switchable quarter-wave plate mounted onto the front of an OLED display to switch between high-power emissive video frame rate display and ultra-low power Black and White E-reader mode [147]. Despite the excellent optical appearance,  $0-\pi$  BTN required cell gaps below  $2\mu\text{m}$  and suffered from manufacturing tolerances that were difficult to achieve. Perhaps the biggest cause of the company's eventual demise in 2010 was that it failed to find the correct niche for its product.

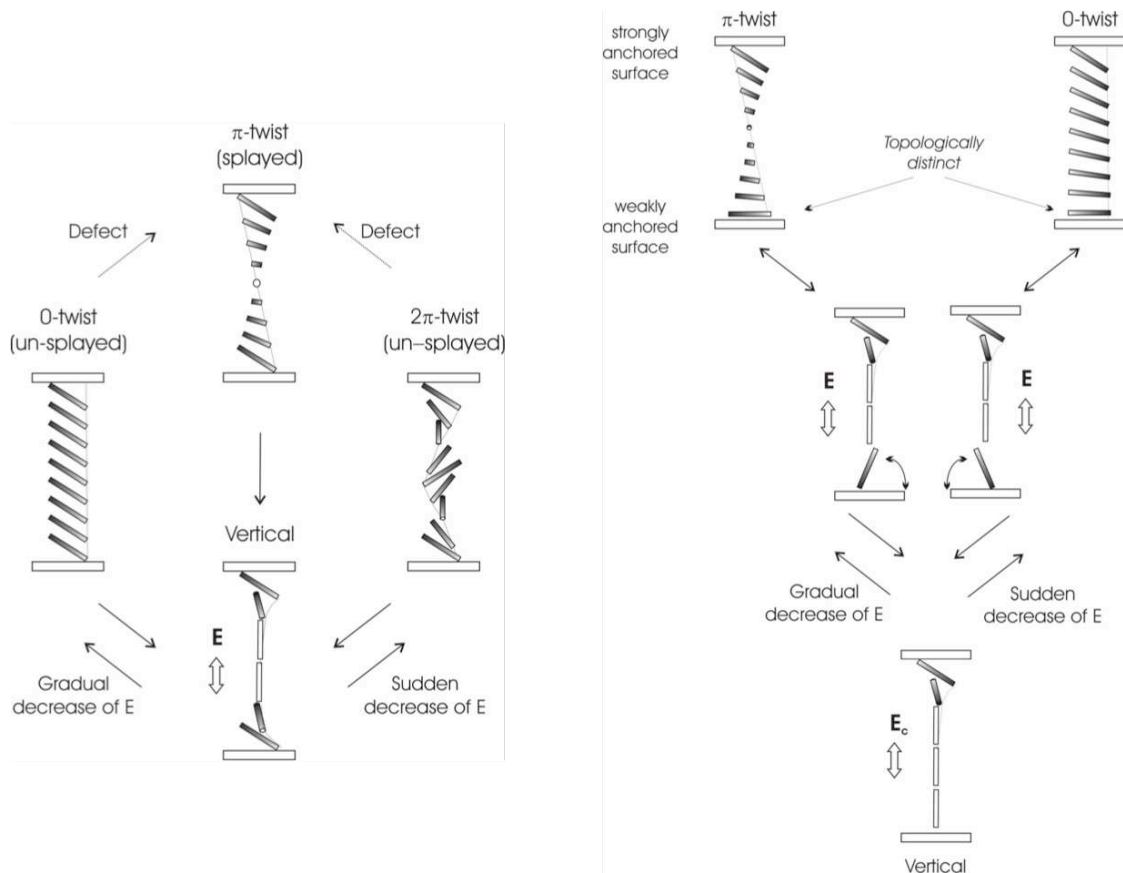


Figure 33. Operation of Bistable Twisted Nematics. a)  $0 - 2\pi$  mode ; b)  $0 - \pi$  mode or *Binem*<sup>TM</sup>.

The Zenithal Bistable Display (ZBD) is rather unusual in several aspects [148, 149]. It uses a grating as a surface alignment layer, designed to impart bistable pre-tilts of the contacting nematic regardless of the overall geometry chosen, figure 34. This allows many different LCD designs to be used, including VAN- HAN mode [148], HAN to TN mode [150, 148], multistable VAN – HAN – TN modes [151], grey scale displays [152], single polariser mixed TN modes [153], scattering modes [154] and ultra-fast Pi cell modes [151]. The device is an early example of, and the only LCD currently on sale, that utilises the flexoelectric effect for latching between the two states. Moreover, the device deliberately uses disclinations at the deep, homeotropic-grating surface to stabilise the low tilt or D state. The potential barrier between this state, and the high tilt defect-free or Continuous state (C state) is mediated by the creation and annihilation of these surface defects. The voltage for latching from one state to the other  $V_{CD}$  is related to the pulse width  $\tau$  by [155]:

$$\begin{aligned} \frac{V_{CD}}{d} &\approx \frac{\gamma_1 l_s}{(e_1 + e_3)\tau} + \frac{2W_\theta}{(e_1 + e_3) + \sqrt{\epsilon_0 \Delta \epsilon K_{33}}} \\ &= \frac{\gamma_1 l_s}{(e_1 + e_3)\tau} + V_{th} \end{aligned} \quad , \quad (105)$$

where  $W_\theta$  is the zenithal anchoring energy of the homeotropic grating surface,  $l_s$  the coefficient of slip for defects moving across that surface,  $e_1 + e_3$  is the sum of the splay and bend flexoelectric coefficients for the liquid crystal material, and the dielectric effect of the grating has been ignored. Controlling the anchoring energy in the range  $0.2 \text{mJcm}^{-2}$  to  $1 \text{mJcm}^{-2}$  allows the threshold voltage  $V_{th}$  to be adjusted to typically about  $1 \text{V}\mu\text{m}^{-1}$ , typically 7V.

The device is usually configured with the grating opposite a standard parallel aligned rubbed polymer surface to create a  $90^\circ$  TN when in the low tilt D state. This state is always formed first on cooling from the isotropic to nematic phase, because the defects are stabilised at the surface when the S order parameter is low. Thus, the interpixel gaps remain in the TN state, and good display reflectivity results when operating in the normally white TN mode.

Typical cell gaps are  $7\mu\text{m}$ , operating at 15 – 20V using standard STN driver electronics, LC mixtures and polarisers. Operating temperatures from  $-25^\circ\text{C}$  to  $40^\circ\text{C}$  and  $-5^\circ\text{C}$  to  $+60^\circ\text{C}$  were achieved using low and high anchoring energies, respectively.

The main technical challenge for *ZBD Displays Ltd.*, was to introduce a low cost and reproducible manufacturing method for a  $0.8\mu\text{m}$  pitch,  $1\mu\text{m}$  high blazed sinusoidal grating into a standard passive matrix LCD production line using Gen 2 glass. This was done by copying a photo-lithographically defined master grating into a lacquer on Polyethylene terephthalate (PET) film, via a nickel sputtering and electro-forming replication technique [149, 156]. The film was shipped from the UK to manufacturers in China, where it is used to emboss the grating into a homeotropic photopolymer deposited on the glass surface, thereby replacing the conventional rubbing step for that plate. This method allows the technology to meet the same price point as conventional STN, where the costs of the compensation foils required for the STN offsets that of the ZBD grating film. Having achieved such low price-points for its chosen niche market, it remains to be seen if ZBD can replace conventional TN and STN displays in other markets.

#### 5.4 Polymer Dispersed Liquid Crystals

A weakness of LCDs that is particularly evident in reflective mode devices is the constraint for polarisers, which absorb more than half of the available light. This inefficiency was avoided in the first dynamic scattering displays, but the contrast and lifetime of those devices was far inferior to retardation based LCDs such as the TN, that their period of success was very short-lived. Hilsum [157] produced a scattering device by mixing glass micro-spheres into a nematic, creating a scattering texture that could be switched to a non-scattering state by an electric field. A more practical device was the polymer-dispersed liquid crystal (PDLC). This is another example of an LCD that initially aimed to produce bright displays, but which found success when the technology was applied

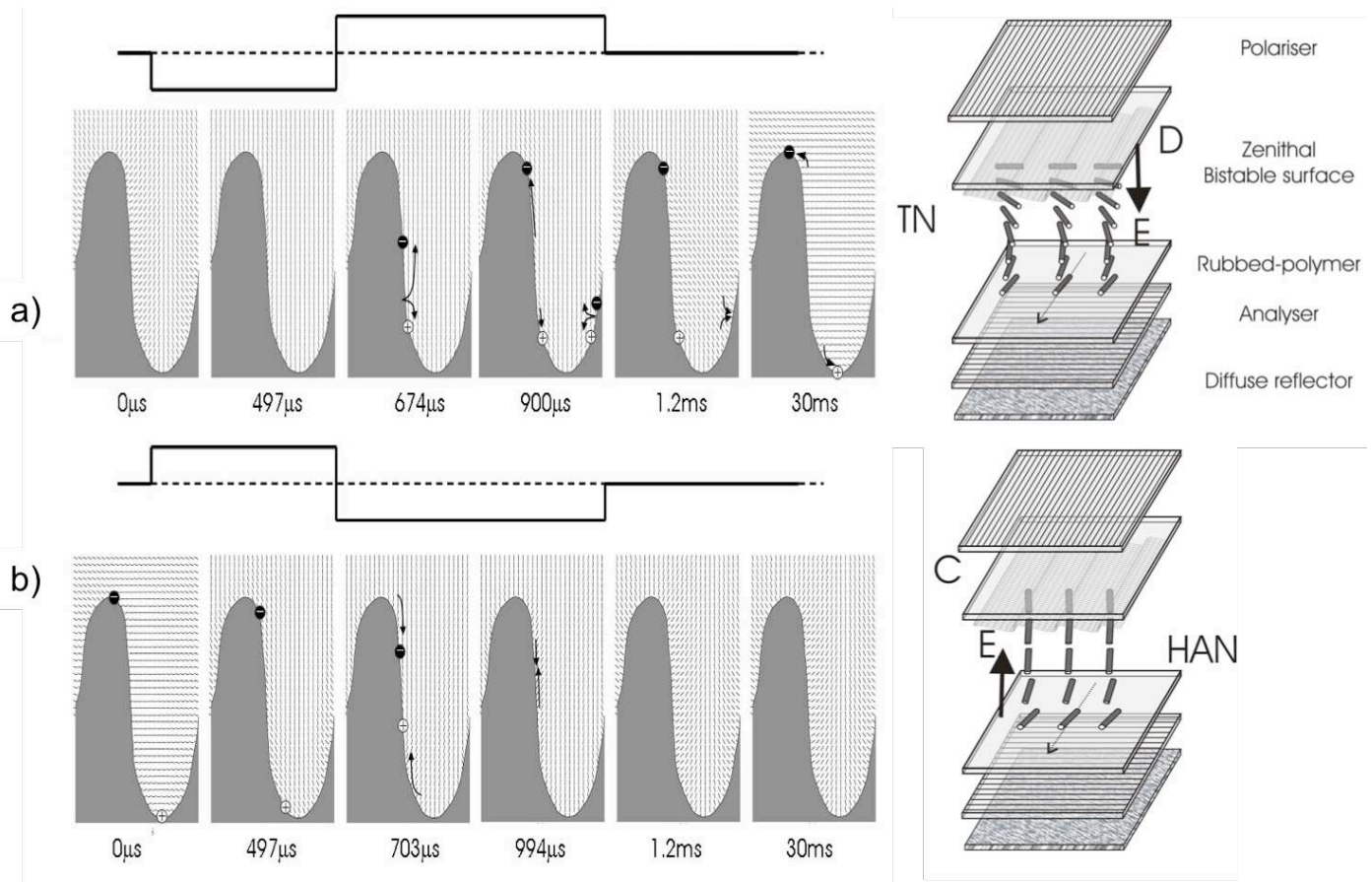


Figure 34 The Zenithal Bistable Display Mode, ZBD™. a) Latching from the C to D state occurs with a bi-polar pulse with the trailing part positive with respect to the grating. The applied field nucleates defects at the bifurcation point on the grating sidewall, and the positive polarity favours the D state with  $-1/2$  disclinations at the convex surface and  $+1/2$  defects at the concave surface. The resulting low surface tilt creates a  $90^\circ$  TN state when placed opposite a conventional monostable rubbed polymer surface as shown. Operating in the normally white mode, with the grating aligned parallel to the front polariser and with  $n$  matched to the liquid crystal ordinary refractive index gives an excellent white state. b) Applying pulses of the opposite polarity causes the defects to retrace their path along the grating surface until they annihilate. The resulting C state is continuous and homeotropic, thereby creating HAN alignment. This appears black when between the crossed polarisers as shown, and the viewing angle self-compensates when in reflective mode.

to a novel product with a niche market; for PDLC this was privacy glass.

Following his successes with cholesteric sensors and the invention of the twisted nematic LCD soon after Schadt and Helfrich (claiming precedence in the US), Ferguson invented a method of encapsulating liquid crystal droplets into a polymer

matrix in the early 1980s [158]. Originally called NCAP by its inventor, PDLC usually takes the form of a plastic layer that can switch between scattering and non-scattering states with an applied electric field [159, 160]. An ITO coated glass or transparent plastic cell is filled with a nematic liquid crystal mixed with a monomer. Curing of the monomer into a solid polymer

form is done either by evaporating the monomer solvent, applying a thermal treatment or, most commonly, through the initiated polymerisation of constituent photo-reactive groups. Phase separation of the liquid crystal occurs as the polymer forms from the monomer, creating droplets within the polymer matrix. Often, a surfactant is included, both to help control the dispersion of droplet size and align the nematic into a radially symmetric or bipolar state, as shown in figure 35. Droplets in the 0.5 to 5 $\mu\text{m}$  range scatter incident

light intensely due to the refractive index mismatch between the polymer and the liquid crystal. Application of an electric field across the sample then causes reorientation of the liquid crystal director, leaving the cross-linked polymer undisturbed. Usually, the liquid crystal has a positive  $\Delta\epsilon$  and an ordinary refractive index  $n_o$  matched to that of the polymer. Thus, the scattering is reduced as the liquid crystal aligns parallel to the field, and light incident close to the normal direction is transmitted unchanged.

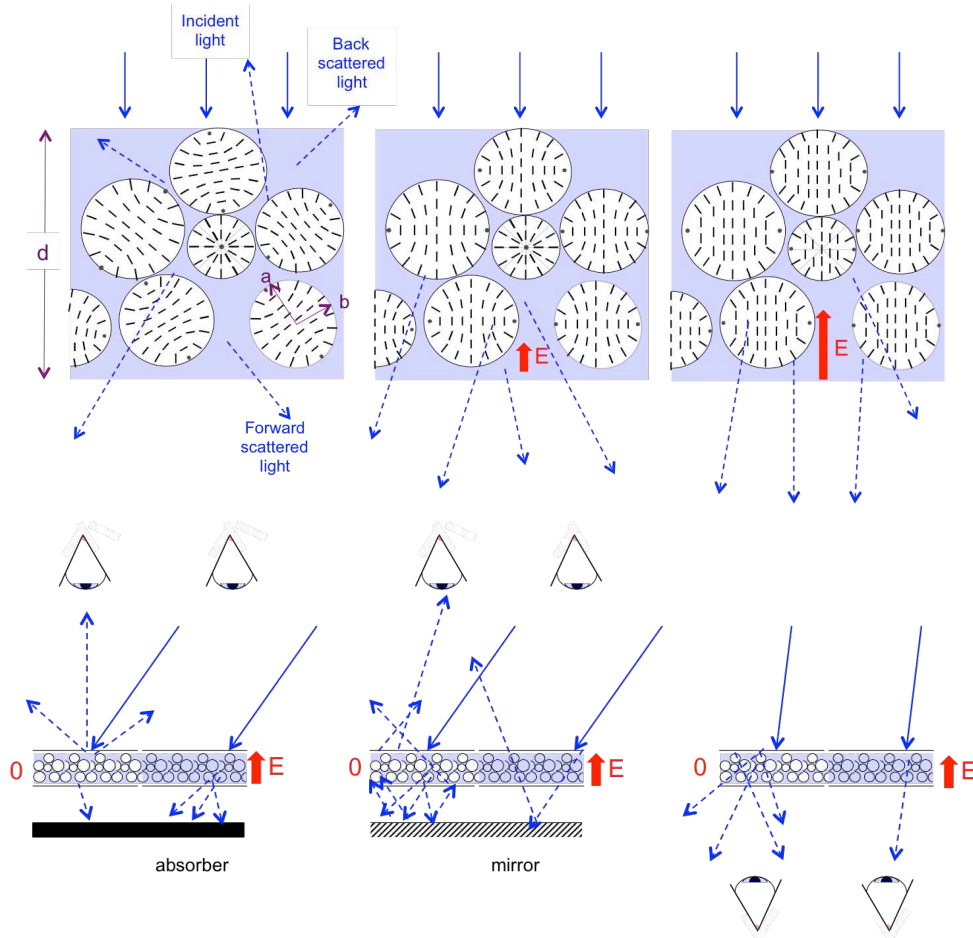


Figure 35 Polymer Dispersed Liquid Crystal for a positive  $\Delta\epsilon$  operating in the scattering to non-scattering mode. a) Droplets of different sizes with random orientations of the director profile, forming either a radial or bipolar configuration. Light is strongly scattered, including back scattering. b) Application of the field initially causes little distortion of the director profile within each droplet, but the profile adjusts to align the disclinations within the plane of the film and the director with a net direction parallel to the field. The scattering reduces somewhat. c) Increasing the field causes distortion of the director field within each droplet towards the vertical orientation, where the refractive index of the droplet and polymer matrix approach the matched condition, and little scattering occurs. d) Conventional back-scattering mode of PDLC; e) Novel, low voltage mode using specular reflection as the black state; f) Common mode for privacy windows, where the plastic film switches between translucent and transparent.

Droplets with radial alignment have a single defect at the droplet centroid (called a “*Boojum*”) leading to spherical symmetry, whereas bipolar droplets have point defects on opposing surfaces and cylindrical symmetry of the director field. Typically, droplets are between 1 and 10 micron, and form the bipolar structure with randomly oriented symmetry axes. The electrical field behaviour is complex. The field required to align the director parallel to the field, and hence approach the minimum deflection of incident light, is inversely proportional to the droplet radius,  $a$  [161]. For a radial droplet, the critical field is approximately related to [162]:

$$E_C = \frac{4}{a} \sqrt{\frac{\bar{k}}{\epsilon_0 \Delta \epsilon}} \quad , \quad (106)$$

where  $\bar{k}$  is a mean elastic constant. The symmetry of a perfectly spherical bipolar droplet prevents analytical solutions being made, and needs the symmetry to be broken. A practical approach is to assume that each droplet is slightly elongated with different semi-major axis  $a$  and semi-minor axis  $b$ . For liquid crystals with positive  $\Delta \epsilon$ , weak applied fields reorient the symmetry axis parallel to the direction of the field. The critical field is then given by [162]:

$$E_C = \frac{1}{3ab} \left( \frac{\sigma_{LC}}{\sigma_P} + 2 \right) \sqrt{\frac{k_{33}(a^2 - b^2)}{\epsilon_0 \Delta \epsilon}} \quad , \quad (107)$$

where  $\sigma_{LC}$  and  $\sigma_P$  are the low frequency conductivities of the liquid crystal and polymer respectively. The response times are given by:

$$\tau_{ON} = \frac{\gamma_1}{\epsilon_0 \Delta \epsilon E^2 + \frac{k_{33}}{a^2 b^2} (a^2 - b^2)} \quad , \quad (108)$$

$$\tau_{OFF} = \frac{\gamma_1 a^2 b^2}{k_{33} (a^2 - b^2)} \quad .$$

Typically, droplets of  $a = 1 \mu\text{m}$ ,  $b = 0.9 \mu\text{m}$ ,  $k_{33} = 10 \text{pN}$ ,  $\gamma_1 = 0.05 \text{kgm}^{-1}\text{s}^{-2}$  and  $\Delta \epsilon = 15$ , and  $\sigma_{LC}/\sigma_P \approx 28$ , giving  $E_C \approx 1.5 \text{V}/\mu\text{m}$ , and  $\tau_{OFF} \approx 20 \text{ms}$ . Substantial scattering needs twenty or so droplets in the direction of incidence, so film thicknesses of  $20 \mu\text{m}$

are typically used. Thus, the voltage of such PDLC films can be high, typically much higher than 30V to achieve saturation of the transparent, non-scattering state.

If the droplets are sufficiently small, and the device spacing high, then the OFF state can lead to significant back scattering. This can be used in a reflective mode display, by mounting the PDLC film onto a black background to provide optical contrast, figure 35d). However, the switching voltage inherently increases both with smaller droplets and higher device spacing. Moreover, the shallow switching response necessitates the use of TFT to matrix address the pixels, limiting the switching voltage to 15V and preventing any useful degree of optical effect. Recently, *Sharp* has produced low voltage TFT PDLC displays where the layer is mounted instead onto a specular mirror [163]. Relatively large droplets keep the voltages sufficiently low for TFT addressing ( $\approx 6 \text{V}$ ), and the forward scattered light is scattered more strongly after being reflected back towards the observer a second time by the mirror. In the ON state, the forward scattering is removed and the viewer sees the specular reflected light. In applications where the display is illuminated by a point source, this will appear black in all directions except where the display is oriented directly between the viewer and light source, figure 35e).

Although never successful for mainstream displays, one market that PDLC has found a niche is for privacy windows. The PDLC can be made as a laminated plastic roll, which can be applied adhesively to existing infrastructure, and trimmed to the appropriate size and shape. The window can then switch between a translucent, "milky white" appearance in the OFF state, to being clear and fully transparent when ON. Although this adds costs to the window, it is increasingly popular in high-end architectural projects for both interior and exterior applications. Uses include privacy control of conference rooms, intensive-care areas or bathroom doors, for example, to providing architectural design features. Moreover, the material can also be adjusted to act as an environmental smart window, switching between heat retention and loss as required [164]. Other applications such as temporary projection

screens, active camouflage, and switchable diffusers are all possible [165].

Another potentially profitable application for PDLC is switchable holographic media [166]. If a coherent image is used to cure the polymer during the fabrication process, switchable diffractive optical elements can be fabricated with droplets ranging from 100nm to 1 $\mu$ m forming holographic gratings from the interference pattern of the illumination. Rather than cause scattering, the droplets locally modulate the refractive index to generate a diffraction grating. Holographic optical elements (HOE) are used for a variety of optoelectronic applications, including focusing, beam-steering, filtering and optical multiplexing. The use of holographic PDLC provides the means for switchable HOE, allowing dynamic beam steering, tuneable filtering, and optical signal processing. For Holographic PDLC the droplet size  $a$  is typically sub-micron and the OFF time is very fast: typically 50 $\mu$ s to 500 $\mu$ s. However,  $E_C$  also increases with decreasing droplet size, and so typically 100 to 200V is required. This high field dominates the ON time, which again is fast, typically 50 $\mu$ s.

## 5.5 Liquid Crystal on Silicon (LCoS)

Rather than apply a semi-conductor onto glass to provide transistors, Liquid Crystal on Silicon (LCoS) places the liquid crystal element directly onto a CMOS integrated circuit [167, 168]. Of course, as the silicon is opaque, the devices must operate in reflection; usually, silver electrodes patterned directly onto a CMOS integrated circuit provide both the pixelated electric field pattern and the highly reflective rear substrate. The chip not only provides the drive signals for the contacting liquid crystal but can also deliver extra functionality, such as grey-scale gamma correction, temperature compensation, edge detection, etc. The devices are typically only 1cm to 2cm in diagonal, and are used for projectors and camera viewfinders. Keeping such low dimensions enables the ultra-high resolution of the silicon circuitry industry to

be applied, with typical pixel pitches for an XGA projection display being below 3 $\mu$ m.

LCoS spatial light modulators are the active element in light projectors for conferences and home cinema systems. This is one of the largest niche markets for LCDs, despite strong competition from micro-electro-mechanical-systems (MEMS) projection displays (Digital Light Projectors, DLP). Recently, there has been great interest in near-eye displays and pico-projectors, such as those used in Virtual and Augmented Reality headsets, and for Google glass. Such displays tend to use a small poly-silicon transmissive TN LCD, rather than reflective LCoS.

The projector systems either use a single LCoS panel, or use three panels tuned for red, green and blue wavelengths and the final image combined using a prism system. A 45° single polarise TN can be used, but VAN mode provides the high contrast needed for home cinema, as utilised by the top of the range projectors from *Sony* and *JVC*, [168]. Considerations such as viewing angle and colour balance become inconsequential in such projection systems, where speed and contrast are the dominant factors, and performance can be optimised for individual colour bands.

A different approach to colour uses a ferroelectric LCoS. Rather than using three separate modulators, the fast response time of the ferroelectric liquid crystal is used to provide operation at 360Hz, thereby allowing frame sequential colour when illuminated by 120Hz alternating colour band illumination [169, 170]. This is used for helmet mounted VR, binocular displays and viewfinders by *Forth Dimension Displays* and *Cinoptics*.

LCoS has also proven successful for non-display applications, particularly for spatial light modulators in optoelectronic systems such as wavelength selective switching, structured illumination and optical pulse shaping [171].

A related technology to LCoS is the Optically Addressed Spatial Light modulator [172]; rather than electrically addressing each pixel, the device is addressed using incident light. The LCD includes un-pixelated ITO electrodes sandwiching a photo-conducting semiconductor and liquid crystal layers. In

the dark state, the dielectric permittivity of the photoconductor is low, and most of the electric field applied across the ITO electrodes is dropped across this layer, leaving the liquid crystal unswitched. However, charge is transferred to the liquid crystal interface where light is incident on the photoconductor, which switches the liquid crystal accordingly. Early devices used GaAs photoconductor and a nematic. Recently [173, 174], an  $\alpha$ -Si OASLM with an FLC modulation layer has been used to produce dynamic computer generated hologram with over  $10^8$  pixels. The speed and the bistability of the FLC allowed the image to be built successfully in a projection system using a series of electrically addressed nematic SLM. The resulting system remains arguably the most complex display to be produced, and the nearest to providing full 3D holographic dynamic images, which remains the ultimate display goal.

## 6 LCD Modes for potential future applications

### 6.1 Introduction

The variety of different LCDs is huge and only a handful has made it to commercial success, whether mainstream or niche. Some of these modes are important to describe, since they include principles yet to be utilised (e.g. the Pi-cell, V-shaped switching FLC and Anti-ferroelectric Liquid Crystals); others are recent modes that are yet to find a market (such as the Blue-phase, or flexoelectric cholesteric modes). It was suggested earlier that the principal motivation for LCD developments has evolved from increasing image complexity, to achieving the widest viewing angle, high resolution and recently colour depth. Alongside these developments has been a constant need for increasingly fast LCD switching. Further speed improvement continues to be important for gaming, virtual and augmented reality (VR, AR), and ultimately for glasses-free 3D displays with eye tracking for multiple viewers, and frame sequential colour.

Moreover, non-display applications of liquid crystals continue to grow in importance and variety. A good example of this is the advent of liquid crystal lasers that have more far-reaching possibilities for optoelectronics. Brief appraisals of each of these modes are included in this section.

### 6.2 Pi- Cell

Nematic liquid crystals are simple to align, usually maintain alignment quality after receiving mechanical or thermal shock, and are well understood and characterised. The down side is often a slow response speed, particularly at low operating temperatures where the Arrhenius form of the viscosity dominates, equation (14). An early example of a fast nematic mode is the Pi-cell [175], where ON and OFF times approaching 1ms are achieved.

The pi-cell is the most well known example of a surface mode liquid crystal [176]. It relies on parallel alignment of high pre-tilt surfaces, between which is a positive  $\Delta\epsilon$  nematic. For low surface pre-tilts, the lowest energy quiescent state is predominantly splayed from one surface to the other. For high pre-tilts, a bend state of the director becomes favoured energetically. This occurs above the pre-tilt given by [177]:

$$\frac{4\theta_s - \pi}{\sin 2\theta_s} = \frac{k_{33} - k_{11}}{k_{33} + k_{11}}, \quad (109)$$

which predicts that the splay and bend states are energetically equivalent states for  $40^\circ < \theta_s \leq 50^\circ$  for typical calamitic nematics ( $0.5 \leq k_{33}/k_{11} \leq 2$ ). Pre-tilts of this magnitude have been hard to achieve historically, with  $\theta_s \approx 25^\circ$  typically being the maximum. With pre-tilts of this magnitude, the splay state is energetically favoured but the bend state is metastable, and can exist alongside the splayed state separated by a  $\pi$  disclination. With an applied voltage coupling to the positive  $\Delta\epsilon$ , the central director of the splayed state can tilt in either a clockwise or anticlockwise direction, concentrating the elastic distortion close to the top or bottom surface, figure 36b). If a sufficiently high field is applied, the elastic distortion may become sufficiently high to break the

anchoring at one of the surfaces and allow a first order alignment transition to the bend or  $\pi$ -state [178]. On removal of the field, the director relaxes back to the meta-stable state where the director remains vertical in the cell centre. Whilst in this state, the director field close to the surfaces can be affected by the application of a lower field in a continuous fashion, thereby modulating the retardation and causing optical contrast between ON and OFF states, with a fast response.

To understand why the pi-cell gives this fast response, the effect of viscous back-flow needs to be considered. Figure 36a) shows the situation for a uniform director produced by anti-parallel surface alignment. When the field is removed, the director is subject to both elastic and viscous restoring forces. Lateral flow of the material is set up in opposing directions in either half of the cell, acting to kick the director in one half in the opposite direction to that of the other, thereby slowing the relaxation to the final state. This back-flow, or

“optical bounce” effect slows the response for ECB and TN devices significantly [68]. However, for the  $\pi$ -state, the final tilt remains vertical in the cell centre and the flow acts in both halves in the same direction as the relaxing director, thereby hastening the relaxation process. Thus, viscous flow supports switching so that the device is very fast – typically switching in about 2 - 5ms for both ON and OFF switching.

The device is oriented with the alignment directions at  $45^\circ$  to crossed polarisers, and the cell gap set to give the half-wave plate condition. This occurs for a higher cell spacing for the bend-state due to the higher overall tilt of the director. The viewing angle of the bend state is better than the splayed state, because of the symmetry of the director arrangement. That is, the change in retardation for off-axis light is increased in one half of the cell and decreased in the other half, so that there is little retardation change. This self-

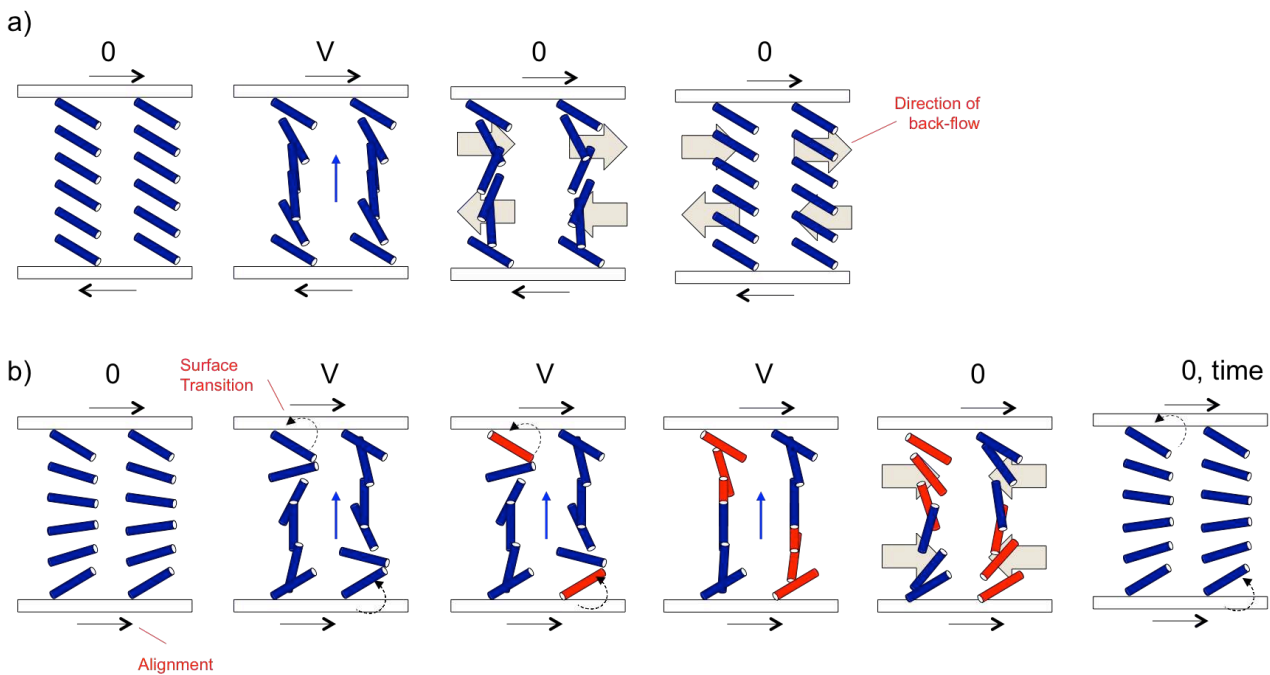


Figure 36. The effect of back-flow and the Pi-cell. a) With anti-parallel alignment, there is flow alignment in opposing directions on removal of the field, hindering the relaxation back to the 0V uniform state. b) Parallel alignment initially gives a splayed state, but application of sufficiently high field to break the surface anchoring allows a bend, or p-state to be formed. When the field is removed, relaxation to the un-switched bend state is supported by the flow throughout the cell. However, the bend state is metastable, so the splay state reforms after sufficient time, usually nucleated from the pixel edges or LCD spacers.

compensation effect leads to the alternative term for the Pi-cell as optically compensated bend-mode (OCB) [179]. Further improvements to the viewing properties can be achieved using film compensators, [180].

The device is yet to be used commercially. It cannot achieve the high contrast ratio enjoyed by the IPS and VAN modes, due to the remnant surface retardation; even with optical compensation, dark state leakage is too high to meet the high contrast ratio requirement of modern TV displays. Moreover, the bend-state is meta-stable, and usually decays back to the splayed state after removal of the field. Unless a constant bias voltage is maintained, domains of the unwanted splay state spread from unswitched areas such as the inter-pixel gaps and close to spacers. However, the principles deployed in this mode remain of interest. For example, a transmissive display has recently been suggested that uses sub-pixelation for the bend state operating in reflection, and the splay state operating with in-plane electrodes in transmissive mode [181].

### 6.3 Analogue Ferroelectric Liquid Crystal Modes

The surface stabilised FLC mode described in section 4.5 is bistable: either the black or white states is retained after the addressing pulse. Grey scale is provided using spatial or temporal dither [126]. Bistability was integral to the original interest in FLCs, since it provided an alternative to TFT. However, once TFT had become sufficiently low cost, interest was retained in utilising the fast optical speed of ferroelectric liquid crystals, but using an analogue response combined with active matrix.

Various analogue ferroelectric liquid crystal modes were studied, as outlined below. Each of the modes described suffers from the need to achieve and maintain uniform smectic layer structures, which has prevented display applications to date. However, the high speeds that are possible means that these modes may yet find utility in non-display and optoelectronic applications.

#### 6.3.1 N\*-SmC\*

Conventional SSFLC uses an N\*-SmA-SmC\* to give a chevron layer arrangement and the implicit bistability that brings. If the ferroelectric liquid crystal has a phase sequence where the SmC\* cools directly from the unwound chiral nematic, the director remains in the rubbing direction at the two surfaces and the layers form in a uniform layer bookshelf geometry but with the layers angled at the cone angle  $\theta_C$  to the rubbing [182]. Cooling with an applied DC field ensures that a single sign of orientation is achieved. Thus, the device is mono-stable, with an analogue response as the director switches about the cone in the bulk of the cell with one polarity of field, and no-response with the opposite polarity. This “half V-shaped” switching can be addressed by TFT to give a fast, analogue response.

A modification is the twisted Ferroelectric LCD [183] which combines a material with a first-order N\*-SmC\* transition with rubbing directions crossed to each other. The unwound N\* forms a conventional TN but, as the twist elastic constant diverges on approaching the smectic C phase, the smectic layers form uniformly at 45° to the rubbing directions. The director still forms a 90° twist, but moves about the SmC\* cone from one surface to the other with the applied DC field, leading to a “V-shaped” switching response. This mode works best with a strongly first order transition, wherein the SmC\* cone angle is independent of temperature and is typically close to the optimum 45°; this allows the director to lie parallel to the crossed rubbing directions.

#### 6.3.2 Anti-ferroelectric liquid crystals

Certain compounds that form chiral tilted smectic phases exhibit higher ordered phases, where there is correlation of the director orientation between adjacent layers. With antiferroelectric liquid crystals (AFLC), the SmC\* c-director and polarisation directions alternate by  $\pi$  from one layer to the next. Application of a DC field switches each alternate layer parallel to

the field, thereby forming a V-shaped switched response [184].

### 6.3.3 Deformed helix mode ferroelectric liquid crystal.

Although formed from chiral liquid crystals, most FLC modes use sufficiently low spaced devices to unwind the pitch. This is not the case for the deformed helix mode, where the pitch is made sufficiently low that even devices at the quarter wave plate condition wind continuously in a helical manner. Application of the field then causes distortion of the sinusoidal director variation and a shifting of the optic axis from that of the helix towards  $\pm\theta_C$  [185].

### 6.3.4 The Electroclinic Effect.

Smectic A phases formed from chiral molecules undergo a field induced director tilt with an applied DC field, forming a structure similar to the SmC\* phase [186]. The strength of this electroclinic effect is greatest immediately above an SmA to SmC\* transition, where the induced tilt is linear with the applied field. As with the AFLC and DH FLC modes, the switching is within the cell plane, and hence it is not only fast but has good viewing angle. However, the limited temperature range and temperature dependence have so far discounted electroclinics from application.

## 6.4 Blue Phase TFT displays

Attendees at the 2008 exhibition that occurs each year alongside the Society of Information Display annual conference were surprised to see an unheralded novel liquid crystal display mode based on the blue phase at the *Samsung* stand. The company demonstrated a 15" TFT monitor operating at a ground breaking 240Hz frame rate. Liquid crystals were known for their slow response, and most attendees were unaware of the Blue-phase. Those that were, most likely believed that the blue phase would never receive such serious interest from a manufacturer, due to the notoriously narrow temperature ranges exhibited by these phases.

Blue phases are a subset of cholesteric liquid crystals, which occur when the cholesteric natural helicity is strong and the pitch is very short, close to the transition to the isotropic phase [187]. Rather than spontaneously twist along a single axis perpendicular to the local director, the director twists along two mutually orthogonal axes to form a double helix cylindrical structure, as shown in figure 37a). The director at the centre of each cylinder lies parallel to the cylinder axis, and the diameter of the cylinder is  $P/4$  so that the director twists through  $45^\circ$  from one side to the other. This means that the director remains continuous across adjacent cylinders oriented with their axes orthogonal to each other, as shown in figure 37b). These double twist cylinders pack into a cubic array as shown in figure 37c), mediated by disclination lines throughout the structure, that occur at the interstices of the cylinders. Of the three possible blue phases, the simple cubic Blue phase I, figure 37f) and body-centred cubic Blue Phase II, figure 37d) have the widest temperature ranges. The occurrence of the disclinations means that the cubic structure is only stable where the pitch and order parameter are very low, typically for about  $1^\circ\text{C}$  to  $2^\circ\text{C}$  below the isotropic to cholesteric phase transition. Optically, the structure appears an iridescent colour due to Bragg reflection from the defects arranged on the regular cubic lattice, figure 37e); hence, the phase became known as the "blue" phase, although other colours are possible depending on the lattice. Otherwise, the phase is optically isotropic due to the cubic symmetry of the phase, and it appears dark between crossed polarisers. Blue-phases exhibit a Kerr effect with an applied field, due to deformation of the local cholesteric structure coupling to the dielectric anisotropy of the liquid crystal [188, 189]. This induces a net birefringence  $\Delta n_E$  with the optic axis in the direction of the applied field [190]:

$$\Delta n_E = \lambda K E^2 \sim -n^3 E^2 \quad , \quad (110)$$

where  $n$  is the isotropic refractive index of the blue phase and the Kerr constant  $K$  is also wavelength dependent.

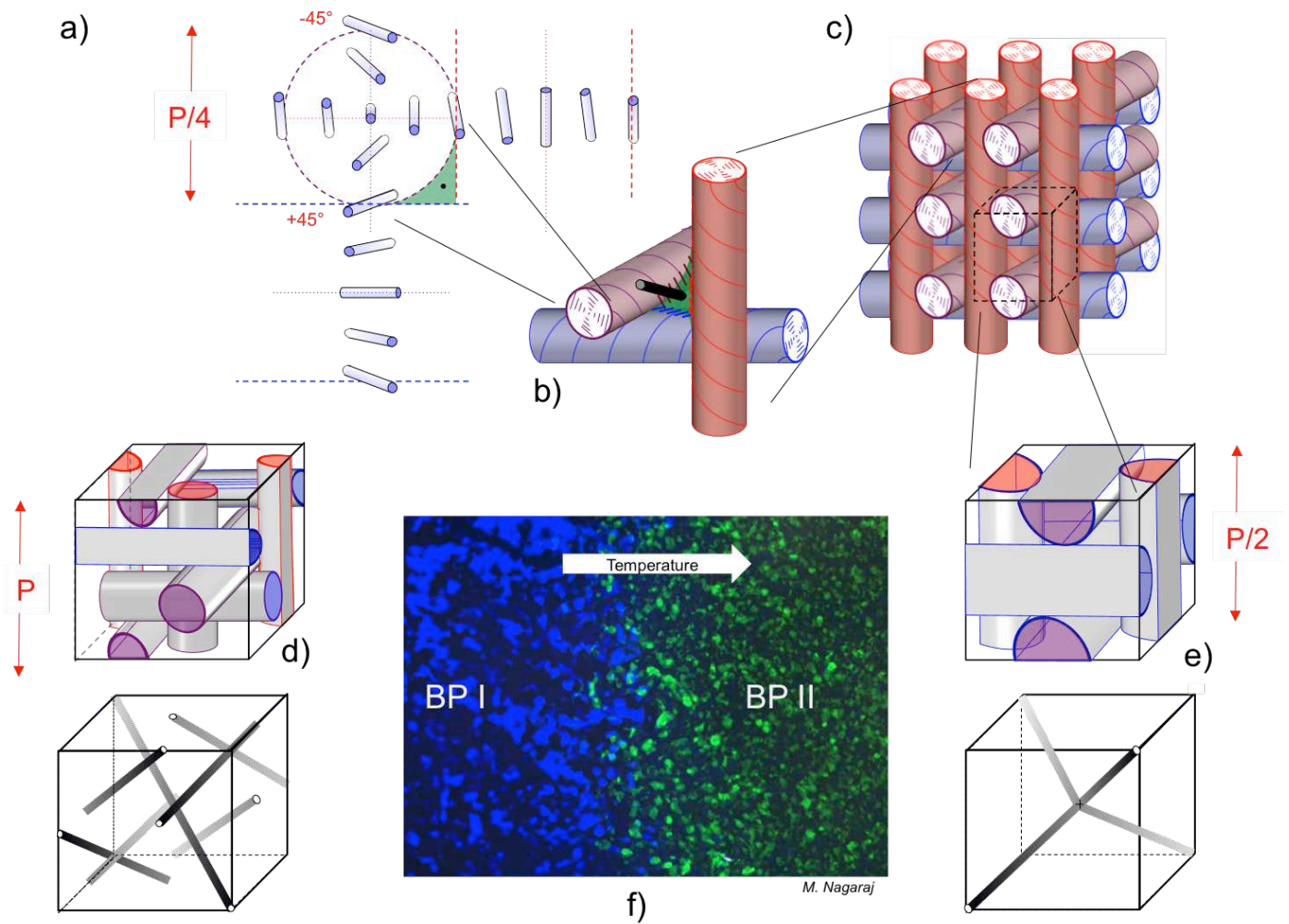


Figure 37 Blue Phase Liquid Crystal. a) The Double helix structure; b) The intersection of three double twist cylinders and the direction of the  $-1/2$  disclination that occurs close to the cylinder intersections; c) Cubic packing of the double twist cylinders; d) Packing of the cubic Blue Phase II, with associated defect lattice; e) Photomicrograph of the transition between Blue Phase I and II; f) Body centred packing of the cubic Blue Phase I and the associated defect lattice.

Although the Kerr effect provided means for electro-optic modulation, the extremely limited temperature range of the blue-phase seemed severely prohibitive to application. This was particularly true for displays, where operation from  $-20^{\circ}\text{C}$  to  $+70^{\circ}\text{C}$  is usually the minimum specification. In 2002, Kikuchi *et al* succeeded in greatly extending the temperature range by photo-polymerising a monomer added to the

liquid crystal at temperatures where the material formed the blue phase [189]. The resulting polymer formed at the defect sites, stabilising the lattice structure over a wide temperature range but without affecting the electro-optic properties of the liquid crystal significantly.

The *Samsung* display used in-plane electrodes to switch the polymer stabilised blue phase from an

optically isotropic structure, to a birefringent medium with the optic axis approximately in the plane of the cell, figure 38. The device does not require alignment layers, and gives excellent high contrast and wide viewing angle due to the isotropic nature of the dark state and in-plane switching effect. The most important issue to resolve was achieving suitably low operating voltages. This was done using shaped protrusions as the electrodes [191], with  $2\mu\text{m}$  wide electrodes and 2 to  $4\mu\text{m}$  electrode gaps. Modelling

showed that using angled electrode walls produced higher transmissivity, by reducing the angle of the optical axis at the electrode edges. Using these structures, operating voltages below the 15V target for TFT addressing were achieved. Indeed, since that original work, a host of different device layouts and liquid crystal materials have been studied [192], indicative of the on-going interest in the Blue Phase mode for applications.

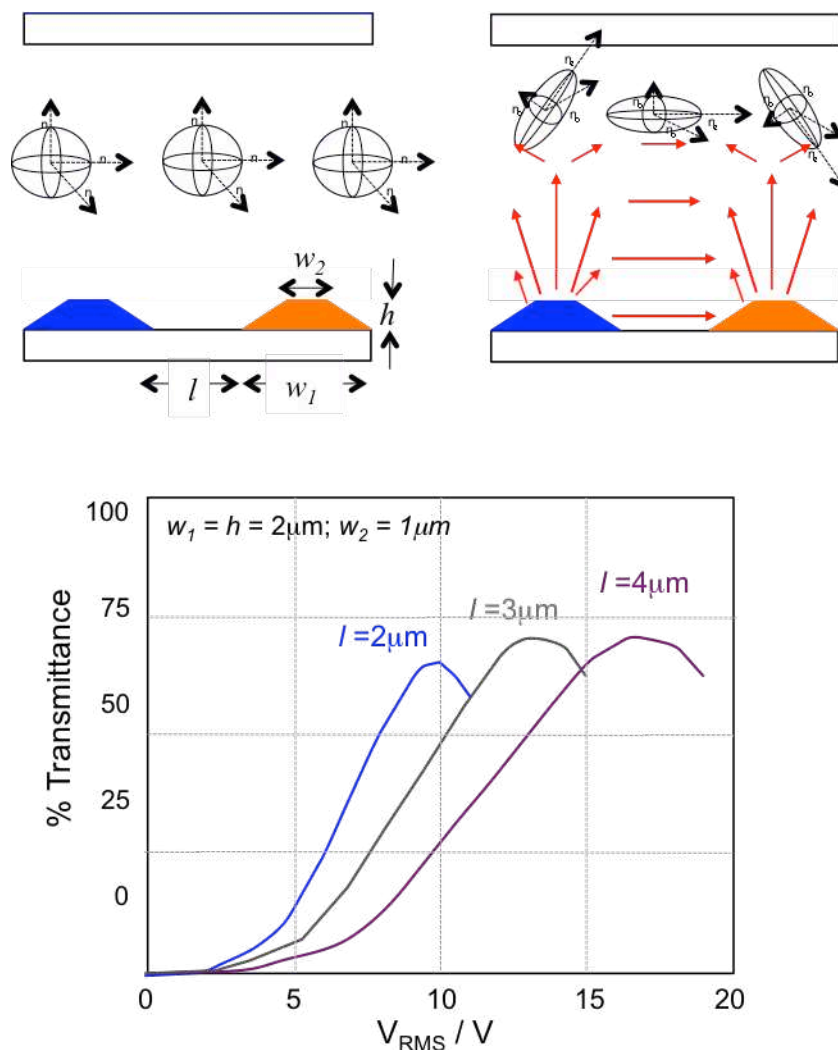


Figure 38 Principal of operation for In-plane switching mode Blue Phase LCD. The applied field induces optical birefringence (shown by the ellipsoid shape of the refractive index indicatrix). Good performance is achieved using shaped protrusions allowing 10V operation to be achieved [187].

## 6.5 Cholesteric Flexoelectricity and the Uniform Lying Helix (ULH) mode

Recently, there has been much renewed interest in the flexoelectro-optic effect in chiral nematic liquid crystals, originally proposed by Patel and Meyer [193] in 1987. This interest stems from the very fast in-plane switching effect, typically 100 $\mu$ s. If an electric field is applied perpendicular to the helical axis of a cholesteric liquid crystal, coupling between the field and the flexoelectric polarization causes splay and bend of the local director field, which in turn causes the local director to tilt away from the helical axis in the direction normal to the field, figure 39a). Without the field, the uniaxial optic axis of the cholesteric lies parallel to the helical axis. The field-induced local tilt of the director causes the optic axis to tilt through angle  $\beta$  in the plane orthogonal to the applied field.

If the cholesteric can be uniformly aligned with the helical axis parallel to the plane of a standard LCD with transverse electrodes (Uniform Lying Helix, ULH), then applying the electric field causes rotation of the optic axis in the cell plane, giving contrast when observed through polarisers parallel and crossed to the helical axis. This in-plane change of retardation axis provides a switchable half-wave plate.

Assuming negligible dielectric anisotropy, the twist angle is approximately linear with the applied field:

$$\tan\beta = \frac{(e_1 - e_3)P}{2\pi(k_{11} + k_{33})} E, \quad (111)$$

and the response time  $\tau$  is:

$$\tau = \frac{\gamma_1 P^2}{2\pi^2(k_{11} + k_{33})} E. \quad (112)$$

Flexoelectric switching is polar, so the ULH can be driven in either direction by swapping the field direction. Thus, equation (112) is appropriate for both ON and OFF switching, since the optic axis can be driven back to the OFF state using signals of the opposite polarity to those for switching. Both expressions show that the strength of the effect is

optimised for small pitch lengths  $P$ , promising speeds below 100 $\mu$ s and greater than 45° switching angles for strongly flexoelectric materials [194], and in-plane switching for good viewing angle. The pitch is unwound by the RMS effect of the field coupling to  $\Delta\epsilon$ , so liquid crystal materials with strong flexoelectric effect but low  $\Delta\epsilon$  are required. This has been achieved using nematic dimers with odd alkyl spacer groups [195].

Fabrication of devices based on this effect requires a method for obtaining the required ULH alignment uniformly and stably over the panel. Strongly planar anchoring at the cell walls leads to the Grandjean texture being formed, where the helical axis lies parallel to the cell normal (sometimes called the Uniform Standing Helix). Homeotropic alignment gives degenerate focal conic domains, and a scattering texture. Various methods have been investigated, including using periodic planar and homeotropic surfaces with the periodicity matched to  $P/2$  [196], surface relief gratings [196, 197] and polymer walls [198]. The director profile for a cholesteric liquid crystal aligned on a homeotropic grating with a pitch of  $P/2$  and a cusped shape to give the lowest elastic distortion of the ULH state [197], as shown in Figure 39b). Although yet to be proven over large areas, these methods show considerable promise for future applications of the ULH mode LCDs.

## 6.6 Liquid Crystal Lasers

With the successful commercialisation of high resolution, high frame rate LCDs for TV, interest in non-display applications for liquid crystals has continued to grow at an amplified rate. One such application particularly relevant to optoelectronics is the invention [199] and demonstration [200, 201] of the liquid crystal laser. This allows straightforward tunability of laser light across the optical wavelength range combined with simple low cost fabrication, and offers the potential for electric field tuning of the lasing wavelength.

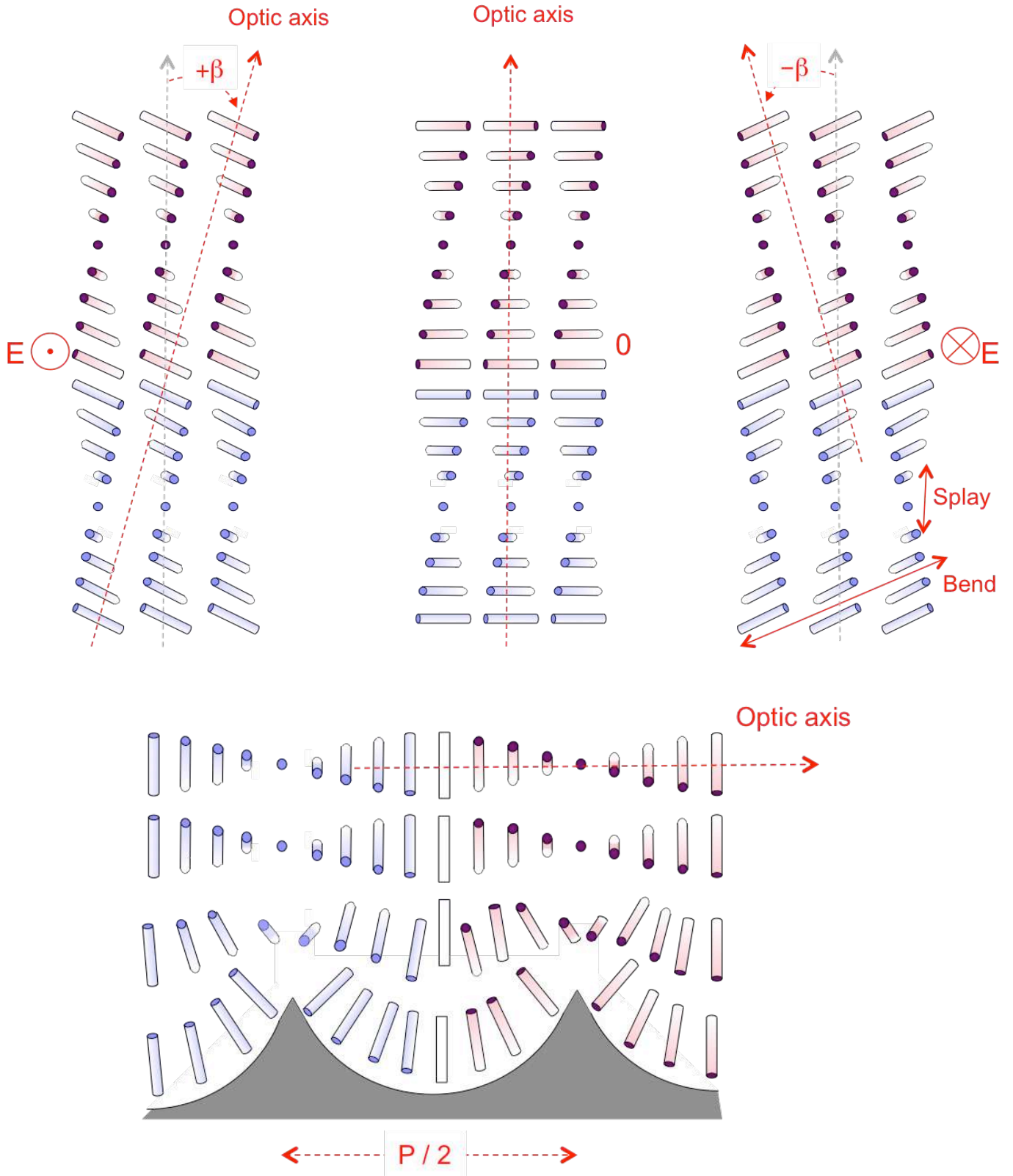


Figure 39 The cholesteric flexoelectric effect. a) Rotation of the optic axis; b) Alignment of  $N^*$  into the ULH texture using cusped grating surfaces [193].

Selective reflection from the cholesteric liquid crystal is an example of a one-dimensional photonic band-gap, wherein circularly polarised light of the correct wavelength range and handedness cannot propagate through the material in the direction parallel (or antiparallel) to the helical axis. This means that spontaneous emission from a fluorophore within the cholesteric is inhibited within the photonic band-gap, leading to photons being emitted at the band edge [202]. That is, optical pumping of a cholesteric with either a fluorescent dye dissolved into it or as constituent part of the mesogenic molecule causes emission of lower energy photons that overlap with the forbidden band of wavelengths corresponding to the range of selective reflection. Where emission occurs across the band-gap lasing will occur at both edges. In the example system shown in figure 40, a tetra-aryl-pyrene derivative dye [203] pumped at 410nm gives emission peaking in the range 450nm – 500nm. Once dissolved into a cholesteric with a photonic band from 500 to 520nm lasing occurs on the lower band edge. Either lowering the cholesteric pitch

or changing to a dye with a longer wavelength emission swaps the lasing wavelength to the upper photonic band edge.

The stimulated emission occurs in a single direction, as shown in figure 40. Such devices offer potential for forming laser arrays, competing against III-V Semiconductor Vertical Cavity Surface Emitting Lasers (VCSEL) but without the need for the multiple fabrication steps. Indeed, the simplicity of fabrication allows ink-jet printing of the liquid crystal to form an array of laser dots, each with a signature emission [204]. The low cost and ability to print onto a plastic backing layer has already earned the technology commercial application for anti-counterfeiting.

Lasing is possible in other liquid crystal phases that include Bragg type structures with optical length scales, including the ferroelectric chiral SmC\* and Blue-phases [205]. The former offers the potential for fast electric field modulation, whereas the latter produces lasing in multiple directions due to the cubic structure of the Bragg lattice.

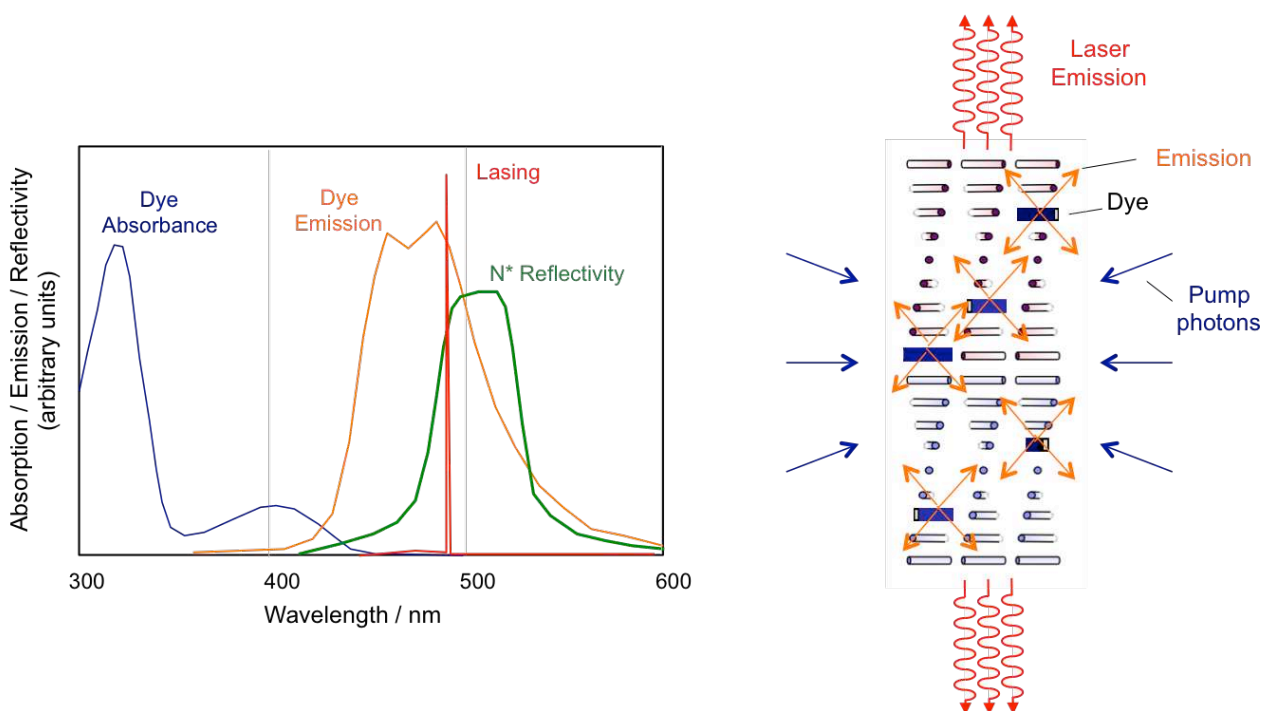


Figure 40 Lasing in dyed cholesteric. a) Example of the optical properties for the fluorescent dye and cholesteric liquid crystal, leading to lasing on the lower band edge of the selective reflection; b) schematic representation of cholesteric lasing.

## 6 Conclusion

The market success of liquid crystal displays is predicated by scientific and technological achievements from across the globe, advances that have needed collaborative efforts of mathematicians, chemists, physicists, engineers and entrepreneurs. The breadth of the subject is unusually broad and involving. A major part of the on-going success of LCDs is the continual evolution and adaptation that these technological advances allow. Throughout the history of the LCDs the naysayers have maintained a mantra that LCDs cannot achieve the complexity, cannot achieve the viewing angle, cannot achieve the resolution, cannot achieve the speed, cannot achieve the colour balance of the latest competing technology. In each case they have proven incorrect. Often, this has been through the invention of new modes, sometimes associated with different arrangements, sometime with different materials and phases. Often, the improvements have come from the use of partnering technologies; the active backplanes, polariser and optical films, back-light units, light guides or manufacturing advances.

As it has always been, the competition is strong. OLED displays are already making inroads into small, high-resolution displays for mobile phones. If performance, cost and lifetimes can all exceed those of the LCD, then they will gain an ever increasing share of the market, from low to high diagonal displays. Low cost reflective passive matrix LCDs retain a large market presence too. However, as the cost of the TFT backplane continues to reduce, the competition from electrophoretic displays is strong and growing. Winning these battles will take yet more ingenuity from the LCD scientists and engineers.

There remain several display markets where no display technology has yet delivered, whether LCD or alternative. Although reflective colour and transfective displays have been marketed, solutions to date have not been adequate to gain market acceptance. LCDs have a natural advantage for transfective mode operation, being based on transparent media that modulates ambient light. Electrophoretics absorb light preventing transmissive

operation and OLEDs emit and so cannot modulate reflected light. Solutions to achieving the required performance at a suitably low cost have yet to be commercialised; perhaps the developments of new nematic modes [e.g. 180] or the application of a new LC phase, such as the Blue-phase III [206] will prove successful.

An area of enormous growth is the use of liquid crystals for non-display applications [207]. In addition to the conventional applications described in the previous sections, liquid crystal main-chain polymers such as *Kevlar* continue to prove one of the biggest LC applications, liquid crystal elastomers are used as the active element in nano-machines and molecular motors [208], liquid crystal semiconductors are attracting interest for photo-voltaic and OLED [209], and the great interest in liquid crystals in chemical and biological sensors continues with unabated enthusiasm [210]. One of the largest areas of growth, however, is in the field of optoelectronics. Whether this is for smart-windows, beam steering and light guiding, printable lasers, switchable lenses, optical computing, adaptable photonic structures, or Terahertz modulators, successful solutions to such applications in the future will require both the ingenuity and the multidisciplinary approach that made our predecessors so successful.

### Acknowledgements

The author wishes to thank Professors Peter Raynes, Cyril Hilsum, Phil Bos, Tim Wilkinson and Dr. Mamatha Nagaraj for invaluable discussions.

### References

- [1] S. Kubrick (Dir.) (1968) “*2001: A Space Odyssey*”, Metro-Goldwyn Mayer, Released 2<sup>nd</sup> April 1968. Premiered in New York from 3<sup>rd</sup> April 1968 at the Loews Capitol Theatre, Broadway, NY.
- [2] B. J. Lechner, (2008). History crystallized: A first person account of the development of matrix-addressed LCDs for Television at RCA in the 1960s. *Information Display*, 08 (1), 26–30.

- [3] G.H. Heilmeyer and L.A. Zanoni (1967). "Electro-optical Device" US patent 3499112 A.
- [4] G.H. Heilmeyer, L.A. Zanoni and L. A. Barton (1968) "Dynamic Scattering: A new electro-optic effect in certain classes of nematic liquid crystals," *Proc. IEEE*, **56**, pp1162 – 1171
- [5] B. Levin and N. Levin (1936) "Improvements in or relating to Light Valves," *UK patent 441, 274*.
- [6] J. A. Castellano, (2005) "Liquid Gold: The story of Liquid Crystal Displays and the Creation of an Industry," *World Scientific, Singapore*
- [7] H. Kawamoto (2001) "The History of Liquid Crystal Displays," *Proc. IEEE* vol. **90**, no. 4, pp460 – 500
- [8] G. W. Gray (1962) "Molecular structure and properties of Liquid Crystals", Academic Press, London.
- [9] G. H. Brown and W.G. Shaw (1957) "The Mesomorphic State: Liquid Crystals", *Chem. Rev.*, **57**, pp 1029 – 1157.
- [10] R. Williams (1963) "Domains in Liquid Crystals," *J. Chem. Phys.* **39**, No. 2, 384-388
- [11] R. Williams (1962) U.S. Patent 3,332,485 A. Filed Nov. 9, 1962 and issued May 30, 1967
- [12] C. Hilsum, (2010). "Flat-panel electronic displays: a triumph of physics, chemistry and engineering", *Philosophical Transactions. Series A, Mathematical, Physical, and Engineering Sciences*, 368(1914), 1027–1082. doi.org/10.1098/rsta.2009.0247
- [13] N. Koide (2014) "*The Liquid Crystal Display Story: 50 Years of Liquid Crystal R&D that lead the Way to the Future*", Springer, Japan.
- [14] M. Schadt and W. Helfrich, (1971) "Voltage-dependent optical activity of a twisted nematic liquid crystal," *Appl. Phys. Lett.*, vol. 18, no. 4, pp.127–128.
- [15] G. W. Gray, K. J. Harrison, and J. A. Nash, (1973) "New family of nematic liquid crystals for displays," *Electron. Lett.*, vol. **9**, no. 6, pp. 130–131.
- [16] A. Ashford, J. Constant, J. Kirton, and E. P. Raynes, (1973) "Electro-optic performance of a new room-temperature nematic liquid crystal," *Electron. Lett.*, vol. **9**, no. 5, pp. 118–120.
- [17] G. H. Heilmeyer, "Liquid crystal displays: An experiment in interdisciplinary research that worked," *IEEE Trans. Electron Devices*, vol. **ED-23**, July 1976.
- [18] F. Reinitzer (1888) "Contributions to the understanding of cholesterol," (*transl.*), *Monatshefte für Chemie (Wien)* vol. **9**, pp 421 – 441.
- [19] O. Lehmann, (1889) *Zeitschrift für Physikalische Chemie*, **4**, p462
- [20] D. Dunmur and T. Sluckin (2011) *Soap, Science, and Flat-screen TVs: a history of liquid crystals*, Oxford University Press ISBN 978-0-19-954940-5.
- [21] I. Haller (1975) "Thermodynamic and static properties of liquid crystals", *Prog. Sol. State Chem.*, **10** (2) pp. 103 – 118
- [22] J. W. Goodby, P. J. Collings, T. Kato, C. Tschierske, H. Gleeson, & P. Raynes (Eds.), (2014) "Handbook of Liquid Crystals", *Wiley VCH, Weinheim. ISBN: 978-3-527-32773-7*.
- [23] R.B. Meyer, L. Liébert, L. Strzelecki and P. Keller (1975) "Ferroelectric liquid crystals," *Journal de Physique*, vol. **26**, pp L69–71.
- [24] M. Klasen-Memmer and H. Hirschmann (2012) "Liquid Crystal Materials for Devices", IN J. Chen, W. Cranton and M Fihn (eds.) "Handbook of Virtual Display Technology", *Springer-Verlag Berlin Heidelberg*.
- [25] D. Dunmur and G. Luckhurst (2014) "Tensor properties and Order Parameters of anisotropic materials" IN J.W. Goodby *et al.* "Handbook of Liquid Crystals: Volume 2", *Wiley VCH, Weinheim*, pp189 – 281.
- [26] J. Constant and E.P. Raynes, (1985) RSRE Internal Memorandum, unpublished
- [27] F. C. Frank, (1958). I. Liquid crystals. "On the theory of liquid crystals", *Discussions of the Faraday Society*, **25** (1), 19- 28.
- [28] J.C. Jones (2000) "*Liquid Crystal Elastic Constants*", *Encyclopaedia of Material Science*
- [29] F. M. Leslie (1966) "Some constitutive equations for anisotropic fluids", *Q. J. Mech. Appl. Math*, **19**, pp 357-370; F.M. Leslie (1968) "Some constitutive equations for anisotropic fluids", *Arch. Ration. Mech. Anal.* **28**, pp 265-283.
- [30] M. G. Clark and F. M. Leslie, (1978) "A calculation of orientational relaxation in nematic liquid crystals," *Proc. Royal Soc. Lond. A*, **361**, pp 463–485.
- [31] D.W. Berreman (1983) "Numerical Modelling of Twisted Nematic Devices", *Phil. Trans. R. Soc. Ser. A: Math. And Phys. Sci.* **309**, (1507) pp 203 -216.

- [32] S.T. Wu and C.S.Wu, (1990). "Rotational viscosity of nematic liquid crystals A critical examination of existing models", *Liquid Crystals*, 8(2), 171–182.  
doi:10.1080/02678299008047339
- [33] R. B. Meyer (1969) "Piezoelectric effects in liquid crystals" *Phys. Rev. Lett.* vol. **22**, pp 918–921.
- [34] E.P. Raynes, (2014) "Mixed systems: phase diagrams and eutectic mixtures", IN J.W. Goodby, P. J. Collings, T. Kato, C. Tschierske, H. Gleeson, & P. Raynes (Eds.), "Handbook of Liquid Crystals: Volume 1", *Wiley VCH, Weinheim*. pp 351 – 363.
- [35] W. Martienssen and H. Warlimont (Eds.) (2005) *Springer Handbook of Condensed Matter and Materials Data*, Springer Verlag; Heidelberg. ISBN 3-540-44376-2
- [36] K. Tarumi, B. Schuler, E. Bartmann and D. Pauluth (1996) "Liquid Crystalline Medium", *US Patent 5,744,060*
- [37] A. Buka and N. Éber (Eds.) (2013) "Flexoelectricity in Liquid Crystals: Theory, Experiments and Applications", *Imperial College Press, London*. ISBN 978-1-84816-799-5.
- [38] G.W. Gray and D.G. McDonnell, (1976) "The Relationship Between Helical Twist Sense, Absolute Configuration and Molecular Structure for Non-Sterol Cholesteric Liquid Crystals", *Molecular Crystals and Liquid Crystals*, **34**, (9), 211–217.
- [39] M. Hird (2011) "Ferroelectricity in liquid crystals—materials, properties and applications, *Liquid Crystals*", **38**, (11-12), pp. 1467-1493.
- [40] F.C. Saunders, K.J. Harrison, E.P. Raynes and D.J. Thompson, (1983) "New photostable anthraquinone dyes with high order parameters", *IEEE Trans. Electr. Dev.*, **ED-30**, pp 499–502.
- [41] I. Jánossy, (1999) "Optical reorientation in dye doped liquid crystals", *J. Nonlin. Opt. Phys. Mat.*, **8**, (3) pp 361 – 377.
- [42] M. Schadt, K. Schmitt, V. Kozinkov and V. Chigrinov (1992) "Surface-Induced Parallel Alignment of Liquid Crystals by Linearly Polymerized Photopolymers", *Jap. J. Appl. Phys.*, **31**, (7) pp
- [43] D. Broer, G. Crawford and S. Žumer, (2011) "Cross-linked Liquid Crystalline Systems: From Rigid Polymer Networks to Elastomers", *CRC Press, Florida*. ISBN 978-1-4200-4622-9.
- [44] R.J. Bushby and N. Boden (2014) "Responses of Discotic Liquid Crystals to Mechanical, Magnetic and Electrical Fields" IN J.W. Goodby *et al.* "Handbook of Liquid Crystals: Volume 3; Part III: Discotic, Biaxial and Chiral Nematic Liquid Crystals", *Wiley VCH, Weinheim*, pp1 - 33.
- [45] C. V. Mauguin, (1911) "Sur les Cristaux Liquides de Lehmann", *Bull. Soc. Fr. Min*, **34**, 71-117.
- [46] V. Fréedericksz and A. Repiewa (1927) "Theoretisches und Experimentelles zur Frage nach der Natur der anisotropen Flüssigkeiten", *Zeitschrift für Physik* **42** (7): 532–546.
- [47] V. Fréedericksz and V. Zolina, (1933) "Forces causing the orientation of an anisotropic liquid". *Trans. Faraday Soc.* **29**: 919–930.
- [48] P. Châtelain, (1941) Sur l'orientation des cristaux liquides par les surfaces frottées, *Comptes rendus de l'Académie des Sciences* **213**, 875–76
- [49] B. Levin and N. Levin (1936) "Improvements in or relating to Light Valves" *British Patent* 441, 274.
- [50] H.J.J. van Boort and R. Groth, (1968) "Low-pressure sodium lamps with indium oxide filter" *Philips Tech. Rev.*, **29**, pp17-18.
- [51] M. Mizuhashi (1980) "Electrical properties of vacuum-deposited indium oxide and indium-tin oxide films", *Thin Solid Films*, **70** (1980) 91-100
- [52] Y. Katsube and S. Katsube (1966) "The Tin-oxide Films Deposited by Vacuum Evaporation (I)", *Shinku: J. Vacuum Soc. Jap.*, **9**, (11), pp443 – 450.
- [53] F.M. Wanlass (1963) "Low stand-by power complementary field effect circuitry" US patent 3, 356,858
- [54] E. H. Land and J.S. Friedman (1933) "Polarizing refracting bodies" *US patent* 1,918,848 A
- [55] J.F. Dreyer (1946) "Dichroic light-polarizing sheet materials and the like and the formation and use thereof"; US Patent 2544659.
- [56] T. Nagatsuka (2014) "Chapter 4.1 – Development of polarizers to support the development of the liquid crystal industry" IN N. Koide (ed.) *The Liquid Crystal Display Story: 50 years of liquid crystal R&D that led*

- the way to the future*, Springer, Japan. pp 81 – 95.
- [57] P. K. Weimer, (1966) “Thin film transistors,” IN ” J. T. Wallmark and H. Johnson, (Eds.) *Field Effect Transistors, Devices*, Englewood Cliffs, N. J. Prentice-Hall.
- [58] E.P.Raynes, (1974) “Improved contrast uniformity in twisted nematic liquid-crystal electro-optic display devices”, *Electron. Lett.*, **10**, pp 141-142.
- [59] A. A. Sonin (1995) “The surface physics of liquid crystals,” *Gordon and Breach Publishers, Luxembourg*.
- [60] A. Hirai, I. Abe, M. Mitsumoto and S. Ishida (2008) “One Drop Filling for Liquid Crystal Display Panel Produced from Larger-sized Mother Glass” *Hitachi Review* **57**, (3), pp 144 - 147.
- [61] M. O’Neill and S. Kelly (2012) Chapter 6: Optical Properties of Light-emitting Liquid Crystals IN R. J. Bushby, S. Kelly and M. O’Neill, *Liquid Crystalline Semiconductors: Materials, properties and applications*, Springer Science and Business Media, London, pp 163 – 195.
- [62] R.C. Jones (1941) “New calculus for the treatment of optical systems”. *I. J. Opt. Soc. Am.*, **31**: p488 – 493.
- [63] K. R. Welford, and J.R. Sambles, (1987). “Analysis of Electric Field Induced Deformations in a Nematic Liquid Crystal for any Applied Field.” *Mol. Cryst. Liq. Cryst*, **147** (1) pp25 -42.
- [64] “LCD Master”, Shintech; <http://shintech.jp/wordpress/en/software-2/lcdm3d.html>; “TechWiz” Sanayi <http://www.sanayisystem.com/eng/index.asp>; DIMOS, Autronic Melchers.
- [65] E. Jakeman and E.P. Raynes (1972) “Electro-optical response times in Liquid Crystals”, *Phys. Lett.*, **39A**, (1), pp. 69 – 70.
- [66] H. Chen, M. Hu, F. Peng, J. Li, Z. An and S.T. Wu, (2015). “Ultra-low viscosity liquid crystal materials”. *Optical Materials Express*, **5**, (3), pp 655 – 661.
- [67] S. T. Wu and D. K. Yang, (2001) *Reflective Liquid Crystal Displays* Wiley, New York.
- [68] D.W. Berreman (1975) “Liquid-crystal twist cell dynamics with backflow”, *J. Appl. Phys.*, **46**, 3746 - 3751.
- [69] P. M. Alt and P. Pleshko, (1974) “Scanning limitations of liquid-crystal displays, *IEEE Trans. Electron Devices*, vol. **ED-21**, pp. 146–155.
- [70] B.J. Lechner, F.J. Marlowe, E.O. Nester, and J. Tufts, (1971) “Liquid Crystal Matrix Displays,” *Proceedings of IEEE*, **59**, (11), pp. 1566–1579.
- [71] T.P. Brody, J.A. Asars and G.D. Dixon, (1973) “A 6x6 inch, 20 lines-per-inch liquid crystal display panel.” *IEEE Trans. Electron Devices*, **ED-20**, 995-1001.
- [72] P.G. LeComber, W.E. Spear and A. Ghaith, (1979) “Amorphous silicon field effect device and possible application,” *Electron. Lett.* vol. **15**, pp. 179- 180.
- [73] A. J. Snell, K. D. Mackenzie, W. E. Spear, P. G. LeComber and A. J. Hughes (1981) “Application of amorphous silicon field effect transistors in addressable Liquid Crystal Display Panels,” *Appl. Phys.* vol. **24**, pp. 357 - 362.
- [74] Y. Okubo, T. Nakagiri, Y. Osada, M. Sugata, N. Kitahara, and K. Hatanaka, (1982) “Large-Scale LCDs Addressed by  $\alpha$ -Si TFT Array,” *SID Digest*, pp. 40–41.
- [75] F. R. Libsch (2009) “Thin-film Transistors in Active Matrix Displays” IN C.R. Kagan and P. Andry “Thin-film Transistors”, *Dekker, New York*. pp187 – 269.
- [76] M.-K., Kang, S. J., Kim, and H.J. Kim, (2014). Fabrication of high performance thin-film transistors via pressure-induced nucleation. *Scientific Reports*, **4**, 6858.
- [77] X. Huang, C. Wu, H. Lu, F. Ren, D. Chen, R.Zhang and Y. Zheng, (2013). Enhanced bias stress stability of a-InGaZnO thin film transistors by inserting an ultra-thin interfacial InGaZnO:N layer. *Applied Physics Letters*, **102**, 193505.
- [78] E. Lueder. (2001) “Liquid Crystal Displays: Addressing Schemes and Electro-optic effects”, *John Wiley and Sons, Chichester*.
- [79] S.M. Kelly and M. O’Neill, (2000). “Chapter 1: Liquid Crystals for Electro-optic Applications” IN H.S. Nalwa, Ed., *Handbook of Advanced Electronic and Photonic Materials, Volume 7: Liquid Crystals, Displays and Laser Materials*. Academic Press, UK.
- [80] S.W. Depp, A. Juliana and B.G. Huth, (1980) “Polysilicon FET devices for Large Area Input/Output Applications”, *Tech. Digest International Electron Devices Meeting*,

- Washington DC, December 1980, *IEEE*, Paper 27.2, pp703 – 706.
- [81] T. Sameshima, S. Usui and M. Sekiya, (1986) “XeCl Excimer laser annealing used in the fabrication of poly-Si TFT’s”, *IEEE Electron Device Letters*, **7** (5), pp276–278.
- [82] K. Nomura, H. Ohta, A. Takagi, T. Kamiya, M. Hirano and H. Hosono, (2004). Room-temperature fabrication of transparent flexible thin-film transistors using amorphous oxide semiconductors. *Nature*, **432** (7016), 488–492.
- [83] J. Fergason (1971) “Liquid Crystal Non-linear light modulators using electric and magnetic fields”, *US Patent 3,918, 796*.
- [84] F.J. Kahn, (1971) “Nematic liquid crystal device”, US Patent 3694053 A
- [85] M. F. Schiekol and K. Fahrenschon, (1971) “Deformation of Nematic Liquid Crystals with Vertical Orientation in Electrical Fields”, *Appl. Phys. Lett.* **19**, 391-393.
- [86] S. Kobayashi, T. Shimojo, K. Kasano, and I. Tsunda, (1972) “Preparation of Alphanumeric Indicators with Liquid Crystals” *SID Digest of Technical Papers*, p68-72.
- [87] R.A. Soref (1973) “Transverse Field Effect in Nematic Liquid Crystals” *Phys. Lett.*, **22**, pp165
- [88] N.A. Clark and S.T. Lagerwall, (1980). “Submicrosecond bistable electro-optic switching in liquid crystals”, *Applied Physics Letters*, **36**, pp899–901.
- [89] C. M. Waters and E.P.Raynes (1982) “Liquid Crystal Devices with particular Cholesteric Pitch / Cell thickness ratio”, *US Patent 4,596,446*.
- [90] T.J. Scheffer and J. Nehring (1984) “A new, highly multiplexable liquid crystal display” *Appl. Phys. Lett.* **45**, 1021-1022.
- [91] K. Katoh, Y. Endo, M. Akatsuka, M. Ohgawara and K. Sawada (1987) “Application of Retardation Compensation; A New Highly Multiplexable Black-White Liquid Crystal Display with Two Supertwisted Nematic Layers” *Jpn J. Appl. Phys.*, **26**, (11) L1784 – L1785.
- [92] R. Kiefer, B. Webber, F. Windscheid, and G. Baur, (1992) “In-plane switching of nematic liquid crystals,” *Proc. Japan Displays’92*, pp. 547–550
- [93] M. Oh-e and K. Kondo, (1995) “Electro-optical characteristics and switching behavior of the in-plane switching mode,” *Appl. Phys. Lett.* **67**, pp. 3895–3897.
- [94] A. Takeda, S. Kataoka, T. Sasaki, H. Chida, H. Tsuda, K. Ohmuro, T. Sasabayashi, Y. Koike, and K. Okamoto, (1998). “A super-high image quality multi-domain vertical alignment LCD by new rubbing-less technology,” *SID Digest 98*, pp. 1077–1100
- [95] Y. Koike and K. Okamoto, (1999) “Super high quality MVA-TFT liquid crystal displays,” *Fujitsu Sci. Tech. J.*, **35**, pp. 221–228.
- [96] S.L. Lee and S.H. Lee, (1996). “Liquid Crystal Display Device with Improved Transmittance and method for manufacturing same:”, KR Patent No. 19960059509, US Patent No. 5,914,762.
- [97] S.H.Lee, S.L.Lee and H.Y.Kim (1998) "High-Transmittance, Wide-Viewing-Angle Nematic Liquid Crystal Display Controlled by Fringe-Field Switching," *Proc. 18th International Display Research Conference (Asia Display)*, p. 371-374.
- [98] J.O. Kwag, K.C. Shin, J.S. Kim, S.G. Kim, and S.S. Kim (2000) “Implementation of New wide viewing angle mode for TFT-LCDs”, *SID Technical Digest*, **31**, pp256 – 259.
- [99] Y. Ishii, S. Mizushima, and M. Hijikigawa, (2001) “High performance TFT-LCDs for AVC applications,” *SID Digest 01*, pp 1090–1093.
- [100] E. Jang, S. Jun, H. Jang, J. Lim, B. Kim and Y. Kim, (2010) “White-light-emitting diodes with quantum dot color converters for display backlights”, *Advanced Materials*, **22** (28), pp3076–3080.
- [101] J.C. Jones (2012) “Bistable LCDs” IN J. C. Janglin, W. Cranton and M. Fihn (eds) *Handbook of Visual Display Technology*, Springer Verlag, Berlin Heidelberg. pp 1507 – 1543.
- [102] J.C. Jones (1999) “The evolution of liquid crystal displays”, *Opto and Laser Europe*, **69**, (12), pp 41-42.
- [103] R. Williams, “Electro-optic elements utilising an organic nematic compound” *US Patent 3,322,485*.
- [104] R. Williams, “Domains in Liquid Crystals” *J. Chem Phys.*, **39**, (2) pp 384 – 388.
- [105] L. M. Blinov (1998) “Behaviour of Liquid Crystals in Electric and Magnetic Fields”, IN D. Demus, J.W. Goodby, G.W.Gray,H.W. Spiess and V. Vill, (Eds.) *Handbook of Liquid*

- Crystals, Volume 1: Fundamentals”, Wiley VCH, Weinham, Germany. pp 437 – 544.
- [106] S. Chandrasekhar (1992) “Liquid Crystals”, Cambridge University Press, UK
- [107] C.H. Gooch and H. A. Tarry (1975) “The Optical Properties of Twisted Nematic Structures with Twist Angles  $\leq 90^\circ$ ”, *J. Phys. D: Appl. Phys.* **8**, 1575 – 1583.
- [108] J.C. Jones and G.P. Bryan-Brown, (2010), “Low cost Zenithal bistable device with improved white state”, *Proc. SID, Int. Symp. Digest, Technical papers, vol. 41*, pp. 207 – 211.
- [109] E. P. Raynes (1986) “The theory of supertwist transitions,” *Mol. Cryst. Liq. Cryst. Lett.* vol. **4**, no. 1, pp1 – 8.
- [110] E.P. Raynes (2014) “ TN, STN and Guest Host Liquid Crystal Display Devices”, IN J. W. Goodby *et al* (Eds.), “Handbook of Liquid Crystals, Volume 8: Applications of Liquid Crystals”, Wiley VCH, Weinheim, Germany. pp 3 -20.
- [111] M.J. Bradshaw and E.P. Raynes (1983) “The Elastic Constants and Electric Permittivities of Mixtures Containing Terminally Cyano Substituted Nematogens”, *Mol. Cryst. Liq. Cryst.* **91**, 145-148.
- [112] T. Sergan, S. Jamal and J. Kelly, (1999). “Polymer negative birefringence films for compensation of twisted nematic devices”, *Displays*, **20**, (5), pp 259–267.
- [113] H.K. Bisoyi and S. Kumar, (2010) “Discotic nematic liquid crystals: science and technology”, *Chemical Society Reviews*, **39**, pp. 264–285.
- [114] M.D. Tillin, M.J.Towler, K.A.Saynor and E.J. Beynon, (1998) “Reflective single polariser low and high twist LCDs”, *SID Tech. Digest*, **29**, pp 311 – 314.
- [115] S. Aftergut and H.S.Cole Jr., (1978) “Method for improving the response time of a display device using the twisted nematic liquid crystal composition”, *US Patent 4,143,947*.
- [116] V. G. Chigrinov, V. V. Belyaev, S. V. Belyaev, and M. F. Grebenkin, (1979) “Instabilities of Cholesteric Liquid Crystals in an electric field”, *Sov. Phys. JETP* **50**, (5), pp 994-999.
- [117] I.C. Sage (1998) “Displays”, IN D. Demus, J.W. Goodby, G.W.Gray, H.W. Spiess and V. Vill, (Eds.) Handbook of Liquid Crystals, Volume 1: Fundamentals”, Wiley VCH, Weinham, Germany. pp 727 – 762.
- [118] O. Okamura, M. Nagata and K. Wada, (1987) “Neutralized STN (NTN) – LCD full colour picture image”, *Inst. Television Eng. Japan, Tech. Rep.* **11**, (27) pp 79 -84.
- [119] S.T. Lagerwall (2014) “Ferroelectric Liquid Crystal Displays and Devices”, IN J. W. Goodby *et al* (Eds.), “Handbook of Liquid Crystals, Volume 8: Applications of Liquid Crystals”, Wiley VCH, Weinheim, Germany. pp 213 -236.
- [120] J.C. Jones, and E.P. Raynes, (1992) "Measurement of the Biaxial Permittivities for Several Smectic-C Host Materials used in Ferroelectric Liquid Crystals Devices." *Liquid Crystals*, **11**, (10) pp199-217.
- [121] J.C. Jones (2015) “On the biaxiality of smectic C and ferroelectric liquid crystals”, *Liquid Crystals* **42**, pp732-759.
- [122] J.C. Jones, C.V. Brown and P.E. Dunn, (2000) “The Physics of  $\tau$ Vmin Ferroelectric Liquid Crystal Displays”, *Ferroelectrics*, **246**, pp 191 – 201.
- [123] J.C.Jones, M.J. Towler, and J.R. Hughes (1993) "Fast, high contrast Ferroelectric Liquid Crystal Displays and the Role of Dielectric Biaxiality" *Displays*, **14**, (2) 86 - 93.
- [124] M.J. Bradshaw, V. Brimmell and E.P. Raynes (1987) “A novel alignment technique for ferroelectric smectics”, *Liquid Crystals*, **2**, (1), pp. 107 – 110
- [125] M.H. Anderson, J.C. Jones, E.P. Raynes and M.J. Towler (1991) "Optical Studies of Thin Layers of Smectic C Materials", *J. Phys. D: Appl. Phys.*, **24**, pp 338 - 342.
- [126] J.C. Jones (2014) “Bistable Nematic Liquid Crystal Displays”, IN J.W. Goodby, P.J. Collins, T. Kato, C. Tschierske, H.F. Gleeson and P. Raynes, *The Handbook of Liquid Crystals. Volume 8: Liquid Crystal Devices*, Chapter 4, Wiley.
- [127] V. Y. Reshetnyak, O.V. Shevchuk and M. Osyptchu (2004) “Director profile in the in-plane switching of nematic liquid crystal cell with strong director anchoring”, *Proceedings of SPIE*, (July 2004), pp 283–292.
- [128] M. Oh-E and K. Kondo (1997). The in-plane switching of homogeneously aligned nematic

- liquid crystals. *Liquid Crystals*, **22**, (4), pp 379–390.
- [129] H. Ki Hong, and H. Ho Shin (2008). Effects of rubbing angle on maximum transmittance of in-plane switching liquid crystal display. *Liquid Crystals*, **35**, (2), 173–177.
- [130] S. Jung, S. Jang, H. Park and W. Park, (2003). “Optimization of the Electro-Optical Characteristics of In-Plane-Switching Liquid Crystal Displays by Three-Dimensional Simulation”, *J. Korean Phys. Soc.*, **43** (5), 935–940.
- [131] D.K. Yang and S.T. Wu (2006) “Fundamentals of Liquid Crystal Devices”, *John Wiley and Sons, Chichester, UK*.
- [132] D.H. Kim, Y.J. Lim D.E. Kim, H. Ren, S.H. Ahn and S.H. Lee (2014) “Past, present, and future of fringe-field switching-liquid crystal display”, *Journal of Information Display*, **15**, (2), pp99–106.
- [133] J.L. Fergason (1964) “Liquid Crystals”, *Scientific American*, **211**, (Aug), pp 76 – 85.
- [134] H. Groskinsky (1968) “The Chameleon Chemical” *Life Magazine*, **64**, (2), pp 40 – 45.
- [135] P Bonnett, T. V. Jones and D. G. McDonnell, (1989) "Shear Stress Measurements in Aerodynamic Testing Using Cholesteric Liquid Crystals", *Liquid Crystals*, **6**, (3), pp 271-280.
- [136] G. H. Heilmeyer and J. E. Goldmacher (1968) “A new electric-field-controlled reflective optical storage effect in mixed liquid crystal systems,” *Appl. Phys. Lett.*, **13**, (4), pp 132 – 133.
- [137] W. Greubel, U. Wolf, H. Krüger, (1973) “Electric field induced texture change in certain nematic/cholesteric liquid crystal mixtures,” *Mol. Cryst. Liq. Cryst.* **24**, pp 103 - 106.
- [138] W. Greubel (1974) “Bistability behavior of texture in cholesteric liquid crystals in an electric field,” *Appl. Phys. Lett.*, **25**, (1) pp. 5 – 7.
- [139] D.-K. Yang, J. L. West, L.-C. Chien and J.W. Doane, (1994) “Control of Reflectivity and Bistability in Displays using Cholesteric Liquid Crystals,” *J. Appl. Phys.*, **76**, pp 1331 - 1333.
- [140] A. Khan, I. Shiyankovskaya, T. Schneider, N. Miller, T. Ernst, D. Marhefka, F. Nicholson, S. Green, G. Magyar, O. Pishnyak, J. W. Doane (2005) “Reflective cholesteric displays: From rigid to flexible,” *J. SID*, **13**, (6), pp. 469 – 474.
- [141] T. Schneider, G. Magyar, S. Barua, T. Ernst, N. Miller, S. Franklin, E. Montbach, D. J. Davis, A. Khan and J. W. Doane (2008) “A Flexible Touch-sensitive Writing Tablet,” *Proc. SID Int. Symp. Digest Tech. Papers*, vol. **39**, pp. 1840 – 1842.
- [142] D. Coates (2009) “Low-power large-area cholesteric displays” *Information Display*, **25**, (3), pp. 16 – 19.
- [143] D. W. Berreman and W. R. Heffner (1980) “New bistable liquid crystal twist cell,” *Appl. Phys. Lett.* **25**, pp 109-111.
- [144] H. Nomura, T. Obikawa, Y. Ozawa and T. Tanaka (2000) “Recent studies on multiplex driving of BTN-LCDs,” *J. SID*, **8**, (4) pp. 289 – 294.
- [145] I. Dozov, M. Nobili and G. Durand (1997) “Fast bistable nematic display using monostable surface switching,” *Appl. Phys. Lett.* **70**, (9), pp. 1179 – 1181.
- [146] S. Joly, P. Thomas, J. Osterman, A. Simon, S. Lallemand, L. Faget, J.-D Laffitte, M. Irzyk, L. Madsen, J. Angelé, F. Leblanc and P. Martinot-Lagarde (2010) “Demonstration of a technological prototype of an active-matrix *Binem* liquid-crystal display,” *J. SID.*, **18**, (12), pp. 1033 – 1039.
- [147] <https://www.youtube.com/watch?v=j3Ob93XGM6A>
- [148] G. P. Bryan-Brown, C.V. Brown and J.C. Jones (1995) "Bistable Nematic Liquid Crystal Device", *Patent US 06249332*.
- [149] J.C. Jones (2008) “The Zenithal Bistable Display: From concept to consumer,” *J. SID*, **16**, (1) pp.143 - 154.
- [150] E.L. Wood, G.P. Bryan-Brown, P. Brett, A. Graham and J.C. Jones, (2000), “Zenithal bistable device (ZBD) suitable for portable applications”, *Proc. SID, Int. Symp. Digest, Technical papers*, **31**, pp. 124 – 127.
- [151] J.C. Jones (2006), “Novel Geometries of the Zenithal Bistable Device,” *Proc. SID Int. Symp. Digest, Technical papers*, vol. **37**, pp. 1626 – 1629.
- [152] J.C. Jones, S.M. Beldon and E.L. Wood (2003) “Gray scale in zenithal bistable displays: The route to ultra-low power color

- displays,” *J. SID*, vol. **11**, no. 2, pp. 269 – 275.
- [153] J.C. Jones, P. Worthing, G Bryan-Brown and E. Wood (2003) “Transflective and single polariser reflective Zenithal Bistable Displays”, *SID Int. Symp. Digest, Technical papers*, **34**, 14.1, pp 190 – 193.
- [154] J.C. Jones (1999) “Bistable nematic liquid crystal device”, *US Patent 7,371,362*.
- [155] T. J. Spencer, C. Care, R.M. Amos and J.C. Jones (2010) “A Zenithal bistable device: Comparison of modelling and experiment”, *Phys. Rev. E.*, **82**, 021702 pp1 – 13
- [156] G.P. Bryan-Brown, D.R.E. Walker and J.C. Jones (2009) “Controlled Grating Replication for the ZBD Technology”, *SID Int. Symp. Digest, Technical papers* **40**, pp 1334 – 1337.
- [157] C. Hilsum, (1976) “Electro-optic Device” *UK Patent 1,442,360*.
- [158] J.L. Ferguson (1984) “Encapsulated liquid crystal and method”, *US patent 4,435,047*.
- [159] D. Coates, (1995) “Polymer-dispersed liquid crystals”. *J Mater. Chem.* **5**, pp 2063–2072.
- [160] P. Dziric (1995) “Liquid Crystal Dispersions”, *World Scientific, Singapore*.
- [161] P. Dziric (1986) “Polymer dispersed nematic liquid crystal for large area displays and light valves”, *J. Appl. Phys.*, **60**, (6) pp 2142 – 2148.
- [162] B.-G. Wu, J. H. Erdmann and J. W. Doane, (1989) “Response times and voltages for PDLC light shutters”, *Liquid Crystals*, **5**, (5), pp 1453-1465
- [163] Y. Asaoka, E. Satoh, K. Deguchi, T. Satoh, K. Minoura, I. Ihara, S. Fujiwara, A. Miyata, Y. Itoh, S. Gyoten, N. Matsuda and Y. Kubota (2009), “29.1: Polarizer-Free Reflective LCD Combined with Ultra Low-Power Driving Technology”, *SID 09 Digest*, pp 395–398.
- [164] M. Kim, K.J. Park, S. Seok, J.M. Ok, H.T. Jung, J. Choe and D.H. Kim (2015) “Fabrication of Microcapsules for Dye-Doped Polymer-Dispersed Liquid Crystal-Based Smart Windows”, *ACS Applied Materials and Interfaces*, **7**(32), 17904–17909.
- [165] For example, <http://intelligentglass.net/categories/switchable-glass/>
- [166] T. J. Bunning, L.V. Natarajan, V.P. Tondiglia and R.L. Sutherland, (2000) “Holographic Polymer Dispersed Liquid Crystals (H-PDLC)”, *Annu. Rev. Mater. Sci.* **30**, pp 83 – 115.
- [167] D. Armitage, I. Underwood and S. -T. Wu (2006) “Introduction to Microdisplays”, *John Wiley and Sons Ltd., Chichester, UK*.
- [168] M. S. Brennesholtz and E. H. Stupp (2008) “Projection Displays”, *John Wiley and Sons Ltd., Chichester, UK*.
- [169] M. J. O’Callaghan and M.A. Handschy, (2001) “Ferroelectric liquid crystal SLMs: from prototypes to products”, *Proc. SPIE 4457, Spatial Light Modulators: Technology and Applications*, 31.
- [170] E. E. Kriezis, L.A. Parry-Jones and S.J. Elston (2003) Optical Properties and applications of ferroelectric and antiferroelectric liquid crystals”, IN L. Vicari “Optical Applications of Liquid Crystals”, *CRC Press, Cambridge, UK*.
- [171] N. Collings, T. Davey, J. Christmas, D. Chu and W. Crossland (2011) “The Applications and Technology of Phase-Only Liquid Crystal on Silicon Devices”, *IEEE Journal of Display Technology*, **7**, (3), pp 112–119.
- [172] D. Armitage, J.I. Thackara and W. D. Eades (1989) “Photoaddressed Liquid Crystal Spatial Light Modulators”, *Appl. Opt.* **28**, (22), pp 4763 - 4771
- [173] M. Stanley, P.B. Conway, S. Coomber, J.C. Jones, D.C. Scattergood, C.W. Slinger, R.W. Bannister, C.V. Brown, W.A. Crossland, A.J. Travis, (2000) “A novel electro-optic modulator system for the production of dynamic images from giga-pixel computer generated holograms”, *Proceedings of SPIE*, **3956**, 13 – 22.
- [174] C. Slinger, C. Cameron and M. Stanley (2005) “Computer-generated holography as a generic display technology”. *Computer* **38**, 46–53.
- [175] P.J. Bos and K.R. Koehler-Beran (1984) “The pi-cell: A fast liquid crystal optical switching device”, *Mol. Cryst. Liq. Cryst.* **113**, pp 329-339.
- [176] J. L. Ferguson and A. L. Berman (1989) “A push/pull surface-mode liquid-crystal shutter: Technology and applications”, *Liquid Crystals*, **5**, (5), 1397–1404.
- [177] X. Y. Yu and H. S. Kwok, (2004) “Bistable bend-splay liquid crystal device”, *Appl. Phys. Lett.*, vol. **85**, (17), pp 3711 – 3713

- [178] E.P. Raynes (1975) "Optically Active Additives in Twisted Nematic Devices", *Rev. de Phys. Appl.*, **10**, pp. 117 – 120.
- [179] Y. Yamaguchi, T. Miyashita and T. Uchida, (1993) "Wide-viewing-angle display mode for the active-matrix LCD Using bend-alignment liquid-crystal cell", *SID 93 Digest*, pp. 273-276.
- [180] P. J. Bos and J. A. Rahman, (1993) "An optically 'self-compensating' electro-optical effect with wide angle of view", *SID 93 Digest*, pp 277-280.
- [181] C. G. Jhun, M. S. Park, P. K. Son, J. H. Kwon, J. Yi and J. S. Gwag, (2011) "Transflective Liquid Crystal Display with Pi-cell", *Mol. Cryst. Liq. Cryst.*, **544**, 88 – 94.
- [182] M.J. Bradshaw and E.P. Raynes (1986) "Smectic Liquid Crystal Devices", *US Patent 4,969,719*.
- [183] J.S. Patel (1992) "Ferroelectric liquid crystal modulator using twisted smectic structure", *Appl. Phys. Lett.* **60**, pp 280–282
- [184] A.D.L. Chandani, E. Gorecka, Y. Ouchi and H. Takezoe H (1989) "Antiferroelectric chiral smectic phases responsible for the tristable switching in MHPOBC". *Jpn. J. Appl. Phys. Lett.*, **28**, pp L1265–L1268
- [185] B.I. Ostrovsky, A.Z. Rabinovich and V.G. Chigrinov (1980) "Behavior of ferroelectric smectic liquid crystals in electric field" IN: L. Bata (ed.) "Advances in liquid crystal research and applications", *Pergamon Press, Oxford, UK*, p 469 – 482.
- [186] S. Garoff and R.B. Meyer (1977) "Electroclinic effect at the A-C phase change in a chiral smectic liquid crystal", *Phys. Rev. Lett.* **38**, pp 848–851.
- [187] D. Coates and G.W. Gray (1973) "Optical studies of the amorphous liquid-cholesteric liquid crystal transition: the blue phase", *Phys. Lett. A* **45**, pp.115–116.
- [188] Y. Haseba and H. Kikuchi (2006) "Electro-optic effects of the optically isotropic state induced by the incorporative effects of a polymer network and the chirality of liquid crystal", *J. SID*, **14**, (6) pp. 551-556
- [189] H. Kikuchi, M. Yokota, Y. Hisakado, H. Yang and T. Kajiyama, (2002) "Polymer-stabilized liquid crystal blue phases", *Nature Materials*, **1** (1), 64–68.
- [190] Z. Ge, S. Gauza, M. Jiao, H. Xianyu and S.T. Wu, (2009) "Electro-optics of polymer-stabilized blue phase liquid crystal displays", *Appl. Phys. Lett.*, **94**, (10), pp 9–12.
- [191] L. Rao, Z. Ge, S.-T Wu and S. H. Lee, (2009) "Low voltage blue-phase liquid crystal displays", *Appl. Phys. Lett.*, **95**, (23), 231101.
- [192] M.D.A. Rahman, S. Mohd Said and S. Balamurugan (2015) "Blue phase liquid crystal: strategies for phase stabilization and device development", *Sci. Tech. Adv. Mat.*, **16**, (3), 033501.
- [193] J. Patel and R.B. Meyer (1987) "Flexoelectric electro-optics of a cholesteric liquid crystal", *Phys. Rev. Lett.* **58**, 1538
- [194] P. Rudquist, M. Buivydas, L. Komitov and S.T. Lagerwall, (1994) "Linear electro-optic effect based on flexoelectricity in a cholesteric with sign change of dielectric anisotropy", *J. Appl. Phys.*, **76**, (12), pp 7778–7783.
- [195] K. L. Atkinson, S. M. Morris, M. M. Qasim, F. Castles, D. J. Gardiner, P. J. W. Hands, S. S. Choi, W. –S. Kim and H. J. Coles (2012) "Increasing the flexoelastic ratio of liquid crystals using highly fluorinated ester-linked bimesogens" *Phys. Chem. Chem. Phys.* **14**, (47) pp 16377-16385.
- [196] L. Komitov, G.P. Bryan-Brown, E.L. Wood and A.B.J. Smout, (1999) "Alignment of cholesteric liquid crystals using periodic anchoring", *J. Appl. Phys.*, **86**, (7) pp 3508 – 3511.
- [197] G. Carbone, D. Corbett, S.J. Elston, P. Raynes, A. Jesacher, A. R. Simmonds and M. Booth, (2011) "Uniform Lying Helix Alignment on Periodic Surface Relief Structure Generated via Laser Scanning Lithography", *Mol. Cryst. Liq. Cryst.*, **544**, (1), pp 37-49.
- [198] C.C. Tartan, P.S. Salter, M.J. Booth, S.J. Morris, and S. J. Elston, (2016) "Localised polymer networks in chiral nematic liquid crystals for high speed photonic switching", *J. Appl. Phys.*, **119**, (18), 183106.
- [199] N.V. Kukhtarev, (1978) "Cholesteric liquid crystal laser with distributed feedback", *Soviet Journal of Quantum Electronics*, **8**, (6), 774-776.
- [200] V. I. Kopp, B. Fan, H. K. M. Vithana and A. Z. Genack, (1998) "Low-threshold lasing at

- the edge of a photonic stop band in cholesteric liquid crystals. *Opt. Lett.* **23**, 1707–1709.
- [201] B. Taheri, A. Munoz, P. Palffy-Muhoray and R. Twieg, (2001) “Threshold lasing in cholesteric liquid crystals”, *Mol. Cryst. Liq. Cryst.* **358**, 73–82.
- [202] E. Yablonovitch (1987) “Inhibited Spontaneous Emission in Solid-State Physics and Electronics”, *Phys. Rev. Lett.* **58**, (20) pp 2059-2062.
- [203] M. Uchimura, Y. Watanabe, F. Araoka,, J. Watanabe, H. Takezoe, and G.I. Konishi, (2010) “Development of laser dyes to realize low threshold in dye-doped cholesteric liquid crystal lasers”. *Advanced Materials*, **22**, (40), pp 4473–4478.
- [204] D.J. Gardiner, W. -K.Hsiao, S. M. Morris, P.J.W. Hands, T.D. Wilkinson, I.M. Hutchings and H.J. Coles, (2012) “Printed photonic arrays from self-organized chiral nematic liquid crystals”, *Soft Matter*, **8** (39), 9977 – 9980.
- [205] H. Coles and S. Morris, (2010) “Liquid-crystal lasers”, *Nature Photonics*, **4**, (10), pp 676–685.
- [206] H.-Y Chen, S. -F. Lu, P.-H., Wu, and C.S. Wang, C.-S. (2016) “Transflective BPIII mode with no internal reflector” *Liquid Crystals*, 8292(August 2016), 1–6.
- [207] Q. Li, (2012) “Liquid Crystals Beyond Displays: Chemistry, Physics, and Applications”, *John Wiley and Sons, New Jersey*. ISBN: 978-1-118-07861-7
- [208] WH. De Jeu (Ed.) (2012) “Liquid Crystal Elastomers: Materials and Applications”, Springer, US. ISBN: 978-3-642-31581-7
- [209] R.J. Bushby, S.M. Kelly and M. O’Neill (Eds) (2012) “Liquid Crystalline Semiconductors: Materials, properties and application”, *Springer-Verlag Berlin Heidelberg*. ISBN 978-90-481-2873-0
- [210] R.J. Carlton, J.T. Hunter, D. S. Miller, R. Abbasi, P.C. Mushenheim, L. N. Tan and N. L. Abbott (2013) “Chemical and Biological Sensing using Liquid crystals”, *Liq. Cryst. Rev.*, **1**, (1) pp 29 – 51.

### Recommended further reading

R. H. Chen (2011) “Liquid Crystal Displays”, *John Wiley and Sons, New Jersey*.

N. Koide (2014) “*The Liquid Crystal Display Story: 50 Years of Liquid Crystal R&D that lead the Way to the Future*”, Springer, Japan.

D. Dunmur and T. Sluckin (2011) *Soap, Science, and Flat-screen TVs: a history of liquid crystals*, Oxford University Press ISBN 978-0-19-954940-5.